

**NUMERICAL ANALYSIS OF ENTROPY  
GENERATION IN LAMINAR VISCOUS FLUID FLOW  
BETWEEN PARALLEL PLATES**

BY

**NAYEF M. AL-SAIFI**

A Thesis Presented to the  
DEANSHIP OF GRADUATE STUDIES

**KING FAHD UNIVERSITY OF PETROLEUM & MINERALS**

DHAHRAN, SAUDI ARABIA

In Partial Fulfillment of the  
Requirements for the Degree of

**MASTER OF SCIENCE**

In

**CHEMICAL ENGINEERING**

January, 2004

UMI Number: 1419519

### INFORMATION TO USERS

The quality of this reproduction is dependent upon the quality of the copy submitted. Broken or indistinct print, colored or poor quality illustrations and photographs, print bleed-through, substandard margins, and improper alignment can adversely affect reproduction.

In the unlikely event that the author did not send a complete manuscript and there are missing pages, these will be noted. Also, if unauthorized copyright material had to be removed, a note will indicate the deletion.

**UMI**<sup>®</sup>

---

UMI Microform 1419519

Copyright 2004 by ProQuest Information and Learning Company.

All rights reserved. This microform edition is protected against unauthorized copying under Title 17, United States Code.

ProQuest Information and Learning Company  
300 North Zeeb Road  
P.O. Box 1346  
Ann Arbor, MI 48106-1346

**KING FAHD UNIVERSITY OF PETROLEUM & MINERALS  
DHAHRAN 31261, SAUDI ARABIA**

**DEANSHIP OF GRADUATE STUDIES**

This thesis, written by

**NAYEF M. AL-SAIFI**

Under the direction of his Thesis Advisor and approved by his Thesis Committee, has been presented to and accepted by the Dean of Graduate Studies, in partial fulfillment of the requirements for the degree of

**MASTER OF SCIENCE IN CHEMICAL ENGINEERING**

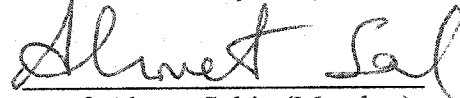
**Thesis Committee**



**Dr. Ramazan Kahraman (Chairman)**



**Dr. Usamah Al-Mubaiyedh (Co-Chairman)**



**Prof. Ahmet Sahin (Member)**



**Dr. H. H. Al-Ali (Member)**



**Dr. K. Loughlin (Member)**



**Prof. Mohamed B. Amin  
(Department Chairman)**



**Prof. Osama A. Jannadi  
(Dean of Graduate Studies)**

**24/3/2004**

**Date**



Dedicated to  
My Loving Parents and Wife

## ACKNOWLEDGMENTS

My unqualified gratitude is to Allah, the Almighty who guided me in every facet of this work in his infinite wisdom and bounties.

I am sincerely grateful to Dr. Ramazan Kahraman, my thesis committee chairman, and Dr. Usamah Al-Mubaiyedh, my thesis co-chairman, who not only made themselves available for consultation at all times, but also served as a source of continuing inspiration throughout the course of this work.

My sincere thanks and appreciation is also due to the other members of the committee, Prof. Ahmet Sahin, Dr. H. H. Al-Ali and Dr. K. Loughlin for their invaluable support, suggestions and constructive criticisms that enormously facilitated this work.

I would like to acknowledge the King Fahd University of Petroleum and Minerals especially for making available all the facilities. I would also like to thank the chemical engineering department and especially the faculty members for their invaluable contributions, and assistance in several ways throughout the course of my graduate program.

Finally, my deep thanks go to my family for their love, support and encouragement for their invaluable help and motivation.

## TABLE OF CONTENTS

	Page
<b>DEDICATION</b>	ii
<b>ACKNOWLEDGMENT</b>	iii
<b>TABLE OF CONTENTS</b>	iv
<b>LIST OF TABLES</b>	vii
<b>LIST OF FIGURES</b>	viii
<b>ABSTRACT (English)</b>	xv
<b>ABSTRACT (Arabic)</b>	xvi
<b>CHAPTER 1 INTRODUCTION</b>	1
1.1 Motivation	1
1.2 Objective of the Study	2
<b>CHAPTER 2 BACKGROUND AND LITERATURE REVIEW</b>	4
2.1 Velocity and Temperature Distributions in Ducts	4
2.2 Entropy Generation Studies	11
2.2.1 Entropy Generation Equations	12
2.2.2 Entropy Generation Analysis in Different Process Components	13
2.2.3 Entropy Generation Analysis in Different Duct Geometries	17
<b>CHAPTER 3 MATHEMATICAL FORMULATIONS</b>	23
3.1 Problem Statement	23
3.2 Entropy Generation Equation	27
3.3 Continuity and Momentum Equations	29
3.3.1 Vorticity and Stream Function Equations	31
3.4 Energy Equation	33
3.5 Fully Developed Velocity Solution	34
3.6 Dimensionless Equations	35
3.7 Viscosity Temperature Relationship	38
3.8 Boundary Conditions	39
3.8.1 Stream Function Boundary Conditions	40
3.8.2 Vorticity Boundary Conditions	41
3.8.3 Temperature Boundary Conditions	43
<b>CHAPTER 4 NUMERICAL FORMULATION</b>	50
4.1 Generalities of the Method of Weighted Residual	50
4.2 Pseudospectral Method	52
4.3 Choice of Basis Function	53
4.4 Chebyshev Polynomials	53
4.5 Chebyshev Derivatives	57
4.6 Solution Techniques	63

<b>CHAPTER 5</b>	<b>RESULTS AND DISCUSSIONS</b>	66
5.1	Convergence of the Numerical Solution	66
5.2	Variable Viscosity Relationship	67
5.3	Constant Wall Temperature	72
5.3.1	Velocity Profiles	72
5.3.1.1	Velocity Profiles for Constant Viscosity	72
5.3.1.2	Velocity Profiles for Variable Viscosity	73
5.3.2	Effect of Inlet-Wall Temperature Difference, Reynolds Number and Liquid Type on Velocity Profile	85
5.3.2.1	Effect of Inlet-Wall Temperature Difference	85
5.3.2.2	Effect of Reynolds Number	90
5.3.2.3	Effect of Liquid Type	95
5.3.3	Temperature Profiles	98
5.3.4	Effect of Reynolds Number and Liquid Type on Temperature Profiles.	102
5.3.4.1	Effect of Reynolds Number	102
5.3.4.2	Effect of Liquid Type	102
5.3.5	Entropy Generation Profiles	105
5.3.5.1	Entropy Generation from Fluid Friction Effect	105
5.3.5.2	Entropy Generation from Heat Transfer Effect	110
5.3.5.3	Effect of Reynolds Number, Liquid Type and $\Delta T$ on Entropy Generation	117
5.3.5.3.1	Effect of Reynolds Number	117
5.3.5.3.2	Effect Liquid Type	120
5.3.5.3.3	Effect of Inlet-Wall Temperature Difference	123
5.3.5.4	$\dot{S}_{\Delta T}$ and $\dot{S}_{\Delta T/\Delta X}$	125
5.4	Constant Heat Flux	129
5.4.1	Velocity Profiles	129
5.4.2	Effect of Reynolds Number and Liquid Type on Velocity Profile.	137
5.4.2.1	Effect of Reynolds Number	137
5.4.2.2	Effect of Liquid Type	139
5.4.3	Temperature Profiles	141
5.4.4	Effect of Reynolds Number and Liquid Type on Temperature Profile.	141
5.4.4.1	Effect of Reynolds number	141
5.4.4.2	Effect of Liquid Type	147
5.4.5	Entropy Generation Profiles	149
5.4.5.1	Patterns of Entropy Generation Profiles	149
5.4.5.2	Effect of Reynolds Number and the Liquid Type on Entropy Generation	152
5.4.5.2.1	Effect of Reynolds Number	152
5.4.5.2.2	Effect of Liquid Type	153

5.4.5.3	$\dot{S}_{\Delta Y}$ and $\dot{S}_{\Delta T_{AX}}$	159
<b>CHAPTER 6</b>	<b>CONCLUSIONS AND RECOMMENDATIONS</b>	<b>162</b>
<b>NOMENCLATURE</b>		<b>166</b>
<b>BIBLIOGRAPHY</b>		<b>169</b>



## LIST OF TABLES

Table		Page
3.1	Dimensionless equations for constant wall temperature and constant properties.	44
3.2	Dimensionless equations for constant wall temperature and temperature dependent viscosity.	45
3.3	Dimensionless equations for constant heat flux and constant properties.	46
3.4	Dimensionless equations for constant heat flux and temperature dependent viscosity.	47
3.5	Boundary conditions for constant wall temperature case.	48
3.6	Boundary conditions for constant heat flux case.	49
4.1	Comparison between exact and pseudospectral solution for $N = 6$ .	61
4.2	Comparison between exact and pseudospectral solution for $N = 14$ .	62
5.1	Numerical solution convergence for axial velocity corresponding to ethylene glycol (physical properties are given in Table 5.2, $T_o = 300$ K, $\Delta T = 30$ K, Reynolds number = 100, $X = 30000$ and $Y = 0$ ).	68
5.2	Physical properties for Water and Ethylene Glycol [Plawsky, 2001].	69

## LIST OF FIGURES

Figure		Page
3.1	Flow of a fluid between parallel plates subjected to constant wall temperature.	24
3.2	Flow of a fluid between parallel plates subjected to constant heat flux.	24
3.3	Determining the entropy generation for constant viscosity case.	25
3.4	Determining the entropy generation for variable viscosity case.	26
4.1	Graphs of the first Chebyshev polynomials, $\phi_k(x)$ , for $k = 0, 1, 2, 3$ and 4.	55
4.2	Flow Chart of solution technique.	65
5.1a	$\mu$ vs. $(T-T_0)$ for water for $T_0 = 300$ K.	70
5.1b	$\mu$ vs. $(T-T_0)$ for ethylene glycol for $T_0 = 300$ K.	71
5.2	U vs. Y for constant viscosity case.	74
5.3	U vs. Y for variable and constant viscosity cases for ethylene glycol at $X = 185$ (physical properties are given in Table 5.2, $Re = 400$ , $\Delta T = 30$ K and $T_0 = 300$ K).	75
5.4	V vs. Y for variable viscosity case for ethylene glycol at $X = 185$ (physical properties are given in Table 5.2, $Re = 400$ , $\Delta T = 30$ K and $T_0 = 300$ K).	78
5.5	U vs. Y for variable viscosity case for ethylene glycol at various X values (physical properties are given in Table 5.2, $Re = 400$ , $\Delta T = 30$ K and $T_0 = 300$ K).	79
5.6	U vs. X for constant and variable viscosity cases for ethylene glycol at $Y = 0$ (physical properties are given in Table 5.2, $Re = 400$ , $\Delta T = 30$ K and $T_0 = 300$ K).	80
5.7	U vs. X for constant and variable viscosity cases for ethylene glycol at various Y values (physical properties are given in Table	

	5.2, $Re = 400$ , $\Delta T = 30$ K and $T_0 = 300$ K).	81
5.8	U vs. X for constant and variable viscosity cases for ethylene glycol at $Y = 0.5$ (physical properties are given in Table 5.2, $Re = 400$ , $\Delta T = 30$ K and $T_0 = 300$ K).	82
5.9	U vs. X for constant and variable viscosity cases for ethylene glycol at $Y = 0.82$ (physical properties are given in Table 5.2, $Re = 400$ , $\Delta T = 30$ K and $T_0 = 300$ K).	83
5.10a	U vs. X for variable viscosity case for ethylene glycol at $Y = 0$ (physical properties are given in Table 5.2, $Re = 400$ , $\Delta T = 30$ K and $T_0 = 300$ K).	84
5.10b	U vs. X for variable viscosity case for ethylene glycol at $Y = 0.46$ (physical properties are given in Table 5.2, $Re = 400$ , $\Delta T = 30$ K and $T_0 = 300$ K).	84
5.11	U vs. Y for variable viscosity case for ethylene glycol at $X = 185$ (physical properties are given in Table 5.2, $Re = 400$ , $\Delta T = 10, 20$ and $30$ K and $T_0 = 300$ K).	86
5.12	U vs. X for constant and variable viscosity cases for ethylene glycol at $Y = 0$ (physical properties are given in Table 5.2, $Re = 400$ , $\Delta T = 10, 20, 30$ K and $T_0 = 300$ K).	87
5.13	V vs. Y for variable viscosity case for ethylene glycol at $X = 185$ (physical properties are given in Table 5.2, $Re = 400$ , $\Delta T = 10, 20, 30$ K and $T_0 = 300$ K).	88
5.14	V vs. X for variable viscosity case for ethylene glycol at $Y = 0.15$ (physical properties are given in Table 5.2, $Re = 400$ , $\Delta T = 10, 20, 30$ K and $T_0 = 300$ K).	89
5.15	U vs. X for variable viscosity case for ethylene glycol at $Y = 0$ (physical properties are given in Table 5.2, $Re = 100$ , $\Delta T = 10$ K and $T_0 = 300$ K).	91
5.16	U vs. X for variable viscosity case for ethylene glycol at $Y = 0$ (physical properties are given in Table 5.2, $Re = 200$ , $\Delta T = 10$ K and $T_0 = 300$ K).	92
5.17	U vs. X for variable viscosity case for ethylene glycol at $Y = 0$ (physical properties are given in Table 5.2, $Re = 100, 200, 300, 400$ , $T_0 = 300$ K, $\Delta T = 10$ K).	93
5.18	U vs. Y for variable viscosity case for ethylene glycol at $X = 1105$	

	(physical properties are given in Table 5.2, $Re = 50$ and $400$ , $T_0 = 300$ K and $\Delta T = 30$ K).	94
5.19	U vs. X for variable viscosity case for ethylene glycol and water at $Y = 0$ (physical properties are given in Table 5.2, $Re = 200$ , $T_0 = 300$ K and $\Delta T = 30$ K).	96
5.20	U vs. Y for variable viscosity case for ethylene glycol and water at $X = 825$ (physical properties are given in Table 5.2, $Re = 200$ , $T_0 = 300$ K and $\Delta T = 30$ K).	97
5.21	$\Theta$ vs. X for variable viscosity case for ethylene glycol at various Y values (physical properties are given in Table 5.2, $Re = 400$ , $T_0 = 300$ K and $\Delta T = 30$ K).	99
5.22	$\Theta$ vs. Y for variable viscosity case for ethylene glycol at various X values (physical properties are given in Table 5.2, $Re = 400$ , $T_0 = 300$ K and $\Delta T = 30$ K).	100
5.23	$\Theta$ vs. X for constant and variable viscosity cases for ethylene glycol at $Y = 0.8$ and $0.9$ (physical properties are given in Table 5.2, $Re = 400$ , $T_0 = 300$ K and $\Delta T = 30$ K).	101
5.24	$\Theta$ vs. X for variable viscosity case for ethylene glycol at $Y = 0$ (physical properties are given in Table 5.2, $Re = 100, 200, 300$ and $400$ , $T_0 = 300$ K and $\Delta T = 30$ K).	103
5.25	$\Theta$ vs. X for variable viscosity case for water and ethylene glycol at $Y = 0$ (physical properties are given in Table 5.2, $Re = 400$ , $T_0 = 300$ K and $\Delta T = 30$ K).	104
5.26	$\dot{S}_{gen}^m$ (fluid friction effect) vs. X for variable viscosity case for ethylene glycol at various Y values (physical properties are given in Table 5.2, $Re = 400$ , $T_0 = 300$ K and $\Delta T = 30$ K).	107
5.27	$\dot{S}_{gen}^m$ (fluid friction) vs. Y for variable viscosity case for ethylene glycol at various Y values (physical properties are given in Table 5.2, $Re = 400$ , $T_0 = 300$ K and $\Delta T = 30$ K).	108
5.28	$\dot{S}_{gen}^m$ (fluid friction) vs. X for variable viscosity case for ethylene glycol at $Y = 0.70$ (physical properties are given in Table 5.2, $Re = 100, 200, 300$ and $400$ , $T_0 = 300$ K and $\Delta T = 30$ K).	109
5.29	$\dot{S}_{gen}^m$ (heat transfer effect only) vs. X for variable viscosity case for	

	ethylene glycol at various Y values (physical properties are given in Table 5.2, $Re = 400$ , $T_0 = 300$ K and $\Delta T = 30$ K).	112
5.30	$\dot{S}_{gen}^m$ vs. X for variable viscosity case for ethylene glycol at various Y values (physical properties are given in Table 5.2, $Re = 400$ , $T_0 = 300$ K and $\Delta T = 30$ K).	113
5.31	$\dot{S}_{gen}^m$ (heat transfer effect) vs. X for variable viscosity case for ethylene glycol at $Y = 0.91$ and $1$ (physical properties are given in Table 5.2, $Re = 400$ , $T_0 = 300$ K and $\Delta T = 30$ K).	114
5.32	$\dot{S}_{gen}^m$ vs. X (heat transfer effect) for constant and variable viscosity cases for ethylene glycol at $Y = 0.92$ (physical properties are given in Table 5.2, $Re = 400$ , $T_0 = 300$ K and $\Delta T = 30$ K).	115
5.33	$\dot{S}_{gen}^m$ (heat transfer effect) vs. Y for constant and variable viscosity cases for ethylene glycol at $X = 185$ (physical properties are given in Table 5.2, $Re = 400$ , $T_0 = 300$ K and $\Delta T = 30$ K).	116
5.34	$\dot{S}_{gen}^m$ (heat transfer effect) vs. X at $Y = 0.90$ for constant and variable viscosity cases for ethylene glycol for two Re values (physical properties are given in Table 5.2, $T_0 = 300$ K and $\Delta T = 30$ K).	118
5.35	$\dot{S}_{gen}^m$ (heat transfer effect) vs. X at $Y = 0.5$ for constant and variable viscosity cases for two Re values (physical properties are given in Table 5.2, $T_0 = 300$ K and $\Delta T = 30$ K).	119
5.36	$\dot{S}_{gen}^m$ (heat transfer effect) vs. X for variable viscosity case for water and ethylene glycol at $Y = 0.90$ (physical properties are given in Table 5.2, $Re = 400$ , $T_0 = 300$ K and $\Delta T = 30$ K).	121
5.37	$\dot{S}_{gen}^m$ (heat transfer effect) vs. Y for variable viscosity case for ethylene glycol and water at $X = 185$ (physical properties are given in Table 5.2, $Re = 400$ , $T_0 = 300$ K and $\Delta T = 30$ K).	122
5.38	$\dot{S}_{gen}^m$ vs. X at $Y = 0.90$ for variable viscosity case for ethylene glycol at different $\Delta T$ values (physical properties are given in Table 5.2, $Re = 400$ and $T_0 = 300$ K).	124

5.39	$\dot{S}_{\Delta Y}$ vs. X for variable viscosity case for ethylene glycol for different Re numbers (physical properties are given in Table 5.2, $T_o = 300$ K, $\Delta T = 30$ K).	127
5.40	$\dot{S}_{\Delta Y \Delta X}$ vs. Re for variable viscosity case for ethylene glycol between X = 0 and X = 7500 (physical properties are given in Table 5.2, $T_o = 300$ K, $\Delta T = 30$ K).	128
5.41	U vs. X for constant and variable viscosity cases for ethylene glycol at Y = 0 (physical properties are given in Table 5.2, Re = 400, $T_o = 300$ K and $Q'' = 10$ W/m <sup>2</sup> ).	130
5.42	U vs. X for constant and variable viscosity cases for ethylene glycol at Y = 0.43 (physical properties are given in Table 5.2, Re = 400, $T_o = 300$ K and $Q'' = 10$ W/m <sup>2</sup> ).	132
5.43	U vs. X for constant and variable viscosity cases for ethylene glycol at Y = 0.95 (physical properties are given in Table 5.2, Re = 400, $T_o = 300$ K and $Q'' = 10$ W/m <sup>2</sup> ).	133
5.44	U vs. X for constant and variable viscosity cases for ethylene glycol at Y = 0.5 (physical properties are given in Table 5.2, Re = 400, $T_o = 300$ K and $Q'' = 10$ W/m <sup>2</sup> ).	134
5.45	U vs. Y for constant and variable viscosity cases for ethylene glycol at X = 10000 (physical properties are given in Table 5.2, Re = 400, $T_o = 300$ K, $Q'' = 10$ W/m <sup>2</sup> ).	135
5.46	V vs. Y for variable viscosity case for ethylene glycol at various X values (physical properties are given in Table 5.2, Re = 400, $T_o = 300$ K and $Q'' = 10$ W/m <sup>2</sup> ).	136
5.47	U vs. X at Y = 0.52 for variable viscosity case for ethylene glycol (physical properties are given in Table 5.2, Re = 100, 200, 300, 400, $T_o = 300$ K and $Q'' = 10$ W/m <sup>2</sup> ).	138
5.48	U vs. X for variable viscosity case for ethylene glycol and water at Y = 0 (physical properties are given in Table 5.2, Re = 400, $T_o = 300$ K and $Q'' = 10$ W/m <sup>2</sup> ).	140
5.49	$\Theta$ vs. X for variable viscosity case for ethylene glycol at Y = 0 (physical properties are given in Table 5.2, Re = 400, $T_o = 300$ K and $Q'' = 10$ W/m <sup>2</sup> ).	142

5.50	⊕ vs. X for variable viscosity case for ethylene glycol at Y = 1 (physical properties are given in Table 5.2, Re = 400, T <sub>o</sub> = 300 K and Q'' = 10 W/m <sup>2</sup> ).	143
5.51	⊕ vs. X for variable viscosity case for ethylene glycol at Y = 0.52 (physical properties are given in Table 5.2, Re = 400, T <sub>o</sub> = 300 K and Q'' = 10 W/m <sup>2</sup> ).	144
5.52	⊕ vs. Y for variable viscosity for ethylene glycol at various X values (physical properties are given in Table 5.2, Re = 400, T <sub>o</sub> = 300 K and Q'' = 10 W/m <sup>2</sup> ).	145
5.53	⊕ vs. X for variable viscosity case for ethylene glycol at Y = 0 (physical properties are given in Table 5.2, Re = 100, 200, 300, 400, T <sub>o</sub> = 300 K and Q'' = 10 W/m <sup>2</sup> ).	146
5.54	⊕ vs. X for variable viscosity case for ethylene glycol and water at Y = 1 (physical properties are given in Table 5.2 Re = 400, T <sub>o</sub> = 300 K and Q'' = 10 W/m <sup>2</sup> ).	148
5.55	$\dot{S}_{gen}''$ vs. X for variable viscosity case for ethylene glycol at various Y values (physical properties are given in Table 5.2, Re = 400, T <sub>o</sub> = 300 K and Q'' = 10 W/m <sup>2</sup> ).	150
5.56	$\dot{S}_{gen}''$ vs. X for constant and variable viscosity cases for ethylene glycol at Y = 0.52 and 0.74 (physical properties are given in Table 5.2, Re = 400, T <sub>o</sub> = 300 K and Q'' = 10 W/m <sup>2</sup> ).	151
5.57	$\dot{S}_{gen}''$ vs. Y for variable viscosity case for ethylene glycol at various X values (physical properties are given in Table 5.2, Re = 400, T <sub>o</sub> = 300 K and Q'' = 10 W/m <sup>2</sup> ).	154
5.58	$\dot{S}_{gen}''$ vs. X for variable viscosity case for ethylene glycol at Y = 0.52 (physical properties are given in Table 5.2, Re = 100, 200, 300, 400, T <sub>o</sub> = 300 K and Q'' = 10 W/m <sup>2</sup> ).	155
5.59	$\dot{S}_{gen}''$ vs. Y for variable viscosity case for ethylene glycol at X = 80.4 (physical properties are given in Table 5.2, Re = 100, 200, 300, 400, T <sub>o</sub> = 300 K and Q'' = 10 W/m <sup>2</sup> ).	156

5.60	$\dot{S}_{gen}''$ vs. X for variable viscosity case for ethylene glycol and water at Y = 0.52 (physical properties are given in Table 5.2, Re = 400, $T_o = 300$ K and $Q'' = 10$ W/m <sup>2</sup> ).	157
5.61	$\dot{S}_{gen}''$ vs. Y for variable viscosity case for ethylene glycol and water at X = 100 (physical properties are given in Table 5.2, Re = 400, $T_o = 300$ K and $Q'' = 10$ W/m <sup>2</sup> ).	158
5.62	$\dot{S}_{\Delta Y}$ vs. X for variable viscosity case for ethylene glycol for different Re numbers (physical properties are given in Table 5.2, $T_o = 300$ K and $Q'' = 10$ W/m <sup>2</sup> ).	160
5.63	$\dot{S}_{\Delta Y \Delta X}$ vs. Re for variable viscosity case for ethylene glycol between X = 0 and X = 1250 (physical properties are given in Table 5.2, $T_o = 300$ K and $Q'' = 10$ W/m <sup>2</sup> ).	161



## THESIS ABSTRACT

**NAME OF STUDENT** : NAYEF M. AL-SAIFI  
**TITLE OF STUDY** : Numerical Analysis of Entropy Generation in Laminar  
Viscous Fluid Flow Between Parallel Plates  
**MAJOR FIELD** : Chemical Engineering  
**DATE OF DEGREE** : January, 2004

Intrinsic irreversibilities associated within various process components lead to generation of entropy which destroys available energy and influences the performance of processes. In this study, entropy generation for fully developed laminar viscous flow is numerically investigated between parallel plates subjected to either constant wall temperature or constant heat flux. The governing partial differential equations representing the continuity, momentum and energy equations are solved numerically using a Chebyshev pseudospectral technique by taking into account the temperature dependence of the viscosity. The governing equations are transformed into stream function and vorticity formulations and solved by using a new technique for treating the boundary conditions of vorticity at the wall. Entropy generated from temperature and velocity fields is shown to depend upon Reynolds number, liquid type and inlet to wall temperature difference. The increase in the Reynolds number values shifts and extends the entropy generation profile downstream. The higher the liquid viscosity, the higher the entropy generation for the flowing fluid between the parallel plates. Further, the entropy generation from heat transfer effect is dominant compared to that from fluid friction effect. The study revealed that the constant viscosity assumption may yield a considerable amount of deviation in entropy generation from that of the variable viscosity case.

The obtained entropy generation profiles are an initial step to the design of fluid flow between parallel plates and to minimize entropy generation.

**MASTER OF SCIENCE DEGREE**  
**KING FAHD UNIVERSITY OF PETROLEUM AND MINERALS**  
**DHAHRAN, SAUDI ARABIA**  
**JANUARY, 2004**

## ملخص الرسالة

اسم الطالب : نايف مسند الصيفي.  
عنوان الرسالة : تحليل حسابي للانتروبي لسائل صفحي بين سطحين متوازيين.  
مجال التخصص : الهندسة الكيميائية.  
تاريخ الدرجة : 2004 م

إن تزايد الانتروبي في العمليات الصناعية يؤدي إلى نتائج سلبية, من ضمنها التأثير على أداء بعض العمليات لاسيما إضعاف فعالية الطاقه في تلك العمليات.

وللحد من هذه الظاهره, لابد من دراسة الانتروبي والبحث في العوامل المسببه في تزايدها. فهذا البحث يقوم بدراسة الانتروبي لسائل صفحي يجري بين سطحين متوازيين و كلاهما معرضان لتسخين إما بتعرضهما إلى درجه حرارة ثابتة أعلى من درجه السائل أو بتسليط تدفق حراري على كلا السطحين ولايجاد منحنيات الانتروبي في هذه الدراسة توجب حل عدة معادلات تفاضليه, وهي معادلة حفظ الطاقه, معادلة حفظ الكتله, ومعادلات العزم و معادلة الانتروبي مع الأخذ في الاعتبار تغير اللزوجه مع درجه الحراره.

ولقد قدم هذا البحث العديد من النتائج الجيدة المساعده في فهم الانتروبي وقام بدراسة بعض العوامل المؤثرة في الانتروبي من ضمنها نوعية السائل و زيادة قيمه رقم رينولد و من هذه النتائج, أن زيادة قيمه رقم رينولد يؤدي إلى زيادة الانتروبي. بالإضافة إلى ذلك لقد وجد أنه كلما زادت لزوجه السائل زاد تولد الانتروبي, وكما أثبتت هذه الدراسة وجود اختلاف في تزايد الانتروبي حينما نقارن بين كون اللزوجه ثابتة أو متغيره لتغير درجه الحراره.

فهذا البحث يقدم معلومات قيمه لدراسات مستقبلية خصوصا في دراسة التقليل من تزايد الانتروبي.

درجة الماجستير في العلوم  
جامعة الملك فهد للبترول والمعادن  
الظهران - المملكة العربية السعودية  
يناير - 2004 م

## CHAPTER 1

### INTRODUCTION

#### 1.1 Motivation

One of the primary objectives in the design of any energy system is to conserve the useful energy applied to run a certain process. This useful energy can be destroyed due to the intrinsic irreversibilities associated within the process components [Gool, 1980]. The thermodynamic irreversibility, for example, can cause a decrease in the net power output of the cycle of the power plant. In a similar manner, it leads to an increase in the power required as an input for refrigeration plant. Furthermore, the available work can be lost in many components such as heat exchangers, mixers, turbines and compressors due to irreversibility [Bejan,1982]. Unfortunately, the irreversibility cannot be avoided but it can be minimized in order to save the available energy. The minimization can be achieved if the irreversibility can be identified in the process components. Entropy generation analysis (EGA), or second law analysis, provides a useful tool to identify the irreversibility in any thermal system as well as to determine the optimum conditions under which the process or devices is operated [Ibanez et al., 2003].

Recently, entropy generation analysis has been extensively applied in many heat transfer processes including forced flow subjected to heat transfer in different geometries of ducts. The entropy generation or thermodynamics irreversibility that associates with fluid flow subjected to heating is usually related to heat transfer across finite temperature difference and viscous friction [Bejan, 1979]. As a result, the rate of entropy generation

per unit volume at an arbitrary point in the medium is a combination of viscous and heat effects. The viscous effect can be described by the Navier Stokes equation while the heat effect can be described by the energy equation. In solving these equations, fluid properties such as specific heat, thermal conductivity and viscosity are usually assumed independent of temperature. Among all physical properties involved in laminar flow problems, the temperature dependent viscosity plays a dominant effect in velocity and temperature distributions which are obtained from momentum and energy equations, respectively [Yang, 1962].

Heat transfer and viscous dissipation are the only sources of entropy generation in forced fluid flow through a duct subjected to heat transfer. However, these two sources can be influenced by different parameters related to the operating conditions and duct geometries such as Reynolds number. Therefore, these parameters can also influence the entropy generation in ducts and the analysis of entropy generation should be accompanied by the investigation of different parameters.

## **1.2 Objective of the Study**

Although there are many studies carried out to investigate entropy generation in many process components, there are still a lot of process components which are not investigated. Entropy generation analysis of forced flow in rectangular ducts has not been investigated so far. Some analytical studies analyzed entropy generation in different duct geometries but those studies were not able to present entropy generation distributions everywhere in the system. A careful inspection of the literature also shows that some other duct geometries are still not studied such as parallel plates. Thus, the study of the entropy

generation in parallel plates can present a good insight to the analysis in the rectangular ducts.

Consequently, the objective of this study is to determine entropy generation distributions and total entropy generation between parallel plates considering the dependency of viscosity on temperature. The investigation covers the following cases:

1. Constant wall temperature in which properties fall in two cases:
  - a) Constant properties.
  - b) Variable properties (temperature dependent viscosity)
2. Constant heat flux in which properties fall in two cases:
  - a) Constant properties.
  - b) Variable properties (temperature dependent viscosity)

In addition, the effects of several parameters are taken into consideration. These parameters are the Reynolds number, liquid type and inlet-wall temperature difference (constant wall temperature case).

## CHAPTER 2

### BACKGROUND AND LITERATURE

#### REVIEW

Recently, extensive studies have been conducted to analyze the entropy generation for fluids flowing or/and heating in many process components in industry including different geometries. Recognizing the fact that entropy generation for a flowing fluid subjected to heating in ducts is due to fluid friction and heat transfer, the former is expressed in terms of velocity and the latter in terms of temperature.

This chapter is aimed at shedding light on representative examples from the literature for entropy generation analysis and treating methods for the solution of momentum and energy equations.

#### **2.1 Velocity and Temperature Distributions in Ducts**

The ultimate solution to laminar viscous flow problems subjected to heating would be to have a general solution to Navier stokes equations and energy equation. Unfortunately, these equations are nonlinear, and there is no known method of obtaining an analytical solution. Exact solutions can only be obtained for these equations after simplifying. For simple cases, an excellent reference has been provided by Schlichting (1979) for different cases of flow and different geometries of ducts. However, when few assumptions and more components of velocity and temperature are considered, the

analytical solution is not available. As a result, the solution of these equations is approximated numerically.

The approximated solutions of the Navier stokes equations or/and energy equation have been investigated from the early times in the literature. An excellent review is provided by Shah and London (1978) in which the numerical solution is presented for different geometries of ducts including pipes, parallel plates and rectangular ducts. Both Navier stokes and energy equations are treated in this review by finite difference method. Although this review involved a comprehensive reference for laminar flow forced convection in ducts, all solutions were limited to constant properties and none of the properties was considered to be temperature dependent property.

Some fluid properties are highly temperature dependent and considering this effect in solving Navier stokes equations and energy equation can provide more accurate results. Among all fluid properties involved in flow problems, temperature dependent viscosity plays a dominant role in influencing the velocity and temperature profiles [Yang, 1962]. Therefore, the complete analysis of momentum and energy equations should include the consideration of temperature dependent viscosity as well as the consideration of all velocity components and temperature.

An inspection of the literature for the analysis of momentum and energy equations shows that these two factors are in general not satisfied for many fluid problems in different geometries of ducts. The literature is very rich with the investigation of the Navier Stokes and Energy equations in different fields including forced flow problems. In this literature review, selective examples will be presented for the investigation of the velocity and temperature profiles rather than a complete and comprehensive investigation since the ultimate objective for this study is to investigate entropy generation profiles.

Thus, the rest of this section will provide selective examples from the literature for the solution of the momentum and energy equations for different numerical schemes in different duct geometries. The introduction of those examples will start by pipe geometry as shown in the following study.

An analytical solution was obtained by Yang (1962) for laminar forced convection of liquids flowing inside circular tubes for both constant wall temperature and constant heat flux. The temperature dependent viscosity was considered in solving the governing equations but the effect of velocity components in the radial and azimuthal direction were neglected.

A similar study carried out by Test (1968). Here, a numerical and experimental study was performed for liquids flowing in tubes considering a temperature dependent viscosity effect. The numerical solution was obtained by solving the momentum, energy and continuity equations assuming Poiseuillean velocity profile and uniform temperature profile at the inlet to the tube. Two equations were obtained as a solution for local Nusselt Number and the local friction factor in the laminar flow whose viscosities are temperature dependent. The friction factor equation was not satisfactory at low Reynolds Numbers. In the energy equation, it was found that the radial convection term is quite significant and serious errors will result in the Nusselt number if this term is neglected. The experimental Nusselt number is not in good agreement with the analytical values while the friction factor values are satisfactory. The calculated velocity profiles did not agree to those obtained from experimental data and this may be related to the nature of the finite difference method which was applied in this study.

One year later, an experimental study was carried out in a circular tube to study the influence of free convection and variable viscosity on forced laminar flow of ethylene



glycol initially at 32 °F subjected to a constant heat flux. In addition, an analytical solution was obtained for the momentum and energy equations coupled through viscosity. This study showed that the requirements for fully developed velocity and temperature profiles in the absence of buoyant forces and with uniform heat flux are satisfied only when the viscosity is exponentially dependent on temperature. Also, this dependency showed that the Nusselt number and pressure gradient are functions of the ratio of the bulk viscosity to the viscosity near the wall and to the Graetz number. The analytical and experimental results are introduced in terms of viscosity ratio exponents for Nu number and pressure gradient. Both are compared and it was found that the results are in good agreement [Shannon and Depew, 1969].

The previous examples presented some of the investigations of velocity and temperature profiles for a forced laminar flow in cylindrical geometry. Now, the investigation of the literature review will be directed towards rectangular geometries since this study is concerned to investigate entropy generation in rectangular geometries. The analysis of flow in rectangular geometries includes the analysis of the flow in parallel plates and rectangular duct. Parallel plates represent a hypothetical situation that serves as a stepping-stone to more complex situations such as rectangular duct. Therefore, the following examples cover first the flow in parallel plates that can be considered as a special case of rectangular duct. Then, the flow in the rectangular duct will be considered.

A numerical study was carried out to obtain an exact solution for the temperature distribution for Poiseuille flow between parallel plates. The temperature of the upper plate was considered to be higher than that of the lower plate and the inlet temperature was less than the lower plate. The study showed the behavior of temperature profiles between parallel plates for Peclet number from 1 to 10 [Deavours, 1974].

Furthermore, Shah and London (1978) presented a comprehensive review involving forced laminar flow between parallel plates. In this reference, continuity, momentum and energy equations are numerically investigated by the finite difference method. Two different temperature boundary conditions are applied to the parallel plates, namely, constant wall temperature and constant heat flux. Several figures are plotted for velocity and temperature in terms of the Nusselt number. The effect of temperature dependent viscosity was neglected in this study.

Although the previous reference provided a comprehensive review for flow between parallel plates, two references will be presented because their analyses are performed by the use of vorticity and stream function formulation that will be used in this study. In the first reference, Chang and Huang (1991) carried out a numerical study on a fully developed laminar forced convection between parallel plates channels with two series of transverse fins. The Navier Stokes and energy equations have been written in terms of vorticity and stream function formulation. The finite difference method has been applied to solve those equations. This study investigated the effect of different parameters on the flow field. These parameters are fins arrangement, Reynolds number and friction factor. The results show that fins arrangement is an influential factor on the flow field when they are arranged as an array while the in-line arrangement behaved ineffectively to the flow. The study did not cover the effect of temperature dependent viscosity on the flow.

In the second reference, Yuan et al. (1998) performed a similar numerical study to that of Chang and Huang (1991) to fully developed laminar flow and heat transfer between parallel plates channel to study the effect of different parameters on the flow but with adiabatic streamwise-periodic rod disturbances. Another parameter was added which

was the ratio of half of the duct to the diameter of rod disturbance where this ratio ranged from four to five. Also, a comparison between the cases of adiabatic rods and isothermal rods has been made. It is shown that the adiabatic rods gave a higher value of the Nusselt number. The effect of temperature dependent viscosity is also not considered in this study.

Finally, some selective examples will be presented for a rectangular duct. One of these studies was performed by Butler and McKee (1973). In this study, a solution is carried out to determine the velocity and the temperature distribution for fully developed flow of viscous fluids in heated rectangular duct by solving the momentum and energy equations. On the top wall of the duct, a constant heat flux was imposed with aspect ration of 0.5, 5, and 10. This study shows that the maximum velocity shifted toward the hotter wall. It is also shown that the average wall stress has a different value for the heated and unheated walls that would cause internal rotation of the flow. The analysis in this study did not cover the alteration of velocity in the radial direction although it included the consideration of the effect of temperature dependent viscosity.

Another study was carried out by Sotiropulos and Abdullah (1990). He introduced a numerical solution to solve continuity and Navier stokes equation in two-dimensional driven cavity for Reynolds number 100, 400 and 1000. The momentum equations were coupled with a Poisson-type equation for the pressure and solved using a method called Beam and Warming approximated factorization method. This method demonstrated an excellent convergence and stability.

Furthermore, Xie and Hartnett (1992) carried out an experimental study for laminar flow heat transfer in a 2:1 rectangular duct to study the variable effect of viscosity on mineral oil. Three heating configurations were adopted: (1) top wall heated, other walls adiabatic; (2) bottom wall heated, other walls adiabatic; (3) top and bottom walls heated

sidewalls adiabatic. In the first case, the effect of heating near the top wall made the liquid less viscous and therefore the velocity would increase. Thus, it is found that the heat transfer was enhanced due to the increase of the velocity near the top heated wall while in the second case the heat transfer is enhanced more because of the additional boundary effect. In the last case, the variable viscosity effect was small due symmetrical variations in the duct cross-section.

The experimental results in the previous study, Xie and Hartnett (1992), are compared with a numerical study carried out by Shin et al. (1993) in a rectangular duct with the same conditions. In this study, the effect of variable viscosity is considered in solving the energy and the momentum equations simultaneously for mineral oil in 2:1 rectangular duct. The effect of the viscous dissipation was neglected in solving those equations. The numerical results are in good agreement with the experimental results carried out by Xie and Hartnett (1992). Moreover, the mechanism of heat transfer enhancement for mineral oil was numerically performed by Chou and Tung (1995) in a 2:1 rectangular duct for the same three heating configurations adopted by Xie and Hartnett (1992). For the case of the top wall heated, the major factor for heat transfer enhancement was the axial velocity distribution due to temperature dependence viscosity. For the case of the bottom wall heated, the major factor to heat transfer enhancement was the axial velocity distribution in the region near the entrance whereas the main cause in the fully developed region was the buoyancy-induced secondary flow. For the case of the top and bottom walls heated, the mechanism of heat transfer enhancement is more like that for bottom wall heated.

Pinelli and Vacca (1994) obtained a solution for the two dimensional incompressible unsteady state Navier Stokes equations by projection method where the

spatial derivatives were evaluated by Chebyshev pseudospectral method in a square cavity for Reynolds number = 10 to 500. The continuity equation was iteratively forced to be satisfied at the boundaries of the cavity and as a result the pressure was satisfied everywhere in the cavity. The solution is compared to other solutions from the literature and it gives good agreement.

## 2.2 Entropy Generation Studies

Although the concept of entropy generation that is based on the second law of thermodynamics has been established from early times, its extensive application did not appear early. The renewed interest in the second law of thermodynamics appeared lately in many applications in engineering problems. Bejan (1982, 1995) carried out an extensive work in the analysis and the minimization of the entropy generation in heat transfer and fluid flow processes.

The purpose of this section is to introduce a literature review for the entropy generation analysis in engineering problems. This section will be divided into three parts. The first part will cover a review for the equations that can describe entropy generation in different phenomena including flow and heat problems. The second part will cover entropy generation analysis in different process equipment including heat exchanger and distillation column. The final part will extensively treat the entropy generation analysis in flow problems in ducts including parallel plates, rectangular duct and pipe. On the other hand, the fundamentals of entropy and its analysis will not be reviewed here and the reader is referred to Bejan (1982, 1988), Nevers and Seader (1980), Gaggioli (1960), Gaggioli and Wepfer (1980), Gool (1980), Kestin (1980), and Marcella (1992).

### 2.2.1 Entropy Generation Equations

To analyze the entropy generation in any process, the analyzer needs to use equations from which the entropy generation can be estimated. These equations can be derived by identifying the sources of entropy generations in any system and then applying the second law of thermodynamics. In this section, the derived equations cover the entropy generated from fluid friction, heat transfer, mass transfer and chemical reactions.

For identifying the entropy generation in forced flow problems subjected to heat transfer, Arpaci (1989) derived the general entropy generation equation for laminar and turbulent flow in rectangular coordinates. The same equation for the laminar case is verified by Bejan (1995). Further, Bejan provides the laminar equations for cylindrical and spherical coordinates. All their derived equations are written in terms of velocity and temperature only because their analyses excluded entropy generation from mass transfer effect and chemical reactions effect.

Poulikakos and Johnson (1989) derived an expression for entropy generation in combined heat and mass transfer phenomena in external flow for laminar and turbulent flows. This expression is applied to forced convection heat and mass transfer in a flat plate and a cylinder in crossflow.

Gyftopoulos and Beretta (1993) derived an approximate expression for the rate of entropy generation in a system including chemical reactions. Their expression is derived for a reaction in a closed system. Further, the validity of their expression included both equilibrium and non-equilibrium states.

Teng et al. (1998) derived a comprehensive equation to determine the local entropy generation in multicomponent system. Their comprehensive equation treated the entropy generated in chemical reaction system and laminar fluid flow involving heat and

mass transfer. Further, the diffusive-viscous effect was considered because it could contribute significantly to entropy generation in multi-component fluid system. Under appropriate simplifying assumptions, this comprehensive equation reduced to those reported in the literature for a single fluid system.

### **2.2.2 Entropy Generation Analysis in Different Process Components**

The widespread application of the entropy generation analysis in process components makes the literature review difficult for this section. Thus, this section will present selective examples from the literature to show the immense use of the entropy generation analysis in many process components. Moreover, the effect of applying this analysis on the process and the effect of some parameters on entropy generation will be introduced if possible.

Leidenfrost et al. (1980) applied the entropy generation analysis on a refrigeration system in order to achieve the proper parameters for running the system. Choosing the proper parameters will lead to minimizing the power needed for the flow of the refrigerant and obtain the minimum losses in the system. It was found that the main parameter that influenced the losses in the system was the condensing temperature. Entropy generation was decreased by lowering the condensing temperature by either increasing the external heat transfer at the condenser or by lowering the inlet temperature to heat exchanging media.

The second law analysis was applied on a combined power and desalination plant in order to locate opportunities for improvement [Gaggioli et al., 1988]. Further, it was shown that the second law analysis was used to provide estimation and saving of the

power. Also, this study showed that the second law analysis could provide an understanding for various processes and their mutual effects.

Badar et al. (1993) carried out an analytical second law analysis for gas liquid heat exchanger in order to optimize the system. The irreversible losses in this system were related to finite temperature difference and pressure drop. The results were shown in terms of optimum number of transfer units as function of dimensionless unit-cost ratio, charging time and reduced temperature difference of the system.

Drost and White (1994) analyzed a rotary magnetic heat pump regenerator by entropy generation analysis. The objectives of their study were to demonstrate the usefulness of local entropy generation analysis to the design of this type of component and to identify design modifications that improve the performance of rotary magnetic heat pump regenerator. Although the design of rotary magnetic heat pump seems complex, the location where the entropy generation analysis was applied in this heat pump is simple. Inside the heat pump, the analysis of entropy generation was applied similar to a liquid water flow inside a duct subjected to constant heat flux. The duct represented the regenerator and the water represented the regenerator fluid. The magnetic material was the source of constant heat flux which provided heat from the top and the bottom of the regenerator. Therefore, improving the design of the heat pump depended on minimizing entropy generation in regenerator. The regenerator fluid gained its entropy generation from heat transfer between the magnetic material to regenerator fluid, conduction of thermal energy along the magnetic material and viscous dissipation in regenerator fluid. The analysis was carried out by obtaining velocity and temperature distributions by assuming laminar flow and substituted those distributions in the entropy generation equation. The analysis was improved by choosing the proper parameters in the design.



These parameters were regenerator length, magnetic material thickness, flow path width, magnetic material inlet temperature, and regenerator fluid inlet temperature and regenerator mass flow.

Ray and Sengupta (1994) performed the entropy generation analysis on a distillation column. In particular, the analysis was applied on trays where the vapor and the liquid are in contact. The entropy generation was numerically calculated from heat, mass and momentum transfer for bubble movement through a moving liquid pool. Two parameters were used to analyze the entropy generation on a distillation column tray. These were sieve hole diameters and weir height. It was found that weir height plays a dominant role compared to sieve hole diameters on entropy generation.

Sama (1995) presented a valuable paper to encourage increased use of the second law of thermodynamics in process design. His work was subdivided into two parts, namely, use of second law in the design of heat exchanger and optimization of designs. The availability concept was introduced and applied on heat exchanger. The optimum design of heat exchangers was explored by studying the saved availability, cost of fuel, cost of heat exchanger and capital cost. Further, second law errors which were defined as the design decisions that cause the waste of thermodynamics availability was discussed in heat transfer process. Finally, three methods were represented for optimization of designs. These are optimization by combination and permutation, optimization by mathematical modeling and optimization using second law insight.

Entropy generation analysis has been applied to investigate irreversibilities in heat exchanger and minimum irreversibility criteria have been established [Saboya and Costa, 1999]. The study involved counter flow, parallel flow and cross flow heat exchangers. In cross flow configurations, four types of heat exchanger configurations have been

investigated, namely, both fluids unmixed, both fluid mixed, fluid of maximum heat capacity rate mixed and the other unmixed and finally fluids of minimum heat capacity rate mixed and the other unmixed. In this analysis, the entropy generation caused by fluid friction was neglected. The study compared those types of heat exchangers and showed that the counterflow heat exchanger is less irreversible than the others.

The entropy generation analysis was conducted in a tubular heat exchanger subjected to constant wall temperature [Zimparov, 2001]. It was shown that the performance of the heat exchanger was improved and the heat transfer was enhanced because of using the entropy generation analysis. In addition, the general evaluation criteria added new information to entropy generation minimization.

The entropy generation in a plane turbulent jet was investigated by taking into account natural oscillations in the jet [Cervantes and Solorio, 2002]. This study was a model modification for an old study. It was shown that the entropy generation grows along the flow direction and depends directly on entrainment with the still ambient fluid. Also, it was shown that the strong increment of the entropy dictated in the highly unsteady region of the flow where its length is specified.

The second law analysis was carried out for a waste heat recovery steam generator [Reddy et al, 2002]. In this study, a general equation for entropy generation was proposed for waste heat recovery steam generator producing superheated steam. It was found that the entropy generation number increases with increasing the non-dimensional temperature difference. In addition, the specific sources that are responsible for entropy generation rate are the temperature difference between stream-to-stream, heat losses to the surroundings, ambient temperature and frictional pressure drop in the generator.

A theoretical entropy production proof was presented to heat exchanger to show that the heat exchange is minimum when the local entropy generation is constant in all parts of the system [Johannessen et al, 2002]. The study showed that minimum entropy generation is independent of the value of the heat transfer coefficient. In addition, the optimal heat exchange conditions are approximated in practice with a counter-current heat exchanger.

### **2.2.3 Entropy Generation Analysis in Different Duct Geometries**

In the preceding section, the entropy generation analysis was reviewed in different engineering equipment and process. In this section, the attention is now turned to the entropy generation analysis in different geometries of ducts. Ducts are always part of any engineering process and the entropy generation inside them may influence the performance of the whole process. As a consequence, the review of entropy generation in ducts is required. Different duct geometries will be considered in this section including triangular, pipe, parallel plates and rectangular ducts.

San et al. (1987) conducted entropy generation analysis for two limiting cases of combined forced convection heat and mass transfer in a two dimensional channel. First, convective heat transfer in a channel was studied for both laminar and turbulent flows for constant wall temperature and constant heat flux. Then, expressions for optimum plate spacing and optimum Reynolds number were derived after minimization of entropy generation. In the laminar case, the fully developed velocity profile was used through the channel while control volume analysis was used in the turbulent flow cases. Second, isothermal convective mass transfer in a channel was studied for laminar and turbulent flow with boundary conditions at the channel walls of both constant concentration and

constant mass flux. Then, the entropy generation was investigated and optimum conditions were derived. It was shown that increasing the plate spacing from the optimum point caused a gradual increase in the entropy generation. Also, the increase in entropy generation was very steep if the plate spacing was decreased from the optimum point.

A numerical study was carried out to study the local entropy generation of the laminar mixed convection flow in vertical parallel plates with a series of fins on one wall [Cheng et al., 1994]. The wall with fins was subjected to constant wall temperature that was higher than the inlet temperature whereas the other wall was subjected to ambient temperature. The local entropy generation was obtained from velocity and temperature data by solving the momentum and energy equations by the stream function vorticity formulation with a constant velocity at the inlet. The study covered a range of Reynolds numbers from 0 to 300, dimensionless fin height from 0 to 0.5 and the parameter of buoyancy force (Rayleigh number) from 0 to 10. The effect of Reynolds number on distortions of entropy generation was shown. Also, the effect of the Reynolds number on the cross-sectional entropy generation was plotted for different parameters. Furthermore, the effect of the local entropy generation on different parameters was studied. These parameters were the effect of Rayleigh on cross sectional entropy generation, the effect of fin height on cross sectional entropy generation and the effect of temperature difference between wall and inlet on the cross-sectional entropy generation. Consequently, the geometric configuration of the finned channel with higher second-law efficiency is proposed.

Sekulic et al. (1996) investigated the entropy generation in different duct geometries under constant wall temperature. The geometries of the ducts included circular, triangular, parallel plates, rectangular and square. To accomplish the analysis of

entropy generation in ducts, Sekulic et al. solved the momentum equation to obtain velocity distributions and the energy equation to obtain temperature distributions. Those distributions inserted into entropy generation equation to get the entropy generation distributions in ducts. The solution of momentum and energy equations was conducted under several assumptions including zero thermal conduction in the fluid stream, all thermophysical properties are constant, fully developed flow and only the consideration of axial velocity component. Different parameters were investigated in this analysis, namely, Reynolds number, inlet to wall temperature ratio and a specific duct length.

Lin and Lee (1996) conducted a second law analysis on a pin-fin array under cross-flow. In this analysis, the main objective was to search for optimal design conditions. This was done by taking into account that increasing the cross-fluid velocity would reduce the heat transfer irreversibilities but also increase the irreversibility due to the increase in the drag force. The study presented the optimal design condition when the fin array are staggered and in line, and both were compared.

Entropy generation for a viscous fluid in a duct subjected to constant wall heat flux was investigated by Sahin (1996). The effect of the dependence of the viscosity on temperature was taken into consideration. It was found that the entropy generation increases along the duct length. Further, in the case of low heat flux, the viscous friction term became dominant.

Sahin (1998) compared the irreversibilities for different duct geometries in order to determine the optimum duct geometry that would minimize losses for a range of laminar flows and constant heat flux. The geometries used were circular, square, equilaterally triangular, rectangular with an aspect ratio of 0.5 and sinusoidal with an

aspect ratio of  $\frac{\sqrt{3}}{2}$ . It was found that the circular geometry is best especially when the frictional contributions become important. In addition, the triangular and rectangular ducts were inferior choices for entropy generation.

A numerical study has been conducted to calculate entropy generation due to laminar mixed convection from an isothermal rotating cylinder by Abu-Hijleh (1998). The study was conducted for three cylinder radii, wide range of Reynolds numbers and buoyancy parameter. The mathematical modeling for the isothermal rotating cylinder was analyzed by the continuity, momentum and energy equations for two directions. It was found that the entropy generation increased as the Reynolds number and buoyancy parameter increased. Moreover, the entropy generation decreased as the cylinder radius was increased. Also, it was shown that the entropy generation was mainly due to the thermal effects at small cylinder radii and due to viscous effects at large cylinder radii.

The entropy generation for a fully developed and forced convection flow has been investigated in a large rectangular duct packed with spherical particles by Demirel and Kahraman (1999). Constant heat flux was applied for the top (heated) and the bottom (cooled) walls. The volumetric entropy generation has been calculated from velocity profile that is obtained from an approximate analytical expression and temperature profile that is determined from velocity and energy equation. Entropy generation per unit volume is calculated and plotted for different values of the ratio of depth of the duct to diameter of packing = 5 and 20. It was shown that the irreversibilities distributions are not continuous through the wall and core regions. Also, the entropy generation is in general due to heat transfer.

A numerical study was conducted by Narusawa (1999) for natural convection in a rectangular cavity to examine the entropy generation. Free boundary and rigid boundary conditions were examined in this study in which the cavity was heated from bottom and cooled at the top. It was pointed out that the entropy generation depends on the aspect ratio of the cavity, the critical Rayleigh number and a non-dimensional parameter related to the ratio of entropy generation by viscous friction to that by thermal transport.

Sahin (2000a) worked out a numerical study to determine the entropy generation and pumping power requirements for a laminar crude oil flow in a pipe subjected to constant heat flux. The effect of viscosity on temperature was taken into consideration. In this study, it was shown that the entropy generation was significantly affected by the dependence of viscosity on temperature.

Analytical entropy generation investigation was carried out by Sahin (2000b) for a fully developed turbulent fluid through a smooth duct subjected to constant wall temperature. The dependency of viscosity on temperature was taken into consideration in this study and the variable viscosity results were compared to those of constant case. It was found that when the fluid is heated the entropy generation per unit heat flux attains a minimum along the duct length and the ratio of pumping power to the total heat flux decreases. Furthermore, the assumption of constant viscosity produced a considerable deviation for the entropy generations and pumping power results.

Baytas (2000) numerically analyzed the entropy generation in an inclined porous cavity subjected to laminar convection heat transfer. The analysis involved the numerical solution of mass, momentum and energy equations, using Darcy's law and Boussinesq-incompressibility approximation. The boundary conditions of the surfaces were kept constant but different temperatures for the two walls and the other walls were kept

thermally insulated. The velocity and temperature profiles were obtained and substituted into entropy generation equation. The entropy generation profiles were considered under different parameters, namely, the angle of inclination, Darcy number and Rayleigh number. It was shown that the heat transfer irreversibilities dominate the fluid friction irreversibilities when Rayleigh number increased.

The method of minimizing entropy generation for two cases was illustrated by asymmetric convective cooling [Ibanez et al., 2003]. The first case is to cool a solid slab subjected to uniform internal heating, whereas; the second case is to cool a Poiseuille flow between two infinite parallel plane walls of finite thickness. In the former case, the entropy generation rate was obtained by the energy balance equation along with Fourier's law for the heat flux. In the latter case, the entropy generation was determined by the energy equation considering viscous dissipation where the velocity was obtained from Poiseuille flow. In both cases, the dimensional heat transfer coefficient (Biot number) was fixed on one wall while the Biot number on the other wall is varying. It was shown that minimum entropy generation rates could be reached by extracting heat in asymmetric way in which Bi numbers are different for the two walls. Also, it was shown when Bi numbers are equal, the entropy generation tends to increase. Furthermore, the cooling in an asymmetric way was very useful in order to optimize operating conditions of heat transfer devices.



## CHAPTER 3

### MATHEMATICAL FORMULATIONS

#### 3.1 Problem Statement

Entropy generation distribution and overall entropy generation of a heated flowing fluid are investigated between parallel plates. The investigation is performed for a fluid entering between the parallel plates with a fully developed velocity profile and constant temperature. The parallel plates are subjected to heating either by constant heat flux or by constant wall temperatures. The two cases are illustrated in Figures 3.1 and 3.2 for constant wall temperature and for constant heat flux, respectively. Both are diagrammed for the upper half of the distance between the parallel plates since the problem is symmetric. The source of entropy generation is related to the change in the fluid temperature and due to the fluid friction. As a result, the momentum and energy equations are solved to determine the temperature and velocity distributions and from these distributions the entropy generation can be determined as shown on Figures 3.3 and 3.4. The effect of temperature dependent viscosity is included in solving momentum and energy equations. This will lead to a coupling between the momentum and energy equations due to the temperature dependent viscosity. A linear relationship for viscosity with temperature is chosen to study the effect of viscosity dependency on temperature. Furthermore, the effect of different parameters is investigated in studying the entropy generation including the Reynolds number, liquid type and inlet-wall temperature difference. In this study, several assumptions are considered. These are steady state, incompressible flow, Newtonian fluid, fully developed flow at the inlet and no buoyancy force.

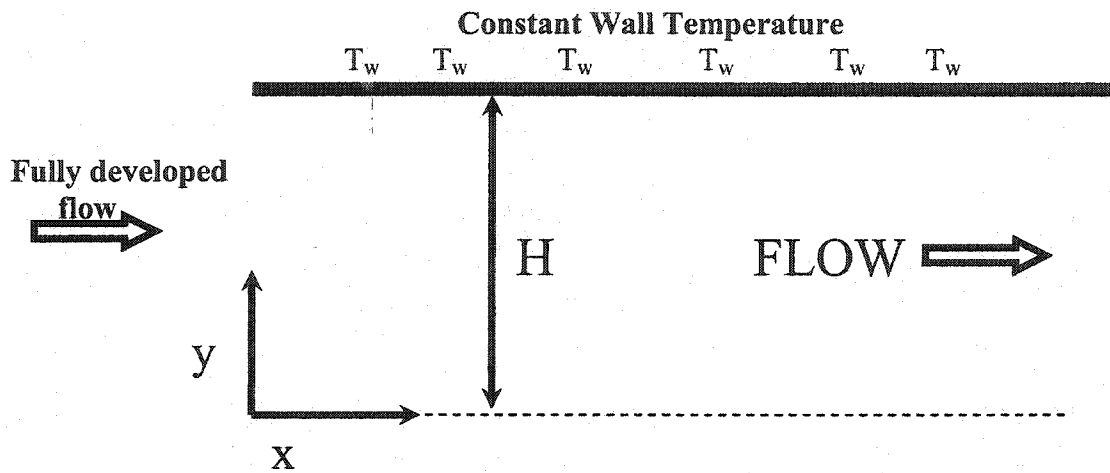


Figure 3.1 Flow of a fluid between parallel plates subjected to constant wall temperature.

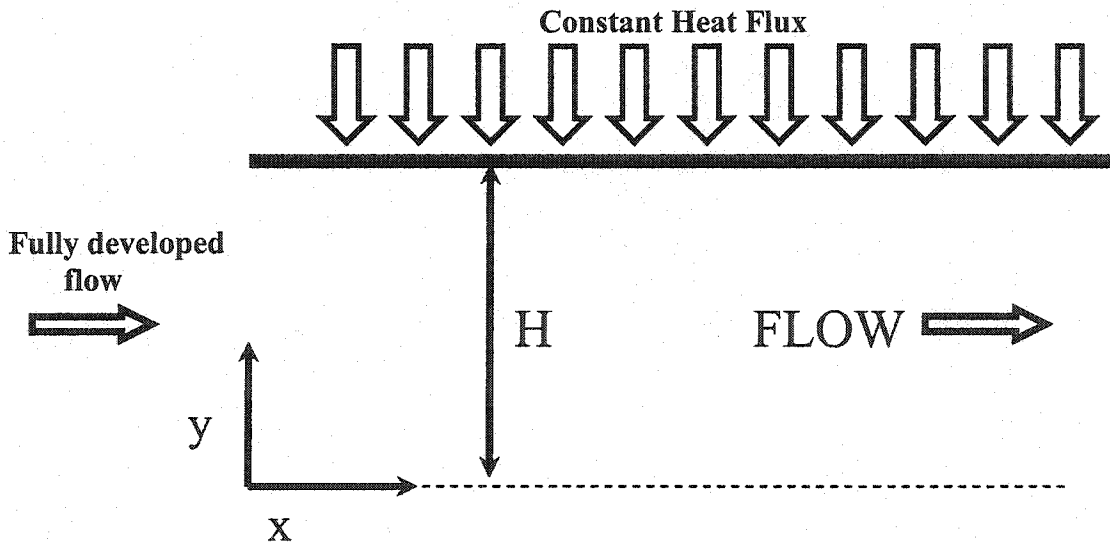
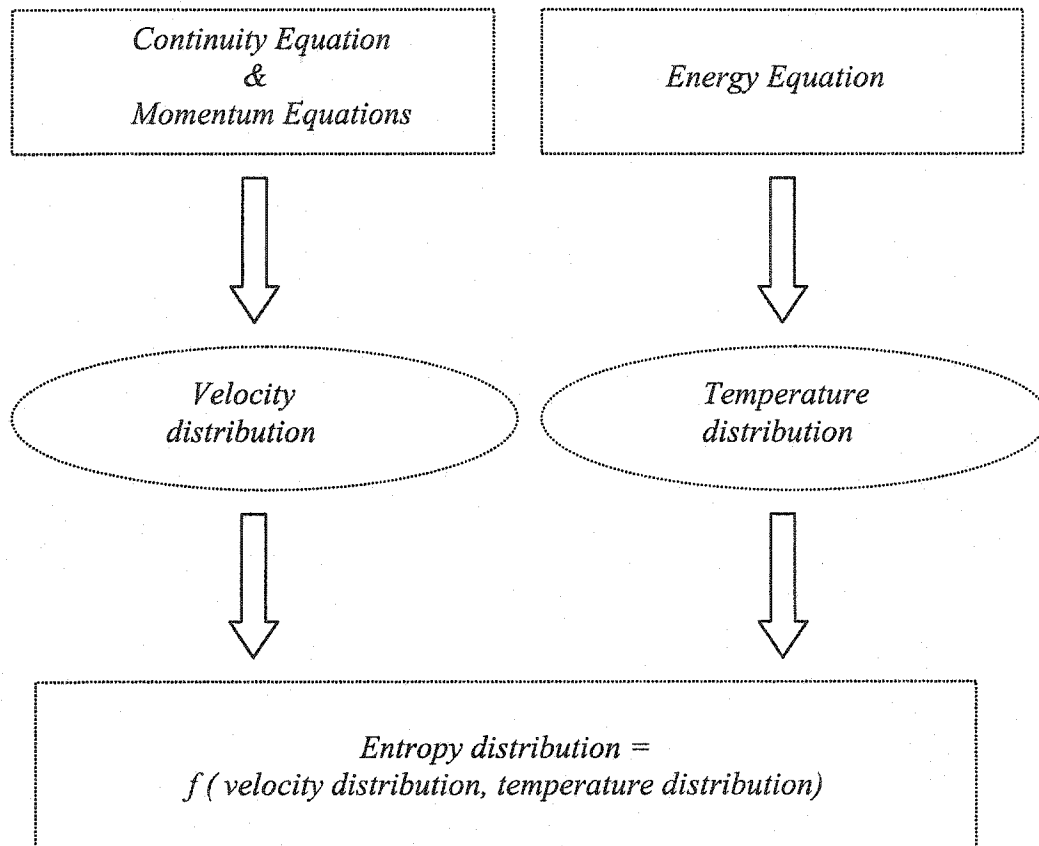
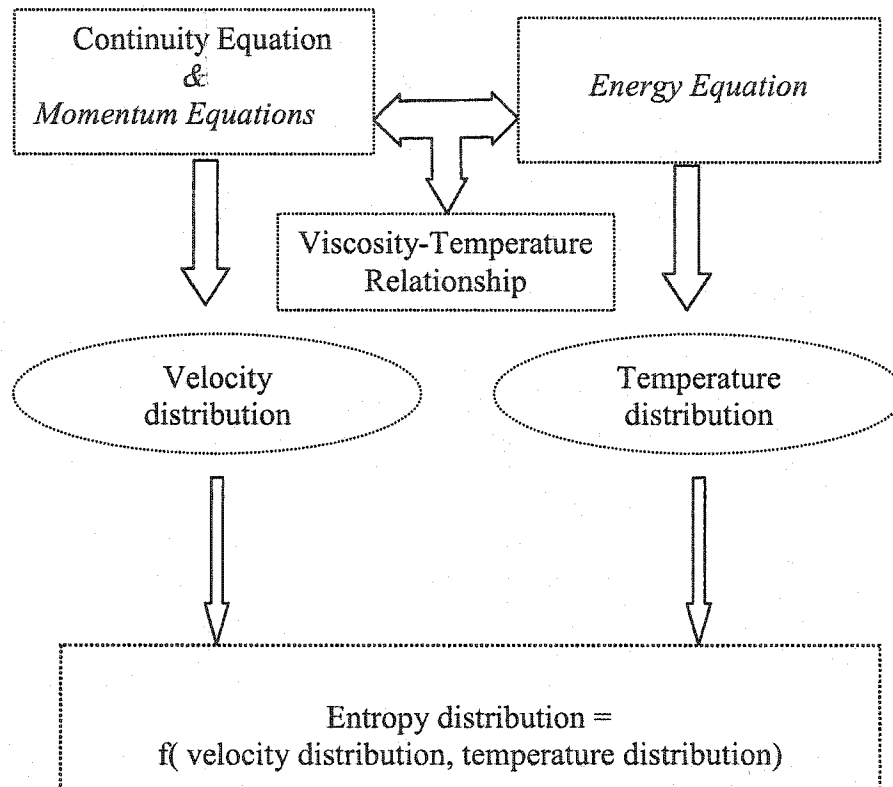


Figure 3.2 Flow of a fluid between parallel plates subjected to constant heat flux.



**Figure 3.3** Determining the entropy generation for constant viscosity case.



**Figure. 3.4** Determining the entropy generation for variable viscosity case.

### 3.2 Entropy Generation Equation

The entropy generation for a flowing fluid through a duct is usually related to heat transfer and viscous friction effects. When a fluid flows inside a duct, three interactions occur in the duct. These are mass fluxes, energy transfer and entropy transfer. These interactions are studied on a differential control volume to determine the local entropy generation equation for two dimensions. The Second law of thermodynamics can be written as:

$$\dot{S}_{gen} = \frac{\partial S}{\partial t} - \frac{\dot{Q}}{T_o} - \sum_{in} \dot{m}s + \sum_{out} \dot{m}s \quad 3.1$$

where :

$\dot{Q}$  : heat transfer rate

$\dot{m}$  : mass flow rate

$s$  : specific entropy

$T_o$  : boundary temperature of the system.

This law can be applied to the control volume to determine the local rate of entropy generation and may be expressed as:

$$\begin{aligned} \dot{S}_{gen} dx dy = & \frac{q_x + \frac{\partial q_x}{\partial x} dx}{T + \frac{\partial T}{\partial x} dx} dy + \frac{q_y + \frac{\partial q_y}{\partial y} dy}{T + \frac{\partial T}{\partial y} dy} dx - \frac{q_x}{T} dy - \frac{q_y}{T} dx \\ & + \left( s + \frac{\partial s}{\partial x} dx \right) \left( v_x + \frac{\partial v_x}{\partial x} dx \right) \left( \rho + \frac{\partial \rho}{\partial x} dx \right) dy + \left( s + \frac{\partial s}{\partial y} dy \right) \\ & \left( v_y + \frac{\partial v_y}{\partial y} dy \right) \left( \rho + \frac{\partial \rho}{\partial y} dy \right) dx - s v_x \rho dy - s v_y \rho dx + \frac{\partial \rho s}{\partial t} dx dy \end{aligned} \quad 3.2$$

where

$q$  : heat flux

$\rho$ : density

$T$ : temperature.

The last equation has nine terms. The first four terms represent the entropy transfer associated with heat transfer, the next four terms account for the entropy conveyed into and out of the system and the last term represents entropy accumulation in the control volume.

Dividing by  $dx dy$ , the local rate of entropy generation becomes:

$$\begin{aligned} \dot{S}_{gen}^m = & \frac{1}{T} \left( \frac{\partial q_x}{\partial x} + \frac{\partial q_y}{\partial y} \right) - \frac{1}{T^2} \left( q_x \frac{\partial T}{\partial x} + q_y \frac{\partial T}{\partial y} \right) + \rho \left( \frac{\partial s}{\partial t} + v_x \frac{\partial s}{\partial x} + v_y \frac{\partial s}{\partial y} \right) \\ & + s \left[ \frac{\partial \rho}{\partial t} + v_x \frac{\partial \rho}{\partial x} + v_y \frac{\partial \rho}{\partial y} + \rho \left( \frac{\partial v_x}{\partial x} + \frac{\partial v_y}{\partial y} \right) \right] \end{aligned} \quad 3.3$$

The term in the square bracket vanishes because it represents the continuity equation.

Equation 3.3 can be written in vectorial notation as:

$$\dot{S}_{gen}^m = \frac{1}{T} \nabla \cdot q - \frac{1}{T^2} q \cdot \nabla T + \rho \frac{Ds}{Dt} \quad 3.4$$

In this equation, the last term includes entropy which can be eliminated by using the Gibbs relation which can be written as:

$$du = Tds - Pd \left( \frac{1}{\rho} \right) \quad 3.5$$

where  $P$  and  $u$  are pressure and internal energy respectively. This relation can be written in terms of substantial derivative notation:

$$\rho \frac{Ds}{Dt} = \frac{\rho}{T} \frac{Du}{Dt} - \frac{P}{\rho T} \frac{D\rho}{Dt} \quad 3.6$$

The internal energy can be represented by using the first law of thermodynamics written for one point in the convective medium as:

$$\rho \frac{Du}{Dt} = -\nabla \cdot q - P(\nabla \cdot v) + \mu \left[ 2 \left( \frac{\partial v_x}{\partial x} \right)^2 + 2 \left( \frac{\partial v_y}{\partial y} \right)^2 + \left( \frac{\partial v_x}{\partial y} + \frac{\partial v_y}{\partial x} \right)^2 \right] \quad 3.7$$

where  $\mu$  is viscosity.

Then, Equation 3.6 and Equation 3.7 are combined to give the overall entropy generation:

$$\dot{S}_{gen}^m = -\frac{1}{T^2} q \cdot \nabla T + \frac{\mu}{T} \Phi - \frac{\rho}{T} \nabla \cdot v - \frac{p}{\rho T} \frac{D\rho}{Dt} \quad 3.8$$

which can be simplified for an incompressible fluid as :

$$\dot{S}_{gen}^m = -\frac{1}{T^2} q \cdot \nabla T + \frac{\mu}{T} \Phi \quad 3.9$$

where  $\Phi$  represents viscous dissipation which is expressed by the quantity inside the square bracket in Equation 3.7. Finally, Fourier's law of heat conduction:

$$q = -k \nabla T \quad 3.10$$

applies to Equation 3.9 and upon substitution gives the volumetric rate of entropy generation:

$$\dot{S}_{gen}^m = \frac{k}{T^2} (\nabla T)^2 + \frac{\mu}{T} \Phi \quad 3.11$$

where  $(\nabla T)^2 = \nabla T \cdot \nabla T$ .

### 3.3 Continuity and Momentum Equations

The velocity distribution can be obtained from the continuity and momentum equations. Since the velocity distribution is required between the parallel plates, several assumptions need to be considered for simplicity. The analysis investigates two velocity components which are the axial and normal components while the third component which represents the velocity in the width direction is set to zero. This assumption is valid if the

width is very large compared to the height. Furthermore, the fluid flow will be assumed at steady state and incompressible.

The continuity and momentum equations that satisfy these assumptions can be written for variable viscosity as:

$$\frac{\partial v_x}{\partial x} + \frac{\partial v_y}{\partial y} = 0 \quad 3.12$$

$$\rho \left( v_x \frac{\partial v_x}{\partial x} + v_y \frac{\partial v_x}{\partial y} \right) = -\frac{dP}{dx} + 2 \frac{\partial \mu}{\partial x} \frac{\partial v_x}{\partial x} + \frac{\partial \mu}{\partial y} \left( \frac{\partial v_y}{\partial x} + \frac{\partial v_x}{\partial y} \right) + \mu \left( \frac{\partial^2 v_x}{\partial x^2} + \frac{\partial^2 v_x}{\partial y^2} \right) \quad 3.13$$

$$\rho \left( v_x \frac{\partial v_y}{\partial x} + v_y \frac{\partial v_y}{\partial y} \right) = -\frac{dP}{dy} + 2 \frac{\partial \mu}{\partial y} \frac{\partial v_y}{\partial y} + \frac{\partial \mu}{\partial x} \left( \frac{\partial v_y}{\partial x} + \frac{\partial v_x}{\partial y} \right) + \mu \left( \frac{\partial^2 v_y}{\partial x^2} + \frac{\partial^2 v_y}{\partial y^2} \right) \quad 3.14$$

where Equation 3.12 represents the continuity equation and Equations 3.13 and 3.14 represent x-momentum and y-momentum equations. In this analysis, the x-direction represents the axial direction whereas the y-direction represents the normal direction. The second and the third terms in the right hand side in Equations 3.13 and 3.14 will vanish if the viscosity is assumed to be constant. Those equations will be solved simultaneously with the energy equation to determine velocity and temperature distributions for both constant wall temperature and constant heat flux. In the case of constant heat flux, the continuous heating to the fluid flow continuously changes the viscosity which, in the case of variable viscosity, couples momentum equations with energy equation. Therefore, the velocity and temperature are continuously changing as the fluid goes downstream and they will not develop. Thus,  $\frac{\partial^2 v_x}{\partial x^2}$  and  $\frac{\partial^2 v_y}{\partial x^2}$ , which represent the second derivatives of axial momentum diffusion components, will be set equal to zero because velocity boundary conditions are unspecified downstream. Order of magnitude analysis shows that it is



possible to eliminate those terms. Both terms have order of magnitude equals to  $u_m/L^2$  where  $u_m$  and  $L$  are average velocity and duct length, respectively. Those terms are compared to those of normal momentum diffusion components which are of order  $u_m/H^2$ , where  $H$  represents the height of the duct.  $L$  is much larger than  $H$ , ( $L \gg H$ ). Therefore, the normal momentum diffusion is much higher than the axial's and hence, the second derivate of axial momentum diffusion can be neglected. Equations 3.12, 3.13, and 3.14 can be transformed in terms of two other quantities which are stream function and vorticity equations to eliminate the pressure.

### 3.3.1 Vorticity and Stream Function Equations

The momentum equations include the pressure term which cannot be treated easily. Pressure is an entity that does not have boundary conditions or independent thermodynamic relation that can satisfy momentum and continuity equations. Several algorithms are available to treat the problem of pressure by iteration procedure among continuity and momentum equations which takes the fact that the continuity equation is indirectly connected to the pressure. However, an interesting two quantities can be very useful in treating the problem of the pressure. These quantities are stream function and vorticity. The stream function and vorticity are defined intelligently to delete pressure term by combining the momentum equations in a single equation and satisfy the continuity equation. The stream function can be defined for the two velocity components as:

$$v_x = \frac{\partial \Psi}{\partial y} \quad 3.15$$

$$v_y = -\frac{\partial \Psi}{\partial x} \quad 3.16$$

On the other hand, the vorticity can be defined as:

$$\omega = -\frac{\partial v_x}{\partial y} + \frac{\partial v_y}{\partial x} \quad 3.17$$

The last three equations can be coupled to obtain an equation that relates the vorticity to the stream function:

$$-\omega = \frac{\partial^2 \psi}{\partial x^2} + \frac{\partial^2 \psi}{\partial y^2} \quad 3.18$$

This equation is applied for constant wall temperature case. However, in the case of constant heat flux, the first term in the right hand side is eliminated due to unknown stream function at very far distance downstream since the stream function does not develop.

The pressure is eliminated from momentum equations by differentiating Equation 3.13 with respect to  $y$  so that  $(\partial^2 p / \partial y \partial x)$  occurs and differentiating Equation 3.14 with respect to  $x$  so that  $(\partial^2 p / \partial y \partial x)$  occurs. Then, the two equations are subtracted to cause the pressure terms to cancel and substitution of Equation 3.15, 3.16 and 3.17 into the resulting equations yields:

$$\begin{aligned} \rho \left( \frac{\partial \psi}{\partial y} \frac{\partial \omega}{\partial x} - \frac{\partial \psi}{\partial x} \frac{\partial \omega}{\partial y} \right) + 2 \left( \frac{\partial \mu}{\partial x} \frac{\partial^3 \psi}{\partial y^2 \partial x} + 2 \frac{\partial^2 \psi}{\partial x \partial y} \frac{\partial^2 \mu}{\partial x \partial y} + \frac{\partial \mu}{\partial y} \frac{\partial^3 \psi}{\partial x^2 \partial y} \right) + \left( \frac{\partial^2 \psi}{\partial y^2} - \frac{\partial^2 \psi}{\partial x^2} \right) \\ \left( \frac{\partial^2 \mu}{\partial y^2} - \frac{\partial^2 \mu}{\partial x^2} \right) - \mu \left( \frac{\partial^2 \omega}{\partial x^2} + \frac{\partial^2 \omega}{\partial y^2} \right) + 2 \frac{\partial \mu}{\partial y} \frac{\partial^3 \psi}{\partial y^3} + 2 \frac{\partial \mu}{\partial x} \frac{\partial^3 \psi}{\partial x^3} = 0 \end{aligned} \quad 3.19$$

This equation is called vorticity equation and applied to constant wall temperature case. However, in the constant heat flux case, vorticity equation differs since the second

derivatives of velocity components with respect to  $x$  are eliminated. Thus, the vorticity equation for the constant heat flux is:

$$\rho \left( \frac{\partial \psi}{\partial y} \frac{\partial \omega}{\partial x} - \frac{\partial \psi}{\partial x} \frac{\partial \omega}{\partial y} \right) + 2 \left( \frac{\partial \mu}{\partial x} \frac{\partial^3 \psi}{\partial y^2 \partial x} + 2 \frac{\partial^2 \psi}{\partial x \partial y} \frac{\partial^2 \mu}{\partial x \partial y} \right) + \left( \frac{\partial^2 \psi}{\partial y^2} - \frac{\partial^2 \psi}{\partial x^2} \right) \left( \frac{\partial^2 \mu}{\partial y^2} \right) - \mu \left( \frac{\partial^2 \omega}{\partial y^2} \right) + 2 \frac{\partial \mu}{\partial y} \frac{\partial^3 \psi}{\partial y^3} = 0 \quad 3.20$$

Equation 3.19 and 3.20 describe the variable viscosity case for constant wall temperature and constant heat flux and they can be used to describe the constant viscosity case if all the terms are deleted except for the terms in the first and fifth brackets.

### 3.4 Energy Equation

The temperature distribution can be obtained from the energy equation. The change of the temperature in two dimensions is:

$$\rho C_p \left( v_x \frac{\partial T}{\partial x} + v_y \frac{\partial T}{\partial y} \right) = k \left[ \frac{\partial^2 T}{\partial x^2} + \frac{\partial^2 T}{\partial y^2} \right] + \mu \left[ 2 \left( \frac{\partial v_x}{\partial x} \right)^2 + 2 \left( \frac{\partial v_y}{\partial y} \right)^2 + \left( \frac{\partial v_x}{\partial y} + \frac{\partial v_y}{\partial x} \right)^2 \right] \quad 3.21$$

where:

$k$  : thermal conductivity

$C_p$  : specific heat

The energy equation consists of three parts, namely, convection which appears in the left hand side, conduction which appears in the first square bracket in the right hand side and viscous dissipation which appears in the second square bracket in the right hand side. The energy equation can be written in terms of stream function by using Equations 3.15 and 3.16:

$$\rho C_p \left( \frac{\partial \psi}{\partial y} \frac{\partial T}{\partial x} - \frac{\partial \psi}{\partial x} \frac{\partial T}{\partial y} \right) = k \left( \frac{\partial^2 T}{\partial x^2} + \frac{\partial^2 T}{\partial y^2} \right) + \mu \left[ 4 \left( \frac{\partial^2 \psi}{\partial x \partial y} \right)^2 + \left( \frac{\partial^2 \psi}{\partial y^2} - \frac{\partial^2 \psi}{\partial x^2} \right)^2 \right] \quad 3.22$$

This equation can be used for constant wall temperature case. However, in the constant heat flux,  $\frac{\partial^2 T}{\partial x^2}$  term is eliminated for the same reasons presented in Section 3.3 and also due to the fact that the normal heat diffusion is much higher than the axial heat diffusion.

### 3.5 Fully Developed Velocity Solution

The fully developed velocity solution is required because the fluid at the inlet is assumed to be fully developed. When the fluid is fully developed, the normal velocity components equal to zero and the axial velocity does not vary in the axial direction. Thus, the only change of velocity is related to the change of the axial velocity in the normal direction and the resulting equation can be written after eliminating zero velocity components from Equations 3.12, 3.13 and 3.14 as:

$$\mu \frac{d^2 v_x}{dy^2} = \frac{\partial P}{\partial x} \quad 3.23$$

This equation is integrated twice to yield:

$$v_x = \frac{1}{2\mu} \left( \frac{\partial P}{\partial x} \right) y^2 + c_1 y + c_2 \quad 3.24$$

in which  $c_1$  and  $c_2$  are determined by invoking the following boundary conditions

$$\frac{dv_x}{dy} = 0 \quad @ \quad y = 0 \quad 3.25$$

$$v_x = 0 \quad @ \quad y = H \quad 3.26$$

where the origin is taken to be at the center of the parallel plates. Applying the boundary conditions to Equation 3.24, the resulting solution yields:

$$v_x = \frac{1}{2\mu} \left( \frac{-dP}{dx} \right) (H^2 - y^2) \quad 3.27$$

In this equation, the pressure gradient can be determined by evaluating the mean velocity that can be determined by:

$$u_m = \frac{Q}{H} \quad 3.28$$

where  $Q$  is the volumetric flow rate which can be obtained by integrating the velocity profile (3.27):

$$Q = \frac{H^3}{3\mu} \left( -\frac{dP}{dx} \right) \quad 3.29$$

Now, the mean velocity can be determined by substituting Equation 3.29 into 3.28:

$$u_m = \frac{H^2}{3\mu} \left( -\frac{dP}{dx} \right) \quad 3.30$$

Equation 3.27 and 3.30 are combined to eliminate the pressure gradient and finally the fully developed solution results:

$$v_x = 1.5u_m \left( 1 - \left( \frac{y}{H} \right)^2 \right) \quad 3.31$$

### 3.6 Dimensionless Equations

The following parameters are used to make the energy, vorticity, stream function and entropy generation equation dimensionless:

$$Y = \frac{y}{H} \quad 3.32$$

$$X = \frac{x}{H} \quad 3.33$$

$$\theta = \frac{T - T_o}{\Delta T} \quad 3.34$$

$$\Delta T = T_w - T_o \quad 3.35$$

$$\bar{\mu} = \frac{\mu}{\mu_o} \quad 3.36$$

$$\bar{\omega} = \frac{\omega}{\left(\frac{u_m}{H}\right)} \quad 3.37$$

$$\bar{\psi} = \frac{\psi}{u_m H} \quad 3.38$$

where  $T_o$ ,  $T_w$  and  $\mu_o$  are inlet temperature, wall temperature and viscosity at  $T_o$ , respectively. In the case of constant heat flux, the dimensionless parameter for the temperature can be defined as:

$$\theta = \frac{T - T_o}{\left(\frac{Q'' H}{k}\right)} \quad 3.39$$

where  $Q''$  and  $k$  are heat flux and thermal conductivity, respectively. The dimensionless stream function, vorticity and energy equations can be written for constant wall temperature case as follows:

$$-\bar{\omega} = \frac{\partial^2 \bar{\psi}}{\partial X^2} + \frac{\partial^2 \bar{\psi}}{\partial Y^2} \quad 3.40$$

$$\begin{aligned} \frac{\text{Re}}{2} \left( \frac{\partial \bar{\psi}}{\partial Y} \frac{\partial \bar{\omega}}{\partial X} - \frac{\partial \bar{\psi}}{\partial X} \frac{\partial \bar{\omega}}{\partial Y} \right) + 2 \left( \frac{\partial \bar{\mu}}{\partial X} \frac{\partial^3 \bar{\psi}}{\partial Y^2 \partial X} + 2 \frac{\partial^2 \bar{\psi}}{\partial X \partial Y} \frac{\partial^2 \bar{\mu}}{\partial X \partial Y} + \frac{\partial \bar{\mu}}{\partial Y} \frac{\partial^3 \bar{\psi}}{\partial X^2 \partial Y} \right) + \left( \frac{\partial^2 \bar{\psi}}{\partial Y^2} - \frac{\partial^2 \bar{\psi}}{\partial X^2} \right) \\ \left( \frac{\partial^2 \bar{\mu}}{\partial Y^2} - \frac{\partial^2 \bar{\mu}}{\partial X^2} \right) - \bar{\mu} \left( \frac{\partial^2 \bar{\omega}}{\partial X^2} + \frac{\partial^2 \bar{\omega}}{\partial Y^2} \right) + 2 \frac{\partial \bar{\mu}}{\partial Y} \frac{\partial^3 \bar{\psi}}{\partial Y^3} + 2 \frac{\partial \bar{\mu}}{\partial X} \frac{\partial^3 \bar{\psi}}{\partial X^3} = 0 \end{aligned} \quad 3.41$$

$$\left( \frac{\partial \bar{\psi}}{\partial Y} \frac{\partial \theta}{\partial X} - \frac{\partial \bar{\psi}}{\partial X} \frac{\partial \theta}{\partial Y} \right) = \frac{2}{Pe} \left( \frac{\partial^2 \theta}{\partial X^2} + \frac{\partial^2 \theta}{\partial Y^2} \right) + \frac{2Br}{Pe} \bar{\mu} \left[ 4 \left( \frac{\partial^2 \bar{\psi}}{\partial X \partial Y} \right)^2 + \left( \frac{\partial^2 \bar{\psi}}{\partial Y^2} - \frac{\partial^2 \bar{\psi}}{\partial X^2} \right)^2 \right] \quad 3.42$$

However, in the constant heat flux, the stream function, vorticity and energy equations can be written as:

$$-\bar{\omega} = \frac{\partial^2 \bar{\psi}}{\partial X^2} + \frac{\partial^2 \bar{\psi}}{\partial Y^2} \quad 3.43$$

$$\begin{aligned} \frac{Re}{2} \left( \frac{\partial \bar{\psi}}{\partial Y} \frac{\partial \bar{\omega}}{\partial X} - \frac{\partial \bar{\psi}}{\partial X} \frac{\partial \bar{\omega}}{\partial Y} \right) + 2 \left( \frac{\partial \bar{\mu}}{\partial X} \frac{\partial^3 \bar{\psi}}{\partial Y^2 \partial X} + 2 \frac{\partial^2 \bar{\psi}}{\partial X \partial Y} \frac{\partial^2 \bar{\mu}}{\partial X \partial Y} \right) + \left( \frac{\partial^2 \bar{\psi}}{\partial Y^2} - \frac{\partial^2 \bar{\psi}}{\partial X^2} \right) \\ \left( \frac{\partial^2 \bar{\mu}}{\partial Y^2} \right) - \bar{\mu} \left( \frac{\partial^2 \bar{\omega}}{\partial Y^2} \right) + 2 \frac{\partial \bar{\mu}}{\partial Y} \frac{\partial^3 \bar{\psi}}{\partial Y^3} = 0 \end{aligned} \quad 3.44$$

$$\left( \frac{\partial \bar{\psi}}{\partial Y} \frac{\partial \theta}{\partial X} - \frac{\partial \bar{\psi}}{\partial X} \frac{\partial \theta}{\partial Y} \right) = \frac{2}{Pe} \left( \frac{\partial^2 \theta}{\partial Y^2} \right) + \frac{2Br'}{Pe} \bar{\mu} \left[ 4 \left( \frac{\partial^2 \bar{\psi}}{\partial X \partial Y} \right)^2 + \left( \frac{\partial^2 \bar{\psi}}{\partial Y^2} - \frac{\partial^2 \bar{\psi}}{\partial X^2} \right)^2 \right] \quad 3.45$$

where the Re and Pe numbers are defined by:

$$Re = \frac{\rho u_m D_h}{\mu_o} \quad 3.46$$

$$Pe = \frac{\rho C_p u_m D_h}{k} \quad 3.47$$

where  $D_h = 2H$ . In the case of constant wall temperature, the Brinkman number is defined as:

$$Br = \frac{\mu_o u_m^2}{k \Delta T} \quad 3.48$$

whereas in the case of constant heat flux, the Brinkman number is suggested by Shah and London (1978) to be defined as:

$$Br' = \frac{\mu_o u_m^2}{Q'' H} \quad 3.49$$

The volumetric entropy generation can be written for variable viscosity and constant wall temperature as:

$$\dot{S}_{gen}^m = \frac{k(\Delta T)^2}{H^2\phi^2} \left[ \left( \frac{\partial\theta}{\partial X} \right)^2 + \left( \frac{\partial\theta}{\partial Y} \right)^2 \right] + Br \frac{k\Delta T}{H^2\phi} \bar{\mu} \left[ 4 \left( \frac{\partial^2\bar{\psi}}{\partial X\partial Y} \right)^2 + \left( \frac{\partial^2\bar{\psi}}{\partial Y^2} - \frac{\partial^2\bar{\psi}}{\partial X^2} \right)^2 \right] \quad 3.50$$

where :  $\phi = \Delta T\theta + T_o$

$\bar{\mu}$  : variable viscosity relation in which  $\bar{\mu} = f(\theta)$

while the volumetric entropy generation for constant heat flux can be written as:

$$\dot{S}_{gen}^m = \frac{(Q'')^2}{k(\phi')^2} \left[ \left( \frac{\partial\theta}{\partial X} \right)^2 + \left( \frac{\partial\theta}{\partial Y} \right)^2 \right] + \frac{Q''Br'}{H\phi'} \bar{\mu} \left[ 4 \left( \frac{\partial^2\bar{\psi}}{\partial X\partial Y} \right)^2 + \left( \frac{\partial^2\bar{\psi}}{\partial Y^2} - \frac{\partial^2\bar{\psi}}{\partial X^2} \right)^2 \right] \quad 3.51$$

where  $\phi' = \frac{Q''H}{k}\theta + T_o$

In the case of constant viscosity  $\bar{\mu}=1$  in Equations 3.50 and 3.51.

### 3.7 Viscosity Temperature Relationship

The viscosity is more sensitive to temperature than other properties such as specific heat, density and thermal conductivity. As a result, the viscosity dependency on temperature will be taken into consideration in this study. Several empirical relations are suggested in the literature. For simplicity, a linear temperature relationship for the viscosity will be used:

$$\mu = \mu_o - b(T - T_o) \quad 3.52$$

where  $b$  is constant. The dimensionless viscosity and its derivatives in Equations 3.41 and 3.44 can be written in dimensionless form as:

$$\bar{\mu} = 1 - \kappa\theta \quad 3.53$$



$$\frac{\partial \bar{\mu}}{\partial X} = -\kappa \frac{\partial \theta}{\partial X} \quad 3.54$$

$$\frac{\partial \bar{\mu}}{\partial Y} = -\kappa \frac{\partial \theta}{\partial Y} \quad 3.55$$

$$\frac{\partial^2 \bar{\mu}}{\partial Y^2} = -\kappa \frac{\partial^2 \theta}{\partial Y^2} \quad 3.56$$

$$\frac{\partial^2 \bar{\mu}}{\partial X^2} = -\kappa \frac{\partial^2 \theta}{\partial X^2} \quad 3.57$$

where  $\kappa$  can be defined for constant wall temperature and constant heat flux as:

$$\kappa = \frac{b\Delta T}{\mu_o} \text{ and } \kappa' = \frac{bHQ''}{\mu_o k}, \text{ respectively.}$$

### 3.8 Boundary Conditions

The boundary conditions considerably influence the entropy generation between the parallel plates especially those for temperature. In this analysis, the boundary conditions are based on symmetry. As a result, the analysis covers the upper half of the parallel plates by taking the center to be the origin. Three boundary quantities will be covered in this section. These are stream function, vorticity and temperature boundary conditions. To solve stream function, vorticity and energy equations, twelve boundary conditions are required for constant wall temperature whereas 9 boundary conditions are required for constant heat flux since the boundary conditions of stream function, vorticity and temperature are not defined downstream.

### 3.8.1 Stream Function Boundary Conditions

At the inlet, the fluid enters the parallel plates with a fully developed velocity profile that was defined in Equation 3.31. This equation can be rewritten in dimensionless form as:

$$U = 1.5 - 1.5 Y^2 \quad 3.58$$

where  $U$  is dimensionless axial velocity which is defined by  $v_x/u_m$ . The boundary condition for the stream function at the inlet can be determined from substituting Equation 3.58 into the dimensionless form of Equation 3.15 to yield the following equation:

$$\bar{\psi} = \frac{3}{2}Y - \frac{1}{2}Y^3 \quad @ \quad X = 0 \quad 3.59$$

However, at a far distance downstream, the boundary condition for the stream function can be defined from Equation 3.16 where  $v_y$  equals to zero (due to fully developed flow) at that location so:

$$\frac{\partial \bar{\psi}}{\partial X} = 0 \quad @ \quad X = L/H \quad 3.60$$

This boundary condition is limited to constant wall temperature while in the case of constant heat flux the stream function is unknown at  $X=L/H$  since the velocity profile will not be fully developed.

On the other hand, the boundary condition for the stream function in the normal direction can be determined from the fact that the difference between any two streamlines equals to the flow rate:

$$Q = \psi_B - \psi_A \quad 3.61$$

where  $\psi_B$  and  $\psi_A$  are two different streamlines. This equation can be written for the upper half of the parallel plate as:

$$Q = \psi(y = H) - \psi(y = 0) \quad 3.62$$

Any solid wall is a streamline and it has a constant value. The stream function at  $y=0$  will be arbitrarily set equal to zero. So, the stream function at  $y=H$  equals to the flow rate. In dimensionless form, the flow rate equals to one. Therefore, the boundary conditions for the stream function in the normal direction can be set to be:

$$\bar{\psi} = 0 \quad @ \quad Y = 0 \quad 3.63$$

$$\bar{\psi} = 1 \quad @ \quad Y = 1 \quad 3.64$$

### 3.8.2 Vorticity Boundary Conditions

The vorticity boundary conditions can be written by the use of Equation 3.17 which can be written in dimensionless form as:

$$\bar{\omega} = -\frac{\partial U}{\partial Y} + \frac{\partial V}{\partial X} \quad 3.65$$

where  $V$  is dimensionless normal velocity which is defined by  $v_y/u_m$ . At the inlet,  $v_y$  equals to zero so  $V = 0$ . Therefore, the second term in the right hand side of Equation 3.65 equals to zero. Then, Equation 3.58 is substituted to Equation 3.65 and integrated to yield:

$$\bar{\omega} = 3Y \quad @ \quad X = 0 \quad 3.66$$

Moreover, to get vorticity boundary condition downstream,  $U$  and  $V$  boundary conditions are required at  $X=L/H$ . The boundary conditions at  $X=L/H$  for  $U$  and  $V$  are defined by:

$$V=0 \quad @ \quad X = L/H \quad 3.67$$

and

$$\frac{\partial U}{\partial X} = 0 \quad @ \quad X=L/H \quad 3.68$$

The last two boundary conditions can be used in the resulting equation from differentiating Equation 3.65 with respect to  $x$ :

$$\frac{\partial \bar{\omega}}{\partial X} = \frac{\partial}{\partial X} \left( -\frac{\partial U}{\partial Y} + \frac{\partial V}{\partial X} \right) \quad 3.69$$

Therefore, both terms on the right hand side equal to zero because of the use of Equations 3.67 and 3.68 to yield:

$$\frac{\partial \bar{\omega}}{\partial X} = 0 \quad @ \quad X = \frac{L}{H} \quad 3.70$$

Equation 3.70 is limited to constant wall temperature because the vorticity is not defined for constant heat flux at far distance downstream since the velocity profile is developing.

The vorticity at  $Y = 0$  can be determined from Equation 3.65. Both terms in the right hand side equals to zero because the centerline is a line of symmetry and therefore  $\partial U / \partial y$  and  $V$  equal to zero. Thus, the vorticity boundary condition at  $Y = 0$  can be written as:

$$\bar{\omega} = 0 \quad @ \quad Y = 0 \quad 3.71$$

At  $Y = 1$ , the vorticity boundary condition cannot be defined from Equation 3.65 or any other equation. Therefore, the vorticity at the wall is written as:

$$\bar{\omega}_i = \beta_i \quad @ \quad Y = 1 \quad 3.72$$

where  $\beta_i$  is unknown value which differs along the wall and is determined by solving stream function, vorticity and energy equations iteratively by using the no-slip boundary condition at the wall as criteria to satisfy the solution. This is explained in detail in section 4.6.

### 3.8.3 Temperature Boundary Conditions

The boundary conditions for the energy equation for the constant wall temperature case are defined as

$$\frac{\partial \theta}{\partial Y} = 0 \quad @ \quad Y = 0 \quad 3.73$$

$$\theta = 1 \quad @ \quad Y = 1 \quad 3.74$$

$$\theta = 0 \quad @ \quad X = 0 \quad 3.75$$

$$\frac{\partial \theta}{\partial X} = 0 \quad @ \quad X = L/H \quad 3.76$$

Equation 3.76 can be applied for constant wall temperature case. In the case of constant heat flux the temperature at  $X=L/H$  is not defined since the temperature profile does not get fully developed. For constant heat flux case, Equations 3.73 and 3.75 also apply for the energy equation. Further, the temperature at the wall is defined to be:

$$\frac{\partial \theta}{\partial Y} = -1 \quad @ \quad Y = 1 \quad 3.77$$

Finally, the boundary conditions for stream function, vorticity and temperature are summarized for constant wall temperature and constant heat flux for the four cases that are solved in this study:

1. Constant wall temperature and constant properties.
2. Constant wall temperature and variable viscosity.
3. Constant heat flux and constant properties.
4. Constant heat flux and variable viscosity.

These four cases are summarized in Table 3.1, Table 3.2, and Table 3.3 and Table 3.4 respectively where their boundary conditions are summarized in Tables 3.5 for constant wall temperature and 3.6 for constant heat flux.

**Table 3.1** Dimensionless equations for constant wall temperature and constant properties.

Vorticity Equation:

$$\frac{\text{Re}}{2} \left( \frac{\partial \bar{\psi}}{\partial Y} \frac{\partial \bar{\omega}}{\partial X} - \frac{\partial \bar{\psi}}{\partial X} \frac{\partial \bar{\omega}}{\partial Y} \right) - \left( \frac{\partial^2 \bar{\omega}}{\partial X^2} + \frac{\partial^2 \bar{\omega}}{\partial Y^2} \right) = 0$$

Stream Function Equation:

$$-\bar{\omega} = \frac{\partial^2 \bar{\psi}}{\partial X^2} + \frac{\partial^2 \bar{\psi}}{\partial Y^2}$$

Energy Equation:

$$\left( \frac{\partial \bar{\psi}}{\partial Y} \frac{\partial \theta}{\partial X} - \frac{\partial \bar{\psi}}{\partial X} \frac{\partial \theta}{\partial Y} \right) = \frac{2}{\text{Pe}} \left( \frac{\partial^2 \theta}{\partial X^2} + \frac{\partial^2 \theta}{\partial Y^2} \right) + \frac{2\text{Br}}{\text{Pe}} \left[ 4 \left( \frac{\partial^2 \bar{\psi}}{\partial X \partial Y} \right)^2 + \left( \frac{\partial^2 \bar{\psi}}{\partial Y^2} - \frac{\partial^2 \bar{\psi}}{\partial X^2} \right)^2 \right]$$

Entropy Equation:

$$\dot{S}_{gen}^m = \frac{k(\Delta T)^2}{H^2 \phi^2} \left[ \left( \frac{\partial \theta}{\partial X} \right)^2 + \left( \frac{\partial \theta}{\partial Y} \right)^2 \right] + \text{Br} \frac{k\Delta T}{H^2 \phi} \left[ 4 \left( \frac{\partial^2 \bar{\psi}}{\partial X \partial Y} \right)^2 + \left( \frac{\partial^2 \bar{\psi}}{\partial Y^2} - \frac{\partial^2 \bar{\psi}}{\partial X^2} \right)^2 \right]$$

$$\phi = \Delta T \theta + T_o$$

**Table 3.2** Dimensionless equations for constant wall temperature and temperature dependent viscosity.

Vorticity Equation:

$$\frac{\text{Re}}{2} \left( \frac{\partial \bar{\psi}}{\partial Y} \frac{\partial \bar{\omega}}{\partial X} - \frac{\partial \bar{\psi}}{\partial X} \frac{\partial \bar{\omega}}{\partial Y} \right) + 2 \left( \frac{\partial \bar{\mu}}{\partial X} \frac{\partial^3 \bar{\psi}}{\partial Y^2 \partial X} + 2 \frac{\partial^2 \bar{\psi}}{\partial X \partial Y} \frac{\partial^2 \bar{\mu}}{\partial X \partial Y} + \frac{\partial \bar{\mu}}{\partial Y} \frac{\partial^3 \bar{\psi}}{\partial X^2 \partial Y} \right) + \left( \frac{\partial^2 \bar{\psi}}{\partial Y^2} - \frac{\partial^2 \bar{\psi}}{\partial X^2} \right) \left( \frac{\partial^2 \bar{\mu}}{\partial Y^2} - \frac{\partial^2 \bar{\mu}}{\partial X^2} \right) - \bar{\mu} \left( \frac{\partial^2 \bar{\omega}}{\partial X^2} + \frac{\partial^2 \bar{\omega}}{\partial Y^2} \right) + 2 \frac{\partial \bar{\mu}}{\partial Y} \frac{\partial^3 \bar{\psi}}{\partial Y^3} + 2 \frac{\partial \bar{\mu}}{\partial X} \frac{\partial^3 \bar{\psi}}{\partial X^3} = 0$$

Stream Function Equation:

$$-\bar{\omega} = \frac{\partial^2 \bar{\psi}}{\partial X^2} + \frac{\partial^2 \bar{\psi}}{\partial Y^2}$$

Energy Equation:

$$\left( \frac{\partial \bar{\psi}}{\partial Y} \frac{\partial \theta}{\partial X} - \frac{\partial \bar{\psi}}{\partial X} \frac{\partial \theta}{\partial Y} \right) = \frac{2}{\text{Pe}} \left( \frac{\partial^2 \theta}{\partial X^2} + \frac{\partial^2 \theta}{\partial Y^2} \right) + \frac{2\text{Br}}{\text{Pe}} \bar{\mu} \left[ 4 \left( \frac{\partial^2 \bar{\psi}}{\partial X \partial Y} \right)^2 + \left( \frac{\partial^2 \bar{\psi}}{\partial Y^2} - \frac{\partial^2 \bar{\psi}}{\partial X^2} \right)^2 \right]$$

Entropy Equation:

$$\dot{S}_{gen}^m = \frac{k(\Delta T)^2}{H^2 \phi^2} \left[ \left( \frac{\partial \theta}{\partial X} \right)^2 + \left( \frac{\partial \theta}{\partial Y} \right)^2 \right] + \text{Br} \frac{k\Delta T}{H^2 \phi} \bar{\mu} \left[ 4 \left( \frac{\partial^2 \bar{\psi}}{\partial X \partial Y} \right)^2 + \left( \frac{\partial^2 \bar{\psi}}{\partial Y^2} - \frac{\partial^2 \bar{\psi}}{\partial X^2} \right)^2 \right]$$

$$\phi = \Delta T \theta + T_o$$

Viscosity Relationships:

$$\bar{\mu} = 1 - \kappa \theta$$

$$\frac{\partial \bar{\mu}}{\partial X} = -\kappa \frac{\partial \theta}{\partial X} \quad \frac{\partial \bar{\mu}}{\partial Y} = -\kappa \frac{\partial \theta}{\partial Y}$$

$$\frac{\partial^2 \bar{\mu}}{\partial Y^2} = -\kappa \frac{\partial^2 \theta}{\partial Y^2} \quad \frac{\partial^2 \bar{\mu}}{\partial X^2} = -\kappa \frac{\partial^2 \theta}{\partial X^2}$$

$$\kappa = \frac{b\Delta T}{\mu_o}$$

**Table 3.3** Dimensionless equations for constant heat flux and constant properties.

Vorticity Equation:

$$\frac{\text{Re}}{2} \left( \frac{\partial \bar{\psi}}{\partial Y} \frac{\partial \bar{\omega}}{\partial X} - \frac{\partial \bar{\psi}}{\partial X} \frac{\partial \bar{\omega}}{\partial Y} \right) - \frac{\partial^2 \bar{\omega}}{\partial Y^2} = 0$$

Stream Function Equation:

$$-\bar{\omega} = \frac{\partial^2 \bar{\psi}}{\partial X^2} + \frac{\partial^2 \bar{\psi}}{\partial Y^2}$$

Energy Equation:

$$\left( \frac{\partial \bar{\psi}}{\partial Y} \frac{\partial \theta}{\partial X} - \frac{\partial \bar{\psi}}{\partial X} \frac{\partial \theta}{\partial Y} \right) = \frac{2}{\text{Pe}} \frac{\partial^2 \theta}{\partial Y^2} + \frac{2\text{Br}'}{\text{Pe}} \left[ 4 \left( \frac{\partial^2 \bar{\psi}}{\partial X \partial Y} \right)^2 + \left( \frac{\partial^2 \bar{\psi}}{\partial Y^2} - \frac{\partial^2 \bar{\psi}}{\partial X^2} \right)^2 \right]$$

Entropy Equation:

$$\dot{S}_{gen}^m = \frac{(Q'')^2}{k(\phi')^2} \left[ \left( \frac{\partial \theta}{\partial X} \right)^2 + \left( \frac{\partial \theta}{\partial Y} \right)^2 \right] + \frac{Q'' \text{Br}'}{H \phi'} \left[ 4 \left( \frac{\partial^2 \bar{\psi}}{\partial X \partial Y} \right)^2 + \left( \frac{\partial^2 \bar{\psi}}{\partial Y^2} - \frac{\partial^2 \bar{\psi}}{\partial X^2} \right)^2 \right]$$

$$\phi' = \frac{Q'' H}{k} \theta + T_o$$



**Table 3.4** Dimensionless equations for constant heat flux and temperature dependent viscosity.

Vorticity Equation:

$$\frac{Re}{2} \left( \frac{\partial \bar{\psi}}{\partial Y} \frac{\partial \bar{\omega}}{\partial X} - \frac{\partial \bar{\psi}}{\partial X} \frac{\partial \bar{\omega}}{\partial Y} \right) + 2 \left( \frac{\partial \bar{\mu}}{\partial X} \frac{\partial^3 \bar{\psi}}{\partial Y^2 \partial X} + 2 \frac{\partial^2 \bar{\psi}}{\partial X \partial Y} \frac{\partial^2 \bar{\mu}}{\partial X \partial Y} \right) + \left( \frac{\partial^2 \bar{\psi}}{\partial Y^2} - \frac{\partial^2 \bar{\psi}}{\partial X^2} \right) \left( \frac{\partial^2 \bar{\mu}}{\partial Y^2} \right) - \bar{\mu} \frac{\partial^2 \bar{\omega}}{\partial Y^2} + 2 \frac{\partial \bar{\mu}}{\partial Y} \frac{\partial^3 \bar{\psi}}{\partial Y^3} = 0$$

Stream Function Equation:

$$-\bar{\omega} = \frac{\partial^2 \bar{\psi}}{\partial X^2} + \frac{\partial^2 \bar{\psi}}{\partial Y^2}$$

Energy Equation:

$$\left( \frac{\partial \bar{\psi}}{\partial Y} \frac{\partial \theta}{\partial X} - \frac{\partial \bar{\psi}}{\partial X} \frac{\partial \theta}{\partial Y} \right) = \frac{2}{Pe} \frac{\partial^2 \theta}{\partial Y^2} + \frac{2Br}{Pe} \bar{\mu} \left[ 4 \left( \frac{\partial^2 \bar{\psi}}{\partial X \partial Y} \right)^2 + \left( \frac{\partial^2 \bar{\psi}}{\partial Y^2} - \frac{\partial^2 \bar{\psi}}{\partial X^2} \right)^2 \right]$$

Entropy Equation:

$$\dot{S}_{gen}^m = \frac{(Q'')^2}{k(\phi')^2} \left[ \left( \frac{\partial \theta}{\partial X} \right)^2 + \left( \frac{\partial \theta}{\partial Y} \right)^2 \right] + \frac{Q'' Br'}{H \phi'} \bar{\mu} \left[ 4 \left( \frac{\partial^2 \bar{\psi}}{\partial X \partial Y} \right)^2 + \left( \frac{\partial^2 \bar{\psi}}{\partial Y^2} - \frac{\partial^2 \bar{\psi}}{\partial X^2} \right)^2 \right]$$

$$\phi' = \frac{Q'' H}{k} \theta + T_o$$

Viscosity Relationships:

$$\begin{aligned} \bar{\mu} &= 1 - \kappa \theta \\ \frac{\partial \bar{\mu}}{\partial X} &= -\kappa \frac{\partial \theta}{\partial X} & \frac{\partial \bar{\mu}}{\partial Y} &= -\kappa \frac{\partial \theta}{\partial Y} \\ \frac{\partial^2 \bar{\mu}}{\partial Y^2} &= -\kappa \frac{\partial^2 \theta}{\partial Y^2} & \frac{\partial^2 \bar{\mu}}{\partial X^2} &= -\kappa \frac{\partial^2 \theta}{\partial X^2} \\ \kappa' &= \frac{b H Q''}{\mu_o k} \end{aligned}$$

**Table 3.5** Boundary conditions for constant wall temperature case.

Vorticity Boundary Conditions:

$$\bar{\omega} = 0 \quad @ \quad Y = 0$$

$$\bar{\omega}_i = \beta_i \quad @ \quad Y = 1$$

$$\bar{\omega} = 3Y \quad @ \quad X = 0$$

$$\frac{\partial \bar{\omega}}{\partial X} = 0 \quad @ \quad X = \frac{L}{H}$$

Stream Function Boundary Conditions:

$$\bar{\psi} = 0 \quad @ \quad Y = 0$$

$$\bar{\psi} = 1 \quad @ \quad Y = 1$$

$$\bar{\psi} = \frac{3}{2}Y - \frac{1}{2}Y^3 \quad @ \quad X = 0$$

$$\frac{\partial \bar{\psi}}{\partial X} = 0 \quad @ \quad X = \frac{L}{H}$$

Temperature Boundary Conditions:

$$\frac{\partial \theta}{\partial Y} = 0 \quad @ \quad Y = 0$$

$$\theta = 1 \quad @ \quad Y = 1$$

$$\theta = 0 \quad @ \quad X = 0$$

$$\frac{\partial \theta}{\partial X} = 0 \quad @ \quad X = L/H$$

**Table 3.6** Boundary conditions for constant heat flux case.

Vorticity Boundary Conditions:

$$\bar{\omega} = 0 \quad @ \quad Y = 0$$

$$\bar{\omega}_i = \beta_i \quad @ \quad Y = 1$$

$$\bar{\omega} = 3Y \quad @ \quad X = 0$$

Stream Function Boundary Conditions:

$$\bar{\psi} = 0 \quad @ \quad Y = 0$$

$$\bar{\psi} = 1 \quad @ \quad Y = 1$$

$$\bar{\psi} = \frac{3}{2}Y - \frac{1}{2}Y^3 \quad @ \quad X = 0$$

Temperature Boundary Conditions:

$$\frac{\partial \theta}{\partial Y} = 0 \quad @ \quad Y = 0$$

$$\frac{\partial \theta}{\partial Y} = -1 \quad @ \quad Y = 1$$

$$\theta = 0 \quad @ \quad X = 0$$

## CHAPTER 4

### NUMERICAL FORMULATION

The forced flow between parallel plates subjected to heating is governed by vorticity, stream function and energy equations. These governing equations are classified as parabolic partial differential equations. The vorticity and energy equations are non-linear in their structure. The complexity of these equations increases when the dependency of viscosity to temperature is taken into consideration. Solving those equations analytically is not possible. As a result, a numerical solution is required to obtain the distributions of vorticity, stream function and temperature. Thus, this chapter is devoted to the numerical formulation of these equations.

#### 4.1 Generalities of the Method of Weighted Residual

Method of Weighted Residuals (MWR) provides a family of numerical techniques for solving differential and integral equations. It includes eigenfunction expansion, pseudospectral, Tau, Galerkin and other projection methods. The numerical techniques of MWR share common mathematical operations and follow similar steps in the implementation of the solution procedures. For example, the trial functions (or basis functions) are generated from the solution of a Sturm-Liouville problem. Further, the solution techniques involve various inner product calculations. A subclass of MWR is spectral method that includes pseudospectral, Galerkin and Tau methods. The spectral method can be used to approximate the integral or differential equation by using a

truncated series expansion and the error (or residual) is forced to be zero in approximate sense by using inner product. To demonstrate the spectral method clearly, consider the following differential equation:

$$L u = f(x) \quad 4.1$$

with the following boundary condition:

$$B u = 0 \quad 4.2$$

where  $L$  and  $B$  are differential operators. A trial function  $\{\varphi_j(x)\}$  is chosen to represent the solution  $u(x)$  and let  $u_N(x)$  be the approximate solution:

$$u(x) \approx u_N(x) = \sum_{j=1}^N a_j \varphi_j(x) \quad 4.3$$

where  $a_j$  are the spectral coefficients. The solution requires that Equation 4.3 must satisfy Equations 4.1 and 4.2. As  $N \rightarrow \infty$ , it is expected for  $u_N(x)$  to approach the exact solution, but for finite  $N$ , a finite error (or residual),  $R$ , is expected. The residual is defined as:

$$R = L u_N(x) - f(x) \quad 4.4$$

In solving the differential equation, the challenge is to choose the appropriate coefficients  $\{a_j\}$  so that the residual becomes as small as possible. In order to make the residual as small as possible, weight function (or test function),  $\gamma_i(x)$  is defined by the inner product condition:

$$(R, \gamma_i) = 0 \quad i=1,2,\dots,\dots \quad 4.5$$

This condition is equivalent to requiring that the residual be orthogonal to the test function. Using  $R$  and  $u_N(x)$  expressions, the condition becomes:

$$\sum_{j=1}^N (L\varphi_j(x), \gamma_i(x)) a_j = (f(x), \gamma_i(x)) \quad i=1,2,\dots,N \quad 4.6$$

and from the resulting system of the equations the coefficients  $\{a_j\}$  can be determined. So far, the test and trial functions have been left unspecified. Choosing the test and trial functions will be illustrated in the coming sections.

Finally, the spectral methods consist of different methods and the forthcoming discussion will be limited to one method which will be applied to solve the vorticity, stream function and energy equations. This method is called pseudospectral method or collocation method.

#### 4.2 Pseudospectral Method

Spectral methods which are Galerkin, Tau and pseudospectral differ in their minimization strategies and the choice of the test function. For example, the test function in pseudospectral method is dirac delta function which can be defined as:

$$\gamma_i = \delta(x - x_i) \quad 4.7$$

where  $\{x_i\}$ ,  $i=1,2,\dots,N$  is a set of collocation points. The pseudospectral method requires that the residual to be zero at the chosen set of points since:

$$(R, \delta(x - x_i)) = R(x_i). \quad 4.8$$

Thus, unknown  $u(x)$  can be approximated by :

$$u_N(x_i) = u(x_i) \quad i= 0,1,\dots,N \quad 4.9$$

hence,

$$\sum_{k=0}^N a_k \varphi_k(x_i) = u(x_i) \quad i= 0,1, \dots,N \quad 4.10$$

Equation 4.10 gives a system of  $N+1$  equations which can be solved to determine the series coefficients,  $a_k$ .

### 4.3 Choice of Basis Function

The choice of basis functions has been unspecified yet during the previous discussion. The basis functions are not specified randomly. Instead, the basis sets must satisfy a number of properties:

- i) easy to compute
- ii) rapid convergence
- iii) completeness ( any solution can be represented to arbitrary high accuracy by taking the truncation  $N$  to be sufficiently large)

These properties are satisfied in different orthogonal polynomials including Legendre and Chebyshev polynomials. The Chebyshev series expansion is similar to a cosine Fourier series and the use of the valuable properties of Fourier series such as Fast Fourier Transform (FFT) can be used in Chebyshev expansion. However, Legendre polynomials does not have known fast transform algorithm. The methods and algorithms for Chebyshev can be applied to Legendre polynomials with technical changes related to their specific properties. The Chebyshev polynomials are selected to provide the basis functions in this study in order to solve vorticity, stream function and energy equations. Thus, the following section is devoted to introduce some of Chebyshev properties and their application in the solution of differential equations by pseudospectral method.

### 4.4 Chebyshev Polynomials

The orthogonal Chebyshev polynomials can be defined for  $x \in [-1, 1]$  by:

$$\varphi_k(x) = \cos(k \cos^{-1} x) \quad k = 0, 1, 2, \dots \quad 4.11$$

By setting  $x = \cos z$ , the following expression can be deduced for the Chebyshev basis function:

$$\varphi_k = \cos(kz) \quad 4.12$$

The first Chebyshev polynomials can be obtained from Equation 4.12:

$$\varphi_0 = 1, \varphi_1 = \cos z = x, \varphi_2 = \cos 2z = 2 \cos^2 z - 1 = 2x^2 - 1 \dots\dots\dots$$

The first five-Chebyshev polynomials are plotted in Figure 4.1. The zeros of these polynomials represent the collocation points which can be obtained from the Gauss-Lobatto points:

$$x_i = \cos \pi i / N \quad i = 0, 1, \dots, N \quad 4.13$$

The main difficulty in pseudospectral method is how to determine the coefficients which appear in Equation 4.10. The coefficients can be defined in an explicit way by following the coming sequences. The Chebyshev polynomials are orthogonal on  $[-1, 1]$  with the weight:

$$w = \frac{1}{\sqrt{1-x^2}} \quad 4.14$$

Let the inner product be defined by:

$$(u, v)_w = \int_{-1}^1 u v w dx \quad 4.15$$

The Chebyshev polynomials are orthogonal in the inner product:

$$(\varphi_k, \varphi_l)_w = \int_{-1}^1 \varphi_k \varphi_l w dx = \frac{\pi}{2} c_k \delta_{k,l} \quad 4.16$$

where  $\delta_{k,l}$  is Kronecker delta and  $c_k$  is



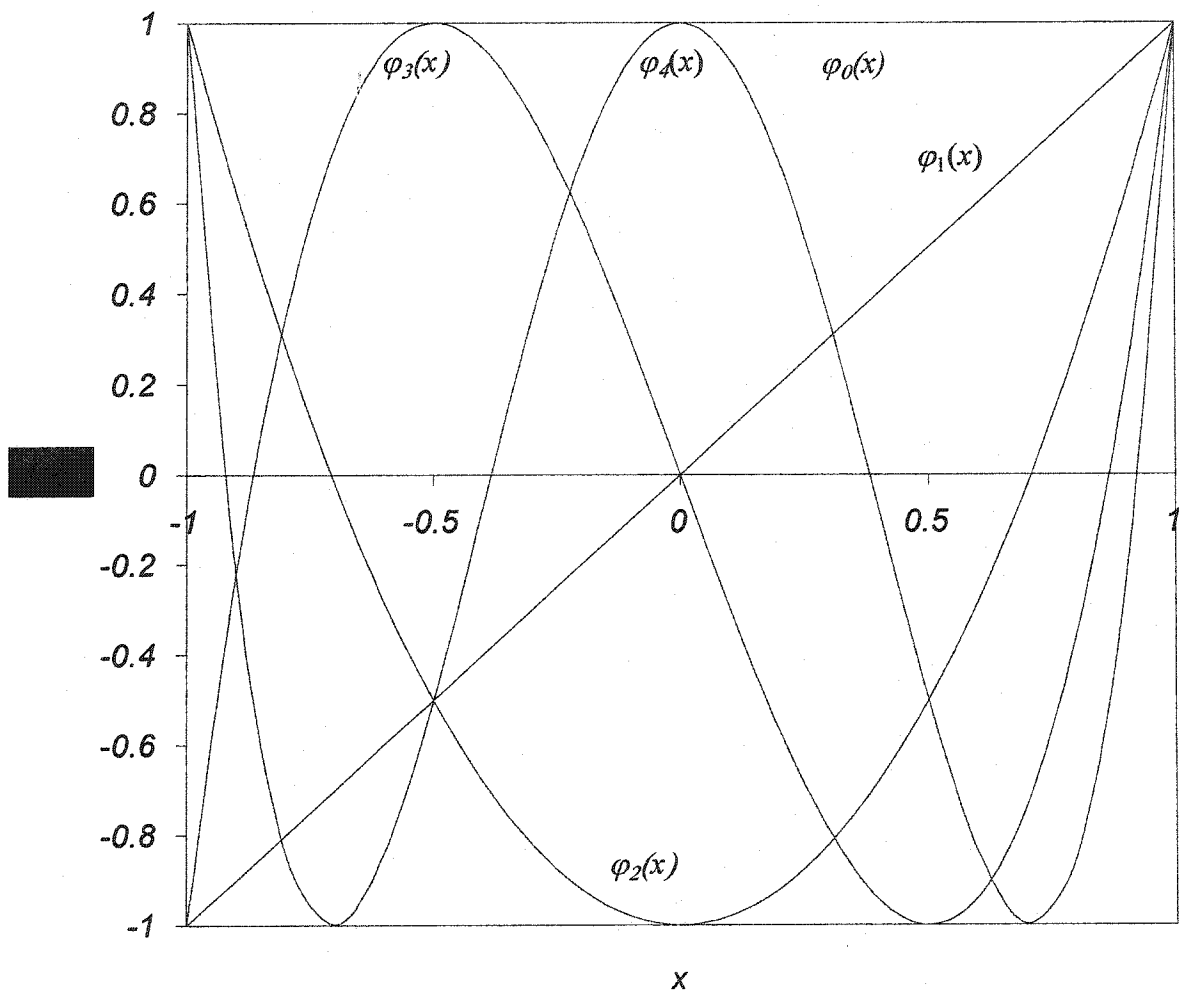


Figure 4.1 Graphs of the first Chebyshev polynomials,  $\varphi_k(x)$ , for  $k=0, 1, 2, 3, 4$ .

$$c_k = \begin{cases} 2 & \text{if } k = 0 \\ 1 & \text{if } k \geq 1 \end{cases} \quad 4.17$$

Equation 4.16 can be approximated by the quadrature formula in which  $x_i$  is calculated from Equation 4.13. The quadratic formula can approximate any function  $f(x)$  by

$$\int_{-1}^1 f w dx \cong \frac{\pi}{N} \sum_{i=0}^N \frac{f(x_i)}{\bar{c}_i} \quad 4.18$$

where

$$\bar{c}_k = \begin{cases} 2 & \text{if } k = 0 \\ 1 & \text{if } 1 \leq k \leq N-1 \\ 2 & \text{if } k = N \end{cases} \quad 4.19$$

Thus, the Chebyshev basis sets in Equation 4.16 can be approximated by:

$$\frac{\pi}{2} c_k \delta_{k,l} = \int_{-1}^1 \varphi_k \varphi_l w dx = \frac{\pi}{N} \sum_{i=0}^N \frac{1}{\bar{c}_i} \varphi_k(x_i) \varphi_l(x_i) \quad 4.20$$

When  $k=l=N$ , this formula remains exact if  $c_k$  is replaced by  $\bar{c}_N$  which is equals to 2.

Therefore Equation 4.20 can be replaced by:

$$\sum_{i=0}^N \frac{1}{\bar{c}_i} \varphi_k(x_i) \varphi_l(x_i) = \frac{\bar{c}_k}{2} N \delta_{k,l} \quad 4.21$$

where  $k \geq 0$  and  $l \leq N$ . This equation is called discrete orthogonality relation based on Gauss-Lobatto points and it is quite useful in Chebyshev pseudospectral method because it provides an explicit approximation to the coefficients,  $a_k$ , which appear in Equation 4.10. This can be achieved by multiplying Equation 4.10 by  $\varphi_l(x_i)/\bar{c}_i$  for each side and summing from  $i=0$  to  $i=N$  then use Equation 4.21 to get the explicit relation for the coefficients:

$$a_k = \frac{2}{\bar{c}_k N} \sum_{i=0}^N \frac{1}{\bar{c}_i} u_i \varphi_k(x_i) \quad k=0, \dots, N \quad 4.22$$

Now, the coefficients for the first and the second derivatives of  $u(x)$  are required in order to solve differential equations. The first and the second derivatives for  $u(x)$  can be represented in terms of basis functions by:

$$u'_N(x) = \sum_{k=0}^N a_k \varphi'_k(x) = \sum_{k=0}^N a_k^{(1)} \varphi_k(x) \quad 4.23$$

$$u''_N(x) = \sum_{k=0}^N a_k \varphi''_k(x) = \sum_{k=0}^N a_k^{(2)} \varphi_k(x) \quad 4.24$$

where the coefficients are defined by:

$$a_k^{(1)} = \frac{2}{c_k} \sum_{\substack{p=k+1 \\ (p+k) \text{ odd}}}^N p a_p \quad k=0, \dots, N-1 \quad 4.25$$

$$a_k^{(2)} = \frac{1}{c_k} \sum_{\substack{p=k+2 \\ (p+k) \text{ even}}}^N p(p^2 - k^2) a_p \quad k = 0, \dots, N-1 \quad 4.26$$

#### 4.5 Chebyshev Derivatives

In pseudospectral method, the solution of differential equations by determining the coefficients is seldom employed in Chebyshev case. Instead, the solution can be obtained by determining the unknown of grid values. This can be obtained by expressing the derivatives at any collocation point in terms of the grid values of the function where the derivative can be expressed as:

$$u_N^{(p)}(x_i) = \sum_{j=0}^N D_{i,j}^{(p)} u_N(x_j) \quad i=0, \dots, N \quad 4.27$$

where  $p$  represents the degree of derivative.  $D_{i,j}^{(p)}$  can be calculated by eliminating the coefficients from Equations 4.23 and 4.24 by using expression (4.22). Then, express  $\varphi_k(x_i)$  and the  $p$  derivatives  $\varphi_k^{(p)}(x_i)$  in terms of trigonometrical functions according to

Equation 4.12. Finally, the sums are evaluated by applying the classical trigonometrical identities.

To illustrate how the pseudospectral method can be applied to solve differential equation where the unknowns are grid values, an example is required.

**Example:**

Let us consider the 1-D second-order linear differential equation:

$$\frac{d^2u}{dx^2} - 4\frac{du}{dx} + 4u = e^x + C \quad x \in [-1, 1]$$

BC's  $u(-1) = 0$   
 $u(+1) = 0$

$$C = \frac{-4e}{1+e^2}$$

the exact solution :

$$u(x) = e^x - \frac{\text{Sinh}1}{\text{Sinh}2} e^{2x} + C/4$$

**Solution:**

Equation 4.27 is substituted in the differential equation to obtain the following:

$$\sum_{l=0}^N D_{jl}^{(2)} u_N(x_l) - 4 \sum_{l=0}^N D_{jl}^{(1)} u_N(x_l) + 4u_N(x_j) = e^{x_j} + C \quad j=0, 2, \dots, N \quad 4.28$$

$$u_N(-1) = 0$$

$$u_N(+1) = 0$$

By choosing  $N=6$ , the collocation points and derivatives are:

$$x = [-1 \quad 0.8660 \quad 0.5 \quad 0 \quad -0.5 \quad -0.8660 \quad 1]$$

$$D_{jl}^{(1)} = \begin{bmatrix} 12.1667 & -14.9282 & 4.0000 & -2.0000 & 1.3333 & -1.0718 & 0.5000 \\ 3.7321 & -1.7321 & -2.7321 & 1.1547 & -0.7321 & 0.5774 & -0.2679 \\ -1.0000 & 2.7321 & -0.3333 & -2.0000 & 1.0000 & -0.7321 & 0.3333 \\ 0.5000 & -1.1547 & 2.0000 & -0.0000 & -2.0000 & 1.1547 & -0.5000 \\ -0.3333 & 0.7321 & -1.0000 & 2.0000 & 0.3333 & -2.7321 & 1.0000 \\ 0.2679 & -0.5774 & 0.7321 & -1.1547 & 2.7321 & 1.7321 & -3.7321 \\ -0.5000 & 1.0718 & -1.3333 & 2.0000 & -4.0000 & 14.9282 & -12.1667 \end{bmatrix}$$

$$D_{jl}^{(2)} = \begin{bmatrix} 86.3333 & -140.4017 & 81.3333 & -44.6667 & 30.6667 & -24.9316 & 11.6667 \\ 42.7846 & -62.6667 & 24.3923 & -6.6667 & 3.6077 & -2.6667 & 1.2154 \\ -3.3333 & 13.1068 & -17.3333 & 9.3333 & -2.6667 & 1.5598 & -0.6667 \\ 1.0000 & -2.6667 & 8.0000 & -12.6667 & 8.0000 & -2.6667 & 1.0000 \\ -0.6667 & 1.5598 & -2.6667 & 9.3333 & -17.3333 & 13.1068 & -3.3333 \\ 1.2154 & -2.6667 & 3.6077 & -6.6667 & 24.3923 & -62.6667 & 42.7846 \\ 11.6667 & -24.9316 & 30.6667 & -44.6667 & 81.3333 & -140.4017 & 86.3333 \end{bmatrix}$$

Substitute  $D_{jl}^{(2)}$  and  $D_{jl}^{(1)}$  and apply boundary conditions in Equation 4.28:

$$\begin{bmatrix} -51.7385 & 35.3205 & -11.2855 & 6.5359 & -4.9761 \\ 2.1786 & -12.0000 & 17.3333 & -6.6667 & 4.4880 \\ 1.9521 & 0 & -8.6667 & 16.0000 & -7.2855 \\ -1.3684 & 1.3333 & 1.3333 & -14.6667 & 24.0350 \\ -0.3573 & 0.6795 & -2.0479 & 13.4641 & -65.5949 \end{bmatrix} \begin{bmatrix} u_6(x_1) \\ u_6(x_2) \\ u_6(x_3) \\ u_6(x_4) \\ u_6(x_5) \end{bmatrix} = \begin{bmatrix} 1.0813 \\ 0.3526 \\ -0.2961 \\ -0.6896 \\ -0.8755 \end{bmatrix}$$

The solution is found to be

$$u_6(x_0) = 0.0000$$

$$u_6(x_1) = 0.2216$$

$$u_6(x_2) = 0.4429$$

$$u_6(x_3) = 0.3516$$

$$u_6(x_4) = 0.1627$$

$$u_6(x_5) = 0.0392$$

$$u_6(x_6) = 0.0000$$

The comparison between pseudospectral and exact solutions has been shown in Table 4.1 for  $N=6$ . The convergence of solution is increased as the number of  $N$  points is increased and this can be verified by using  $N=14$  as shown in Table 4.2.

The truncated series 4.27 can be modified to two-dimensions. These derivatives are required in this study in order to represent stream function, vorticity and energy equations. To show how these derivatives can be presented, selected derivatives are shown:

$$\left. \frac{\partial^2 \psi}{\partial x^2} \right|_{i,k} = \sum_{j=0}^N Dx_{i,j}^{(2)} \psi [(k-1) * N + j] \quad 4.29$$

$$\left. \frac{\partial^2 \omega}{\partial y^2} \right|_{i,k} = \sum_{j=0}^N Dy_{k,j}^{(2)} \omega [(j-1) * N + i] \quad 4.30$$

$$\left. \frac{\partial^3 \psi}{\partial y^3} \right|_{i,k} = \sum_{j=0}^N Dy_{k,j}^{(3)} \psi [(j-1) * N + i] \quad 4.31$$

All other derivatives are calculated in the same way and then they are substituted to vorticity, stream function and energy equations and solved simultaneously.

**Table 4.1** Comparison between exact and pseudospectral solution for  $N=6$ .

Unknown grids	Pseudospectral solution N=6	Exact solution
$u_6(1.000)$	0.000000000000000	0.000000000000000
$u_6(0.8660)$	0.22158833611989	0.22193844430186
$u_6(0.5000)$	0.44294812692560	0.44389705589030
$u_6(0.000)$	0.35160260729292	0.35194572633611
$u_6(-0.5000)$	0.16274001051126	0.16330060085857
$u_6(-0.8660)$	0.03915564374364	0.03926561729417
$u_6(-1.000)$	0.000000000000000	0.000000000000000

**Table 4.2** Comparison between exact and pseudospectral solution for  $N=14$ .

Unknown grids	Pseudospectral solution N=14	Exact solution
$u_{14}(1.000)$	0.000000000000000	0.000000000000000
$u_{14}(0.97493)$	0.04979178600830	0.04979178600822
$u_{14}(0.90097)$	0.17390808380990	0.17390808381019
$u_{14}(0.78183)$	0.31379829260617	0.31379829260636
$u_{14}(0.62349)$	0.41384450474992	0.41384450475063
$u_{14}(0.43388)$	0.44751317240387	0.44751317240408
$u_{14}(0.22252)$	0.41953249290887	0.41953249290965
$u_{14}(0.000)$	0.35194572633609	0.35194572633611
$u_{14}(-0.22252)$	0.26883535022965	0.26883535023028
$u_{14}(-0.43388)$	0.18790537179341	0.18790537179336
$u_{14}(-0.62349)$	0.11892710081015	0.11892710081051
$u_{14}(-0.78183)$	0.06569924503458	0.06569924503463
$u_{14}(-0.90097)$	0.02869116311253	0.02869116311264
$u_{14}(-0.97493)$	0.00708510155216	0.00708510155235
$u_{14}(-1.000)$	0.000000000000000	0.000000000000000



#### 4.6 Solution Techniques

The solution of stream function, vorticity and energy equations is required for four cases. Two of them investigate the stream function, vorticity and temperature distributions on constant wall temperature in which the viscosity is constant in one case and variable with temperature in the other case. Whereas the two other cases investigate the distributions of stream function, vorticity and temperature with constant wall heat flux in variable and constant viscosity. The techniques of the solution will be explained for one case and the other cases will follow similar techniques. As an example, the investigation of stream function, vorticity and temperature will be shown for the variable viscosity case and constant wall temperature. The solution can be obtained by solving Equations 3.40, 3.41 and 3.42 simultaneously with the boundary conditions 3.59, 3.60, 3.63, 3.64, 3.66, 3.70, 3.71, 3.72, 3.73 to 3.76 and with viscosity relations 3.53 to 3.57. The main difficulty in solving those equations is the lack of the knowledge of vorticity on the wall. The vorticity on the wall is taken to be  $\beta_i$ , which changes from point to point on the wall. This difficulty can be recovered by the following sequence. The values of Re, Br and Pe is computed by choosing properties for any chosen liquid. The system of equations is solved with boundary conditions by giving the vector  $\beta_i$ , guessed values. The solution of  $\omega$ ,  $\Psi$  and  $T$  that is determined is checked by using the following criteria on the wall:

$$v_x = \frac{\partial \psi}{\partial y} \Big|_{y=1} = 0 \quad 4.32$$

If this condition is satisfied, the vorticity, stream function and temperature are the required solution. Otherwise, the values of  $\beta_i$  need to be updated by using Newton-Raphson technique and again the system of the equations needs to be solved with the new  $\beta_i$  till

the criteria is satisfied. After the convergence of the solution, the velocity components can be obtained from Equations 3.15 and 3.16. The solution can be double-checked by substituting the two velocity components in the continuity equation. The number of points that is taken in the two-directions is 40x40 collocation points. Finally, the entropy generation rate per unit volume is determined from Equation (3.50) since the velocity and temperature distributions are achieved. The sequence of this procedure is shown on Figure 4.2.

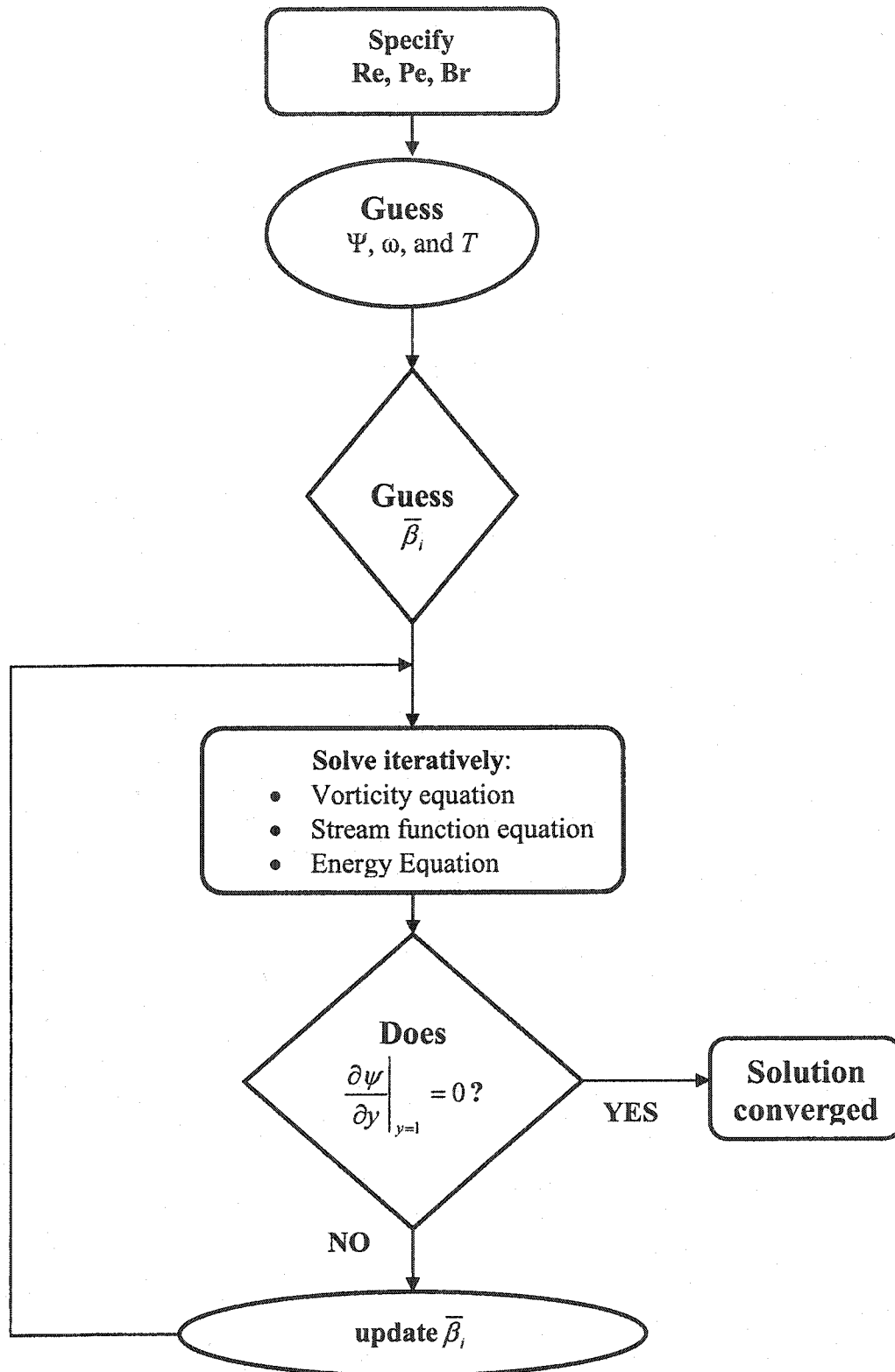


Figure 4.2 Flow chart of solution technique.

## CHAPTER 5

### RESULTS AND DISCUSSIONS

The numerical schemes outlined in the previous chapter were employed to determine the entropy generation for laminar flow between parallel plates subjected to heat transfer. The pseudospectral method was applied to accomplish this task by solving the stream function, vorticity, and energy equations for constant and variable viscosity. Constant wall temperature and constant heat flux cases were considered. In the variable viscosity, where the viscosity is a function of temperature, a linear relationship represented by Equation 3.52 is used to describe viscosity behavior with temperature for two liquids. Thus, the test of the linear relationship for the two liquids is presented. Moreover, it is necessary to demonstrate the convergence of the numerical solution.

#### 5.1 Convergence of the Numerical Solution

Convergence of the numerical solution using the pseudospectral method increases as the mesh size is increased. The mesh size is expressed by  $N_x \times N_y$ , where  $N_x$  and  $N_y$  represent the number of collocation points in  $x$  and  $y$  directions, respectively. The convergence of the numerical solution is demonstrated in Table 5.1. Here the axial velocity at  $X = 3000$  and  $Y = 0$  is reported for different values of  $N_x$  and  $N_y$ . The conditions for these calculations correspond to the physical properties of ethylene glycol as shown in Table 5.2,  $T_o = 300$  K,  $T_w = 330$  K and  $Re = 100$ . It is clear that increasing  $N_x \times N_y$  improves the accuracy of the numerical solution. In particular,  $N_x$  plays a more

significant role on the convergence of the numeral solution than  $N_y$ . As shown in Table 5.1, the axial velocity reached an asymptotic value of 1.499842 converged up to six decimal digits for  $N_x = 40$  and  $N_y = 20$ . In this study, we have adopted a mesh size of  $N_x = 40$  and  $N_y = 40$  to produce all the numerical results. The solution of these equations has been obtained by choosing a tolerance equals to  $1e-8$ . All codes written for this study were programmed in FORTRAN 90.

## 5.2 Variable Viscosity Relationship

Many relationships can be utilized to study the viscosity behavior with temperature. The choice of viscosity relationship depends on several factors including the type of fluid. Two liquids are chosen in this study, ethylene glycol and water. The properties of the more viscous liquid (ethylene glycol) and the less viscous liquid (water) are shown in Table 5.2. Equation 3.52 is suggested to be applied in this study for both liquids:

$$\mu = \mu_o - b(T - T_o) \quad 3.52$$

The applicability of this relationship is satisfactory for the selected temperature ranges that are chosen in this study. The maximum chosen range for the temperature difference between the inlet fluid and the wall was 30 K. Figures 5.1a and 5.1b show the applicability of this linear relationship over the selected range in this study for both water and ethylene glycol.

**Table 5.1** Numerical solution convergence for axial velocity corresponding to ethylene glycol (physical properties are given in Table 5.2,  $T_o = 300$  K,  $\Delta T = 30$  K, Reynolds number = 100,  $X = 30000$  and  $Y = 0$ ).

$N_x$	$N_y$	U
10	10	1.4985948
20	20	1.4996592
30	30	1.4998007
40	20	1.4998429
40	30	1.4998428
40	40	1.4998429

**Table 5.2** Physical properties for water and ethylene glycol [ Plawsky, 2001].

	Water	Ethylene Glycol
Viscosity relation	$\mu = \mu_0 - b(T - T_o)$	$\mu = \mu_0 - b(T - T_o)$
$T_o$ (K)	300	300
$\mu_o$ (N.s/m <sup>2</sup> )	$855 \times 10^{-6}$	$1.57 \times 10^{-2}$
$\rho$ (kg/m <sup>3</sup> )	997	1114.4
$k$ (W/m.K)	$613 \times 10^{-3}$	$252 \times 10^{-3}$
$C_p$ (J/kg.K)	4184	2415
Pr	5.83	151
$b$ (N.s/m <sup>2</sup> K)	$1.08 \times 10^{-5}$	$33.4 \times 10^{-5}$

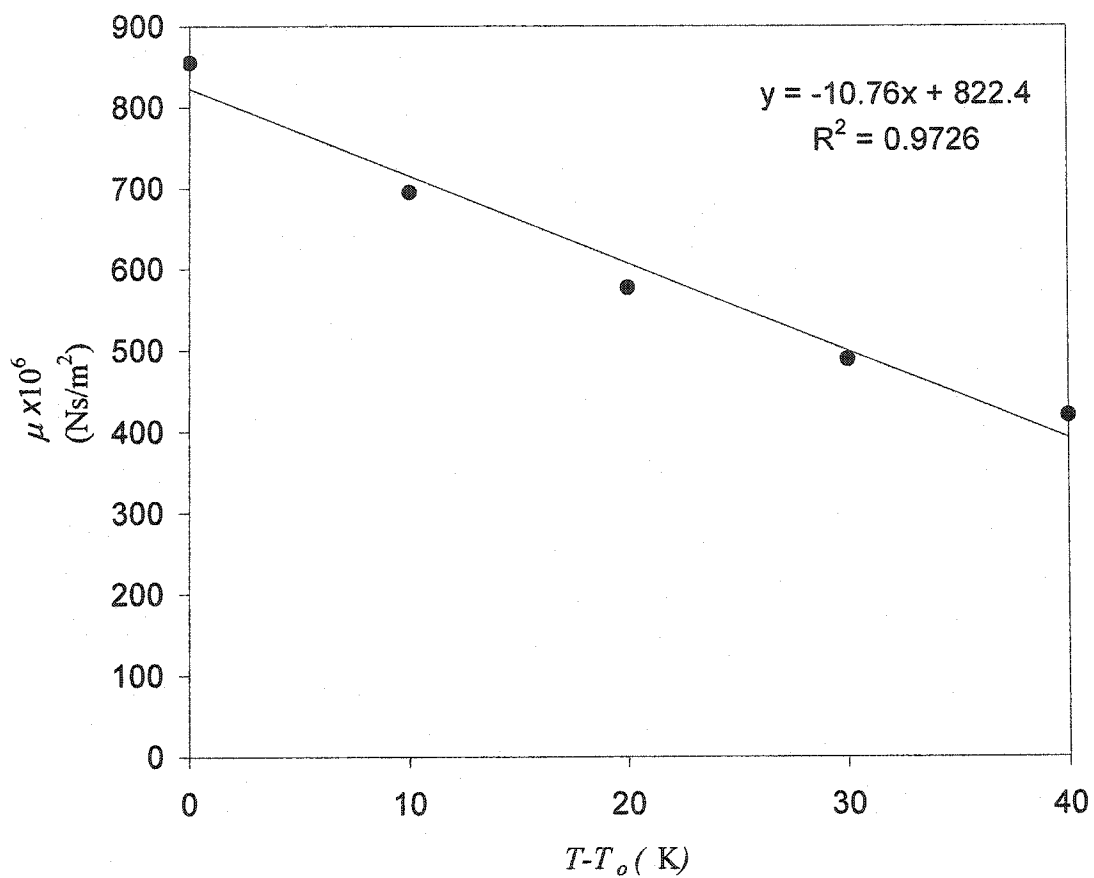


Figure 5.1a  $\mu$  vs.  $(T - T_0)$  for water for  $T_0 = 300$  K.



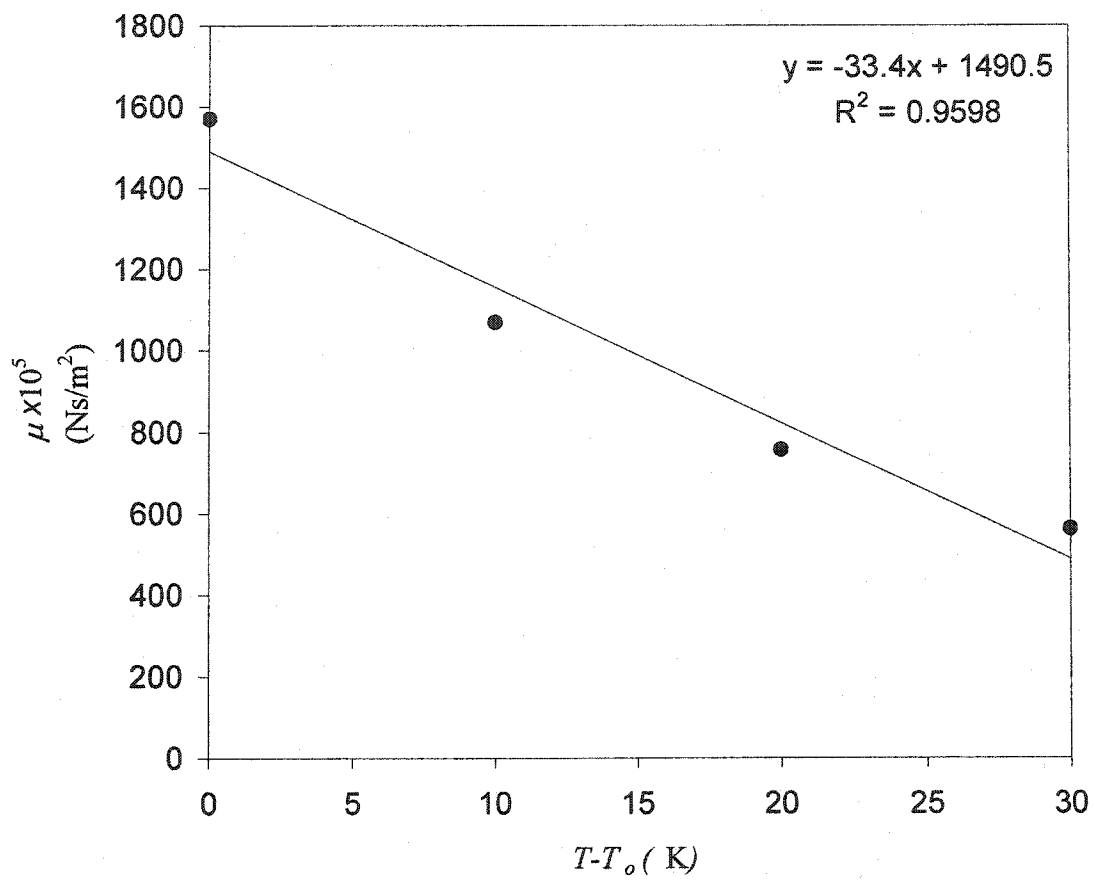


Figure 5.1b  $\mu$  vs.  $(T - T_0)$  for ethylene glycol for  $T_0 = 300$  K.

## 5.3 Constant Wall Temperature

### 5.3.1 Velocity Profiles

After resolving the stream function, vorticity and energy equations, Equations 3.15 and 3.16 were successfully applied to acquire the velocity profiles,  $v_x$  and  $v_y$ . The velocity profiles can be influenced in the case of variable viscosity by different parameters. These are inlet-wall temperature difference ( $\Delta T$ ), Reynolds number (Re) and liquid type. In this section, the velocity profiles are presented for both constant and variable viscosity. These profiles were acquired under several assumptions (as mentioned in Section 3.1) including fully developed flow at the inlet.

#### 5.3.1.1 Velocity Profiles for Constant Viscosity

For the constant viscosity case, the inlet fully developed velocity profile that is only a function of  $y$  is not influenced by the wall temperature that heats the inlet fluid as it proceeds further between the parallel plates since the momentum and energy equations are decoupled. As a result, the axial velocity,  $v_x$ , remains unchanged as the fluid flows downstream along the parallel plates and the  $v_y$  component is equal to zero. However, as just mentioned above, the axial velocity changes in the normal direction. The velocity can be expressed for fully developed fluid by Equation 3.58:

$$U = 1.5 - 1.5Y^2 \quad 3.58$$

The axial velocity profile vs.  $Y$  is plotted in Figure 5.2 for the upper half of the parallel plates where the origin is chosen at the center. At the center where  $Y=0$ , the axial velocity equals to 1.5 which is the maximum velocity while at  $Y=1$  the axial velocity equals to zero due to the no slip condition at the wall. The change of the Reynolds number, the

liquid type and the inlet-wall temperature difference do not influence the shape of the fully developed profile when the viscosity is constant provided that the flow is laminar.

### **5.3.1.2 Velocity Profiles for Variable Viscosity**

In the variable viscosity case, however, the temperature dependent viscosity influences the velocity profiles between the parallel plates in which the wall temperature heats the entering fluid. Here, the momentum and energy equations are coupled through viscosity since it is a function of temperature. The velocity component  $U$  for the variable viscosity case is compared to that of the constant viscosity case in Figure 5.3. The effect of consideration of variable viscosity is obvious. In this figure, the axial velocity profile is plotted vs.  $Y$  at  $X = 185$  and Reynolds number = 400 for both constant and variable viscosity with 30 K difference between the inlet and the wall temperature for ethylene glycol. When ethylene glycol enters the parallel plates with a fully developed velocity profile, it is subjected to heat transfer from the wall due to the difference in temperature between the fluid and the wall. This heating causes a decrease in viscosity as the fluid proceeds further in the duct. The ethylene glycol tends to become less viscous near the wall than at the center because of the effect of heating which is higher near the wall. The decrease in viscosity near the wall is accompanied by a decrease in shear stresses between the liquid molecules and therefore an increase in the velocity as it is shown in the figure at a distance near  $Y = 1$ . On the other hand, near the center where  $Y$  is close to zero, the magnitude of velocity is lower for the variable viscosity than the constant viscosity case. This can be explained based on the volumetric flow rate per unit width:

$$Q = \int v_x dy \quad 5.1$$

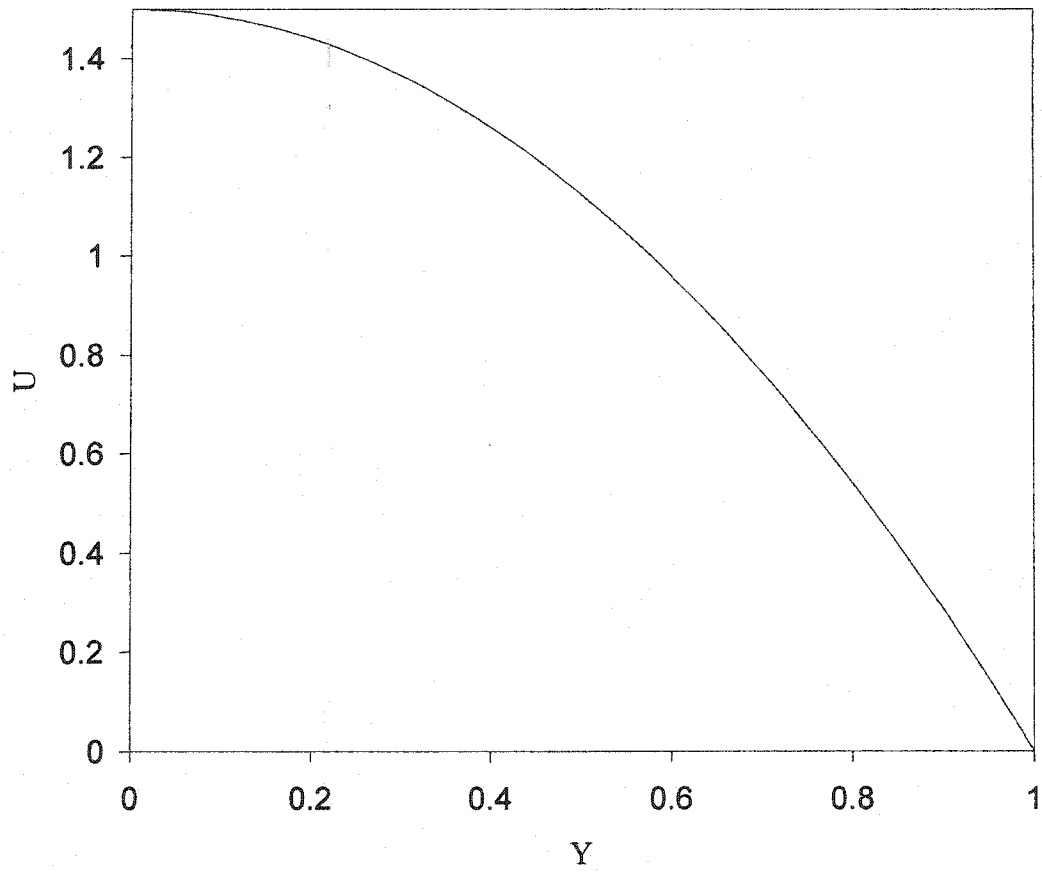


**Figure 5.2**  $U$  vs.  $Y$  for constant viscosity case.

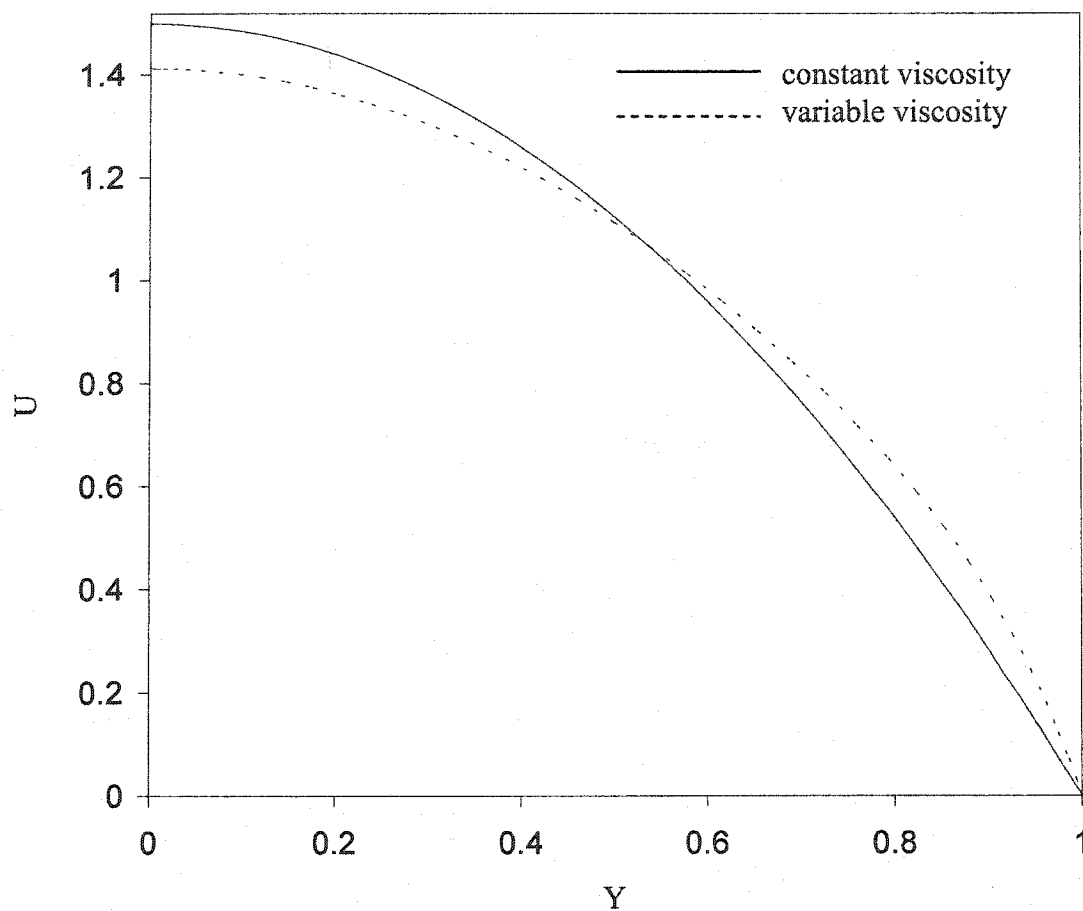


**Figure 5.3**  $U$  vs.  $Y$  for variable and constant viscosity cases for ethylene glycol at  $X = 185$  (physical properties are given in Table 5.2,  $Re = 400$ ,  $\Delta T = 30$  K and  $T_0 = 300$  K).

The volumetric flow rate for the two cases should be equal. Since the velocity increases near the wall, it has to decrease later far away from the wall such that the area under the curve remains the same.

Due to the fact that the temperature is varying in the axial direction and the viscosity is temperature dependant, the velocity field will be modified accordingly. Specifically, the axial velocity is a function of the axial direction and due to the continuity equation (3.12)

$$\frac{dv_y}{dy} \neq 0 \quad 5.2$$

This will give rise to non-zero value for normal velocity as shown in Figure 5.4.

To sum up the discussion of axial velocity in the normal direction, a look at U vs. Y is required at distance far from the inlet. The heat transfer occurs along the duct until the temperature difference between the fluid and the wall equals to zero at the end of the duct, no temperature-jump condition. The velocity profile at no temperature-jump condition reforms to the fully developed profile since there is no temperature difference between the wall and the fluid. The no temperature-jump condition occurs at  $X = 120000$ . The velocity profile at this location coincides with the fully developed profile as plotted in Figure 5.5.

As expected, the axial velocity varies in the axial direction due to the dependence of viscosity on temperature. U vs. X is presented in Figures 5.6, 5.7, 5.8 and 5.9 at various Y values. For the same reasons mentioned before, near the heated wall U first increases due to the large temperature gradient and then decreases and becomes very close to that of the constant viscosity case at height X values at which the temperature gradient diminishes. Whereas near the center ( $Y = 0$ ) U first decreases and then increases to balance the

changes which takes place near the wall, as also explained above. Furthermore, in Figure 5.7, the minimum velocity is shifted to the left as the  $Y$  values increase. To see this picture clearly, Figure 5.10a and Figure 5.10b are plotted for  $U$  vs.  $X$  for  $Y = 0$  and  $0.46$  respectively. In Figure 5.10a, the minimum velocity appears approximately at  $X = 1000$  while the minimum velocity for Figure 5.10b appears at  $X = 200$ . Figure 5.10b is closer to the heating plate where the velocity profile develops faster.

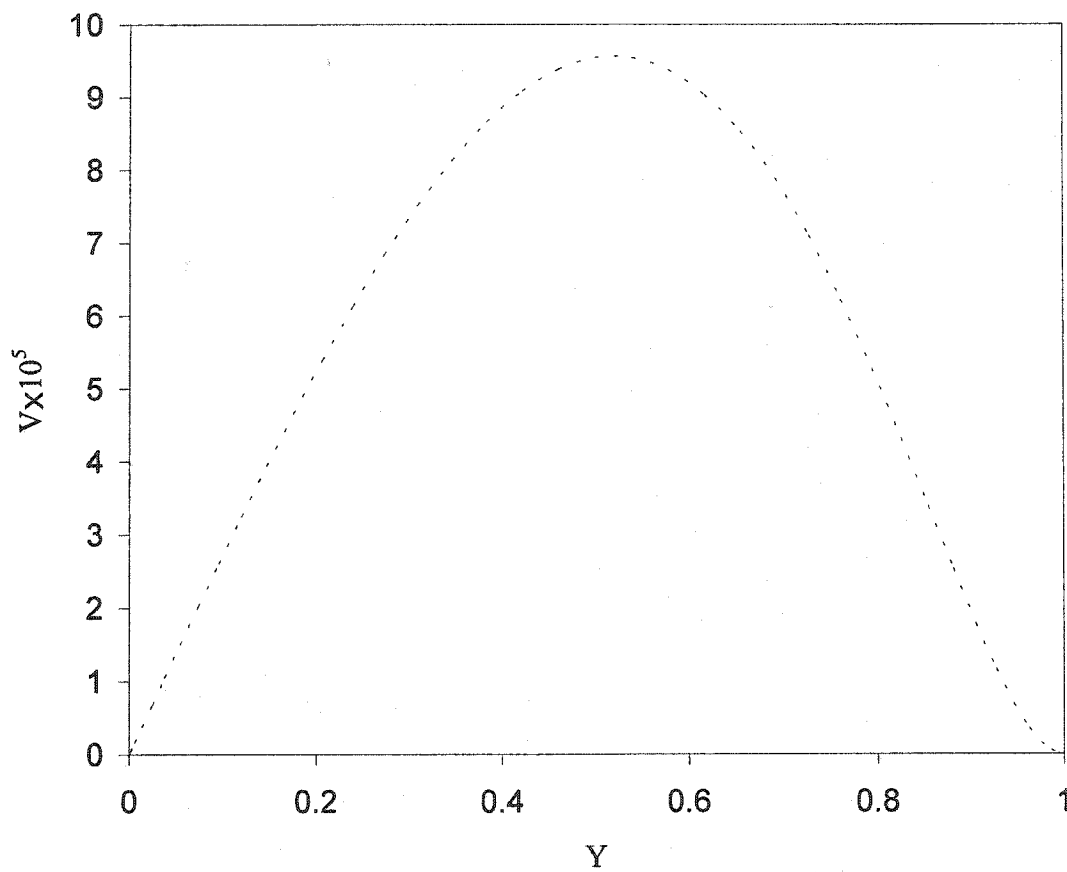


**Figure 5.4**  $V$  vs.  $Y$  for variable viscosity case for ethylene glycol at  $X = 185$  (physical properties are given in Table 5.2,  $Re = 400$ ,  $\Delta T = 30$  K and  $T_0 = 300$  K).



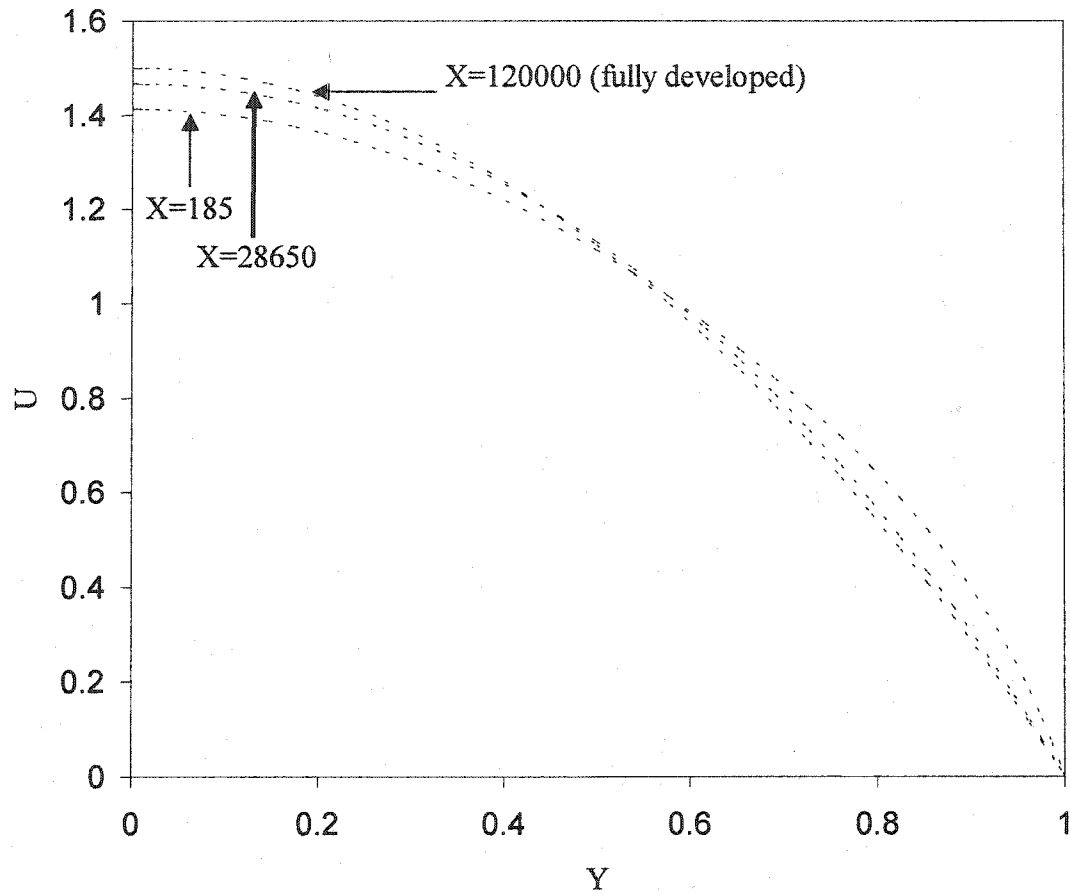


**Figure 5.5**  $U$  vs.  $Y$  for variable viscosity case for ethylene glycol at various  $X$  values (physical properties are given in Table 5.2,  $Re = 400$ ,  $\Delta T = 30$  K and  $T_o = 300$  K).

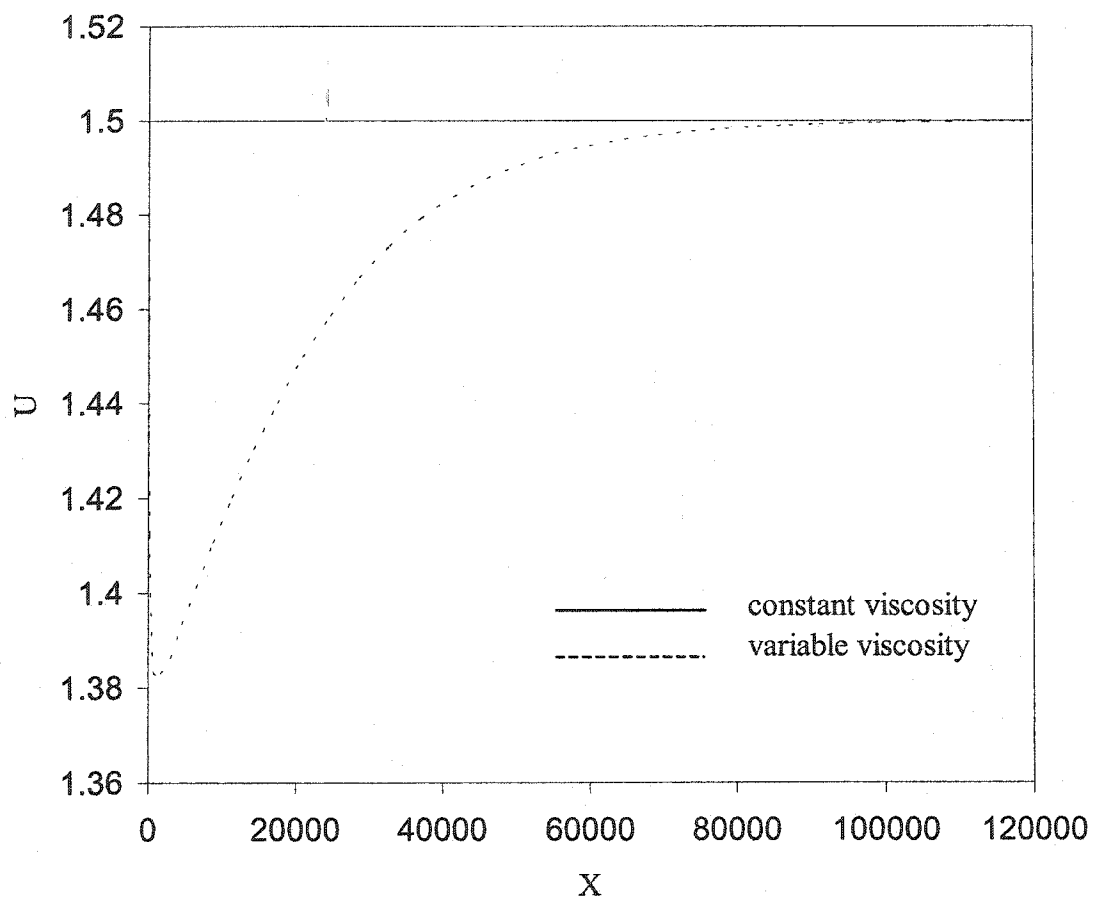


**Figure 5.6**  $U$  vs.  $X$  for constant and variable viscosity cases for ethylene glycol at  $Y = 0$  (physical properties are given in Table 5.2,  $Re = 400$ ,  $\Delta T = 30$  K and  $T_o = 300$  K).

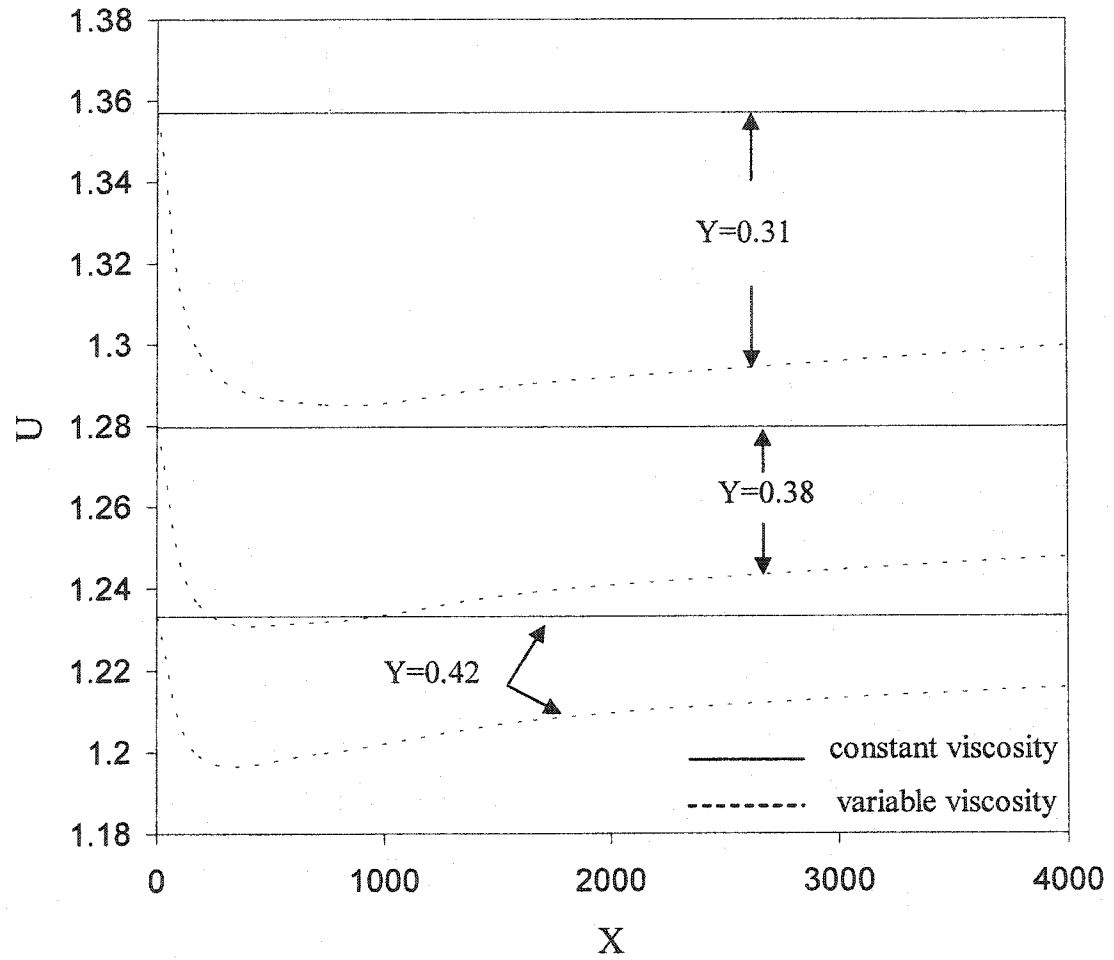


**Figure 5.7**  $U$  vs.  $X$  for constant and variable viscosity cases for ethylene glycol at various  $Y$  values (physical properties are given in Table 5.2,  $Re = 400$ ,  $\Delta T = 30$  K and  $T_0 = 300$  K).

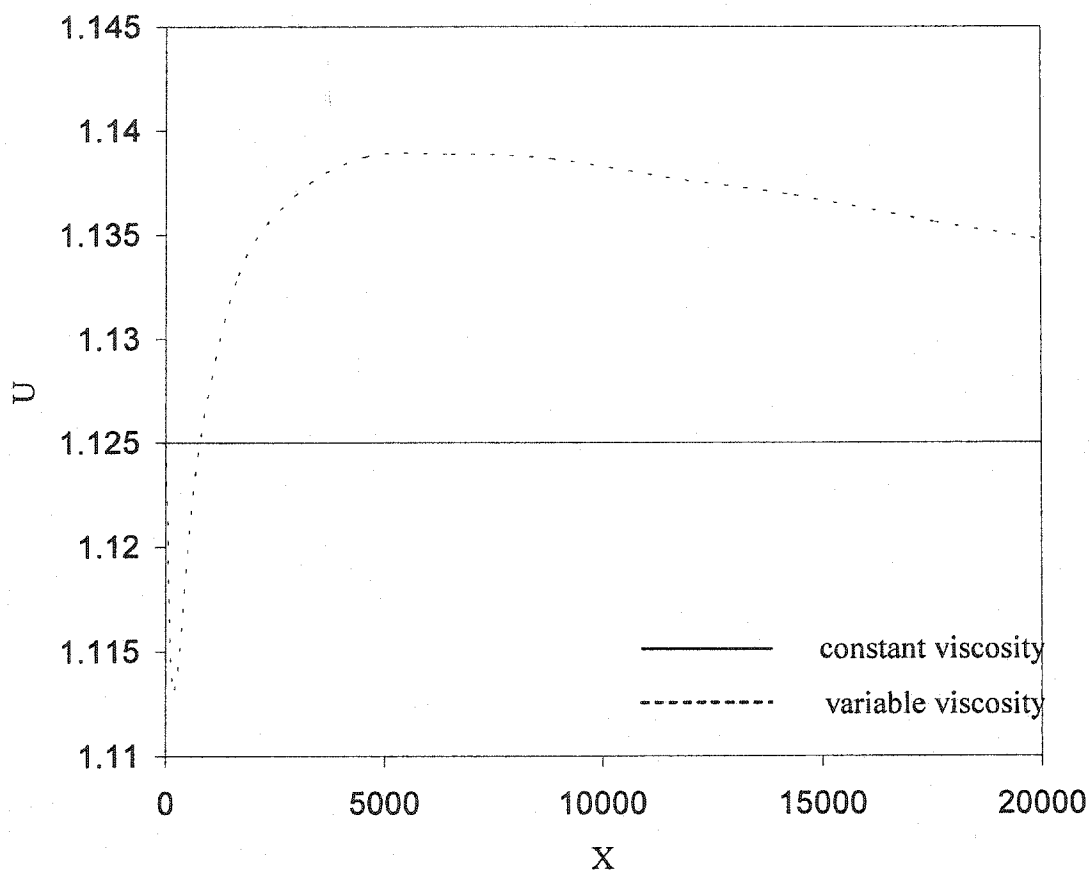


**Figure 5.8**  $U$  vs.  $X$  for constant and variable viscosity cases for ethylene glycol at  $Y = 0.5$  (physical properties are given in Table 5.2,  $Re = 400$ ,  $\Delta T = 30$  K and  $T_0 = 300$  K).

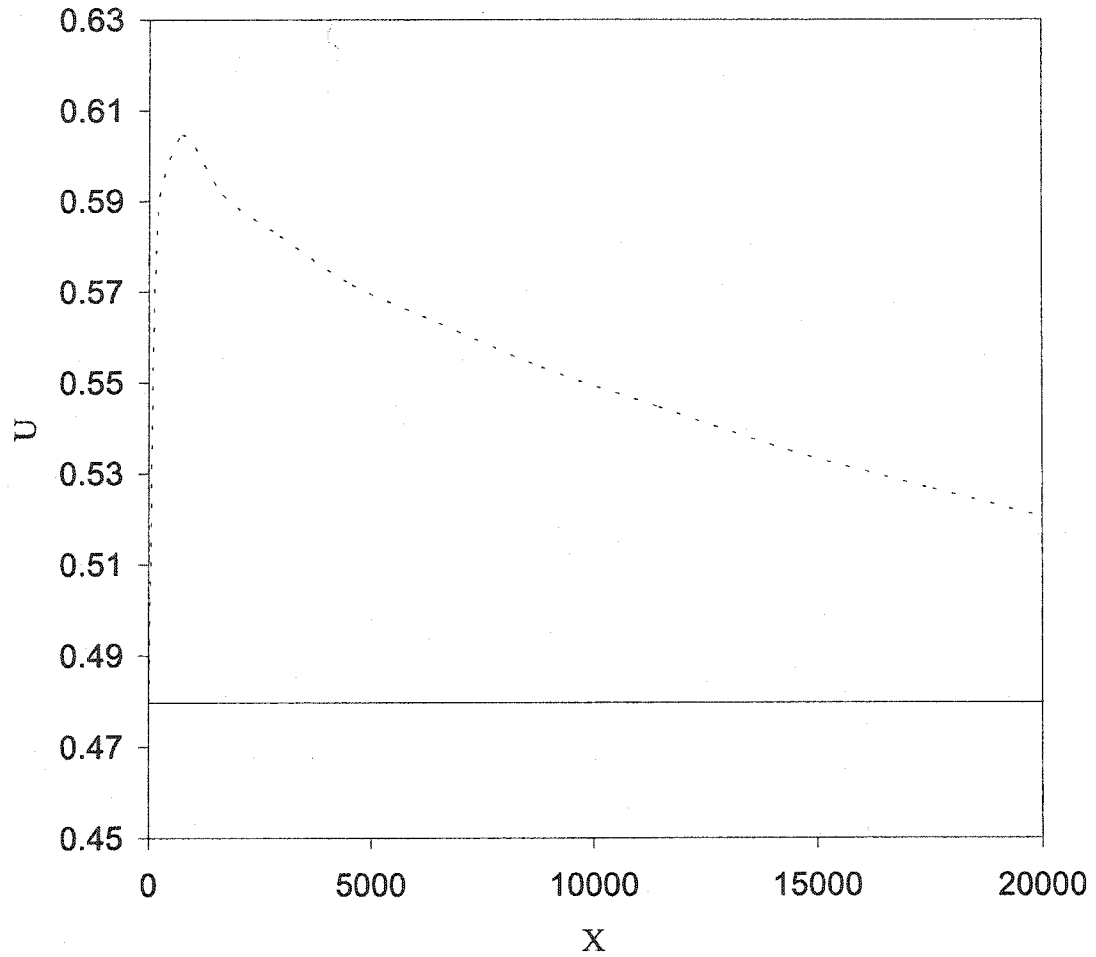


**Figure 5.9**  $U$  vs.  $X$  for constant and variable viscosity cases for ethylene glycol at  $Y = 0.82$  (physical properties are given in Table 5.2,  $Re = 400$ ,  $\Delta T = 30$  K and  $T_0 = 300$  K).

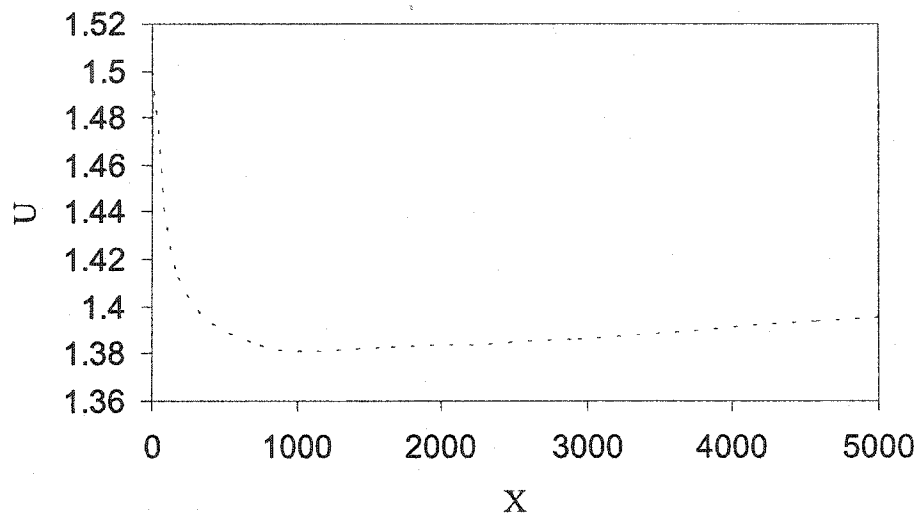


**Figure 5.10 a** U vs. X for variable viscosity case for ethylene glycol at  $Y = 0$  (physical properties are given in Table 5.2,  $Re = 400$ ,  $\Delta T = 30$  K and  $T_0 = 300$  K).

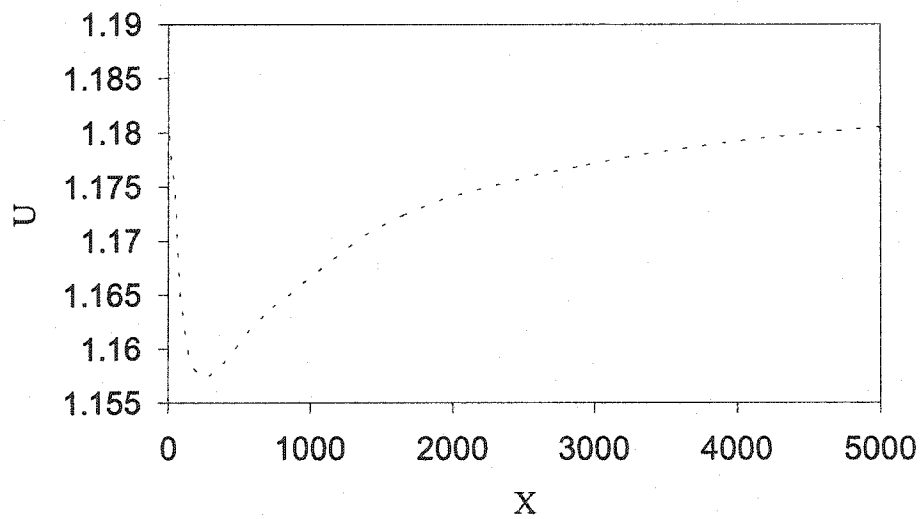


**Figure 5.10 b** U vs. X for variable viscosity case for ethylene glycol at  $Y = 0.46$  (physical properties are given in Table 5.2,  $Re = 400$ ,  $\Delta T = 30$  K and  $T_0 = 300$  K).

### **5.3.2 Effect of Inlet-Wall Temperature Difference, Reynolds Number and Liquid Type on Velocity Profiles**

The velocity profiles for variable viscosity are influenced by several parameters. These parameters are inlet-wall temperature differences, Reynolds number and liquid type.

#### **5.3.2.1 Effect of Inlet-Wall Temperature Difference**

The viscosity is a function of temperature. The higher the temperature, the less viscous the fluid becomes. To study the effect of inlet-wall temperature difference on the liquid, the inlet temperature is fixed at 300 K while the wall temperature is specified to 310 K, 320 K and 330 K for three different runs. The three runs are plotted as U vs. Y in Figure 5.11 for ethylene glycol with Reynolds number = 400 at  $X = 185$ . As the temperature difference increases between the wall and inlet fluid, the change in the velocity profile becomes more pronounced as compared to the constant viscosity change, see also Figure 5.12. This phenomenon can be noticed in the other velocity components with the same fluid properties as shown in Figures 5.12, 5.13 and 5.14.

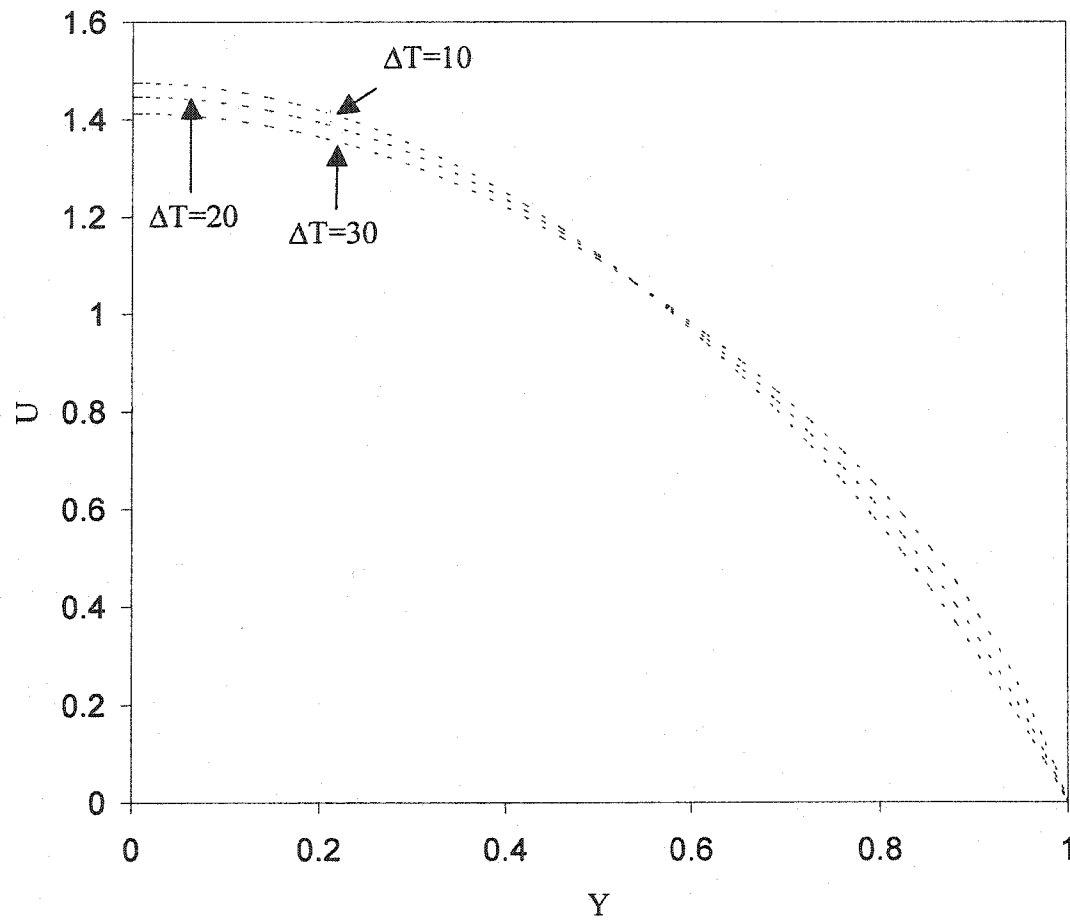


**Figure 5.11**  $U$  vs.  $Y$  for variable viscosity case for ethylene glycol at  $X = 185$  (physical properties are given in Table 5.2,  $Re = 400$ ,  $\Delta T = 10, 20$  and  $30$  K and  $T_o = 300$  K).



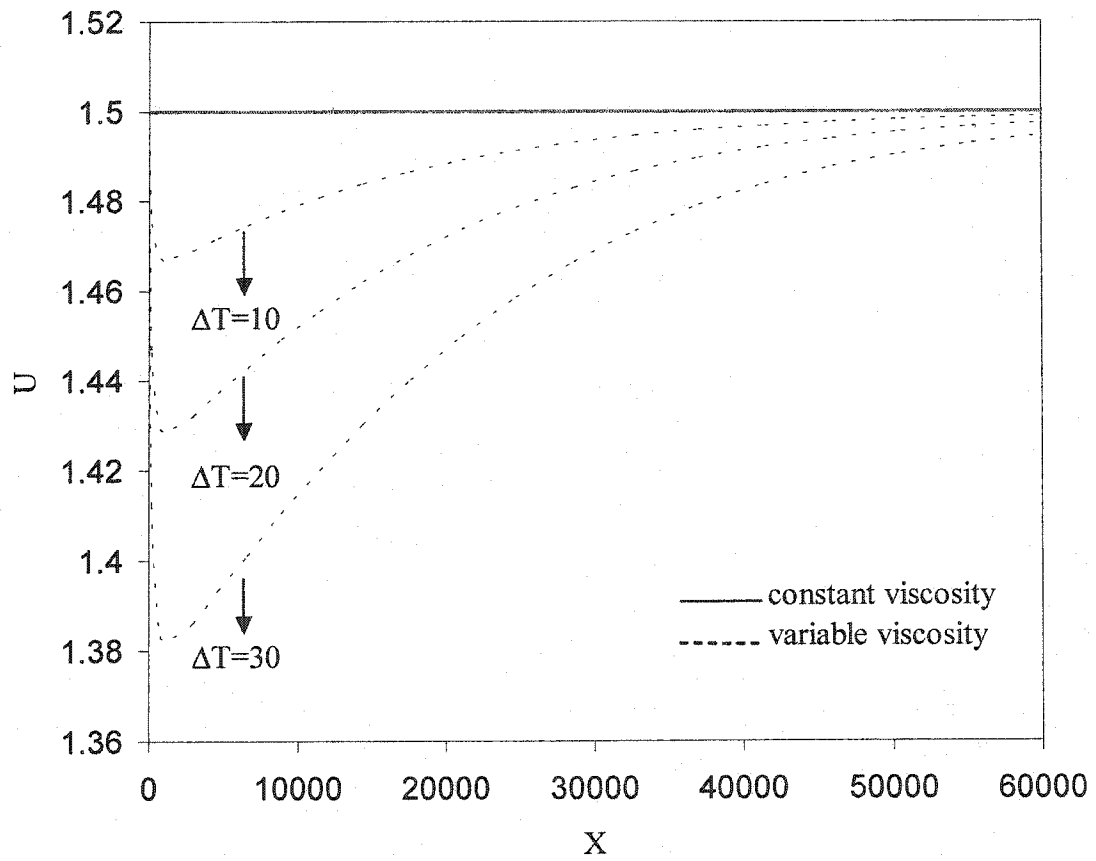


**Figure 5.12**  $U$  vs.  $X$  for constant and variable viscosity cases for ethylene glycol at  $Y = 0$  (physical properties are given in Table 5.2,  $Re = 400$ ,  $\Delta T = 10, 20, 30$  K and  $T_0 = 300$  K).

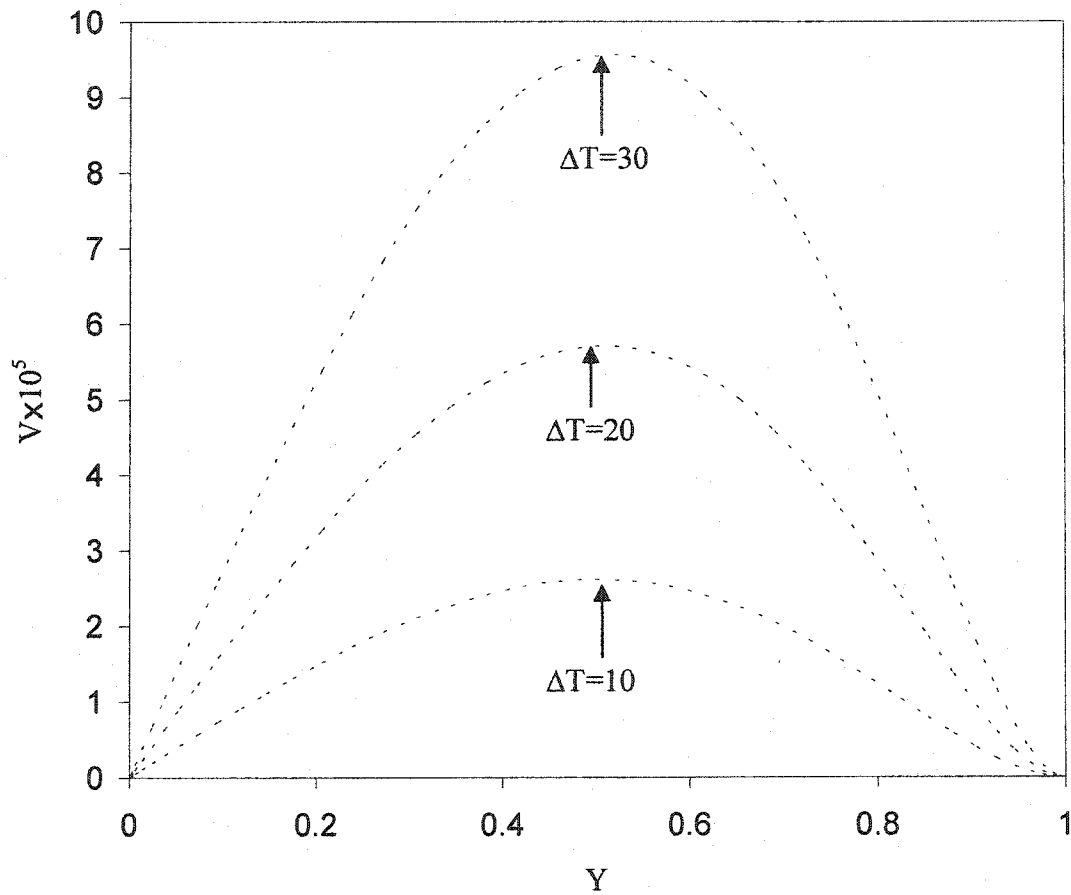


**Figure 5.13**  $V$  vs.  $Y$  for variable viscosity case for ethylene glycol at  $X = 185$  (physical properties are given in Table 5.2,  $Re = 400$ ,  $\Delta T = 10, 20, 30$  K and  $T_0 = 300$  K).

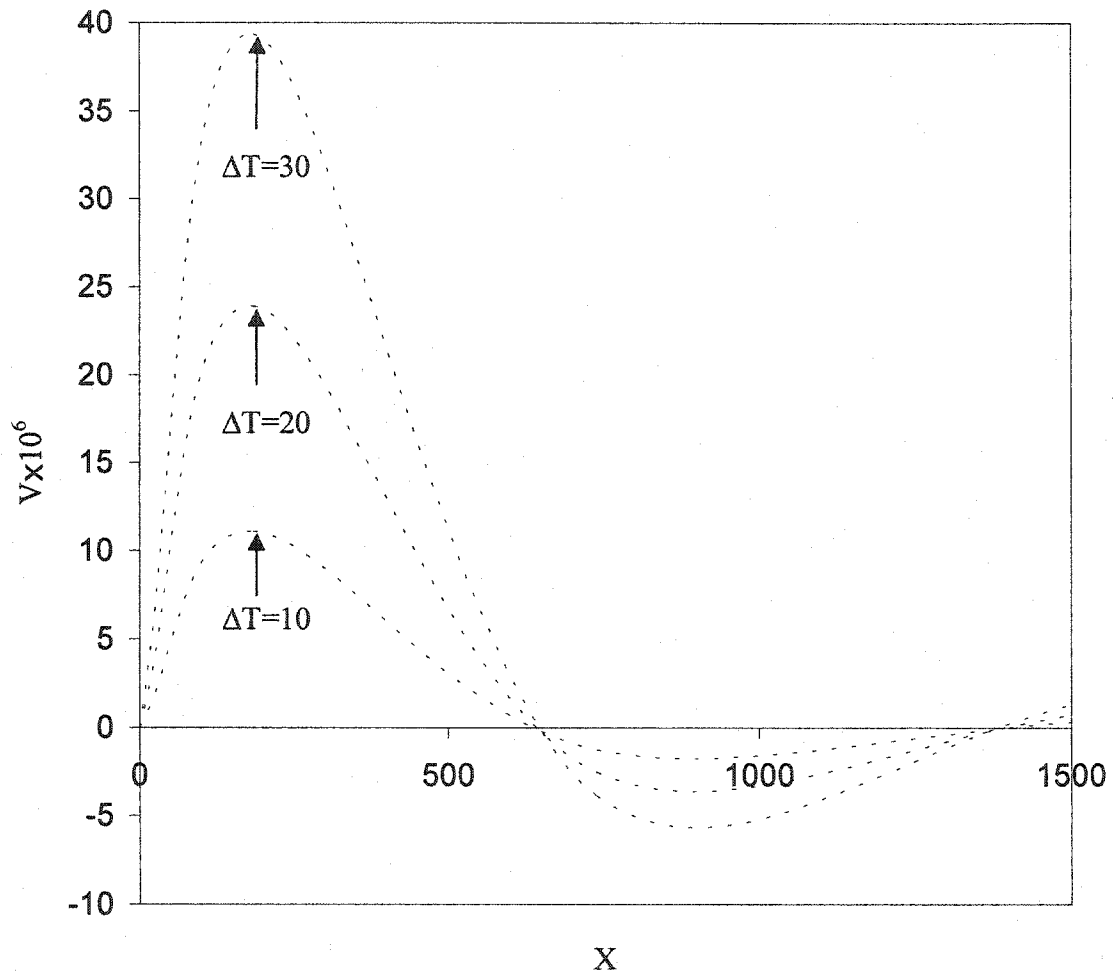


**Figure 5.14**  $V$  vs.  $X$  for variable viscosity case for ethylene glycol at  $Y = 0.15$  (physical properties are given in Table 5.2,  $Re = 400$ ,  $\Delta T = 10, 20, 30$  K and  $T_o = 300$  K).

### **5.3.2.2 Effect of Reynolds Number**

Reynolds number is one of the parameters that influences the velocity profiles. In the previous discussion, the pattern of the axial velocity profiles at the center was discussed in the axial direction and it was shown that the profiles become fully developed at a far distance downstream. This conclusion is true for any Reynolds number provided that the flow is laminar. Figures 5.15 and 5.16 show this behavior for Reynolds numbers 100 and 200 for ethylene glycol where  $\Delta T = 10$  K. It is clear that the profile at Reynolds number = 100 develops faster than that of Reynolds number = 200. The same behavior is presented more clearly in Figure 5.17 in which  $U$  vs.  $X$  is plotted for different values of Reynolds numbers at  $Y = 0$  and  $\Delta T = 10$  K. It was shown from last three figures that at low Reynolds number, the profile developed after a short distance between the parallel plates. As the Reynolds number increases, the pattern of the profiles is shifted downstream. Moreover, as the Reynolds number becomes larger, the length it takes to establish the final profile grows in a direct proportion. Finally, in order to see the effect of Reynolds number from different angles, Figure 5.18 is plotted for  $U$  vs.  $Y$  at two different Reynolds numbers at  $X = 1105$ . At the center, the figure shows that the velocity for  $Re = 50$  is higher than that of  $Re = 400$ . This is because the temperature gradient for  $Re = 50$  is higher than that of  $Re = 400$ .

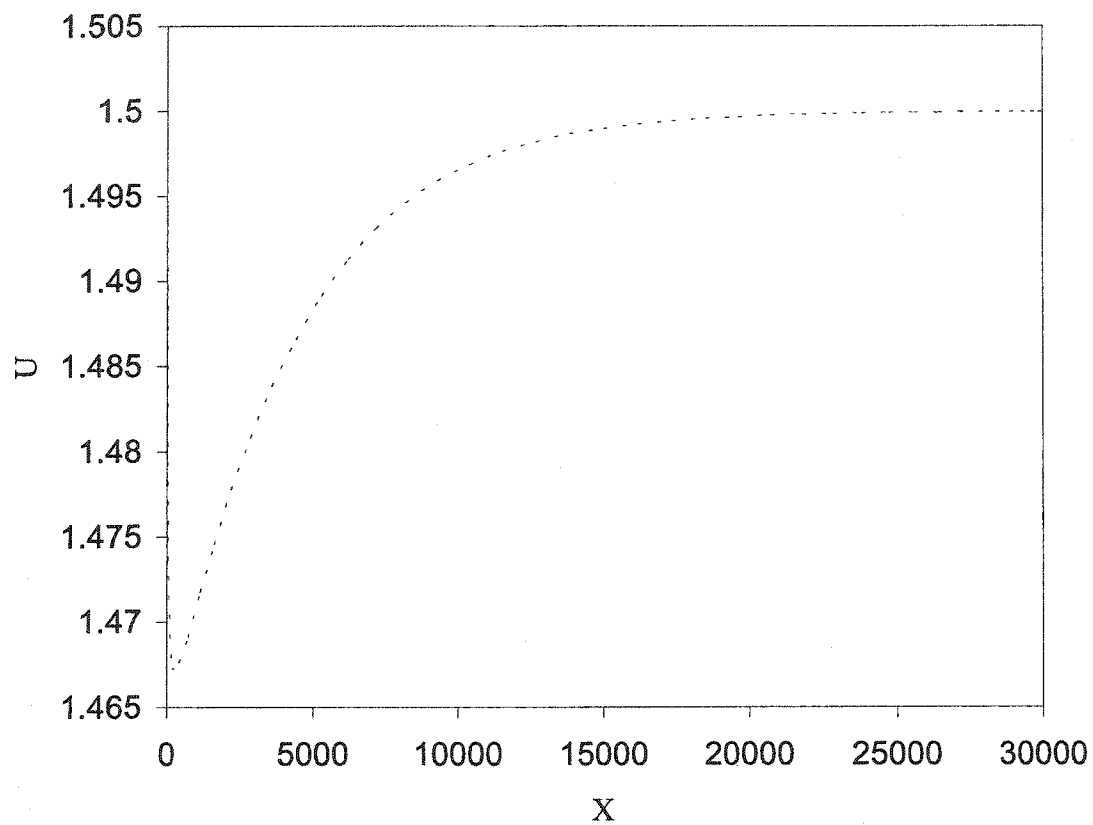


**Figure 5.15**  $U$  vs.  $X$  for variable viscosity case for ethylene glycol at  $Y = 0$  (physical properties are given in Table 5.2,  $Re = 100$ ,  $\Delta T = 10$  K and  $T_0 = 300$  K)

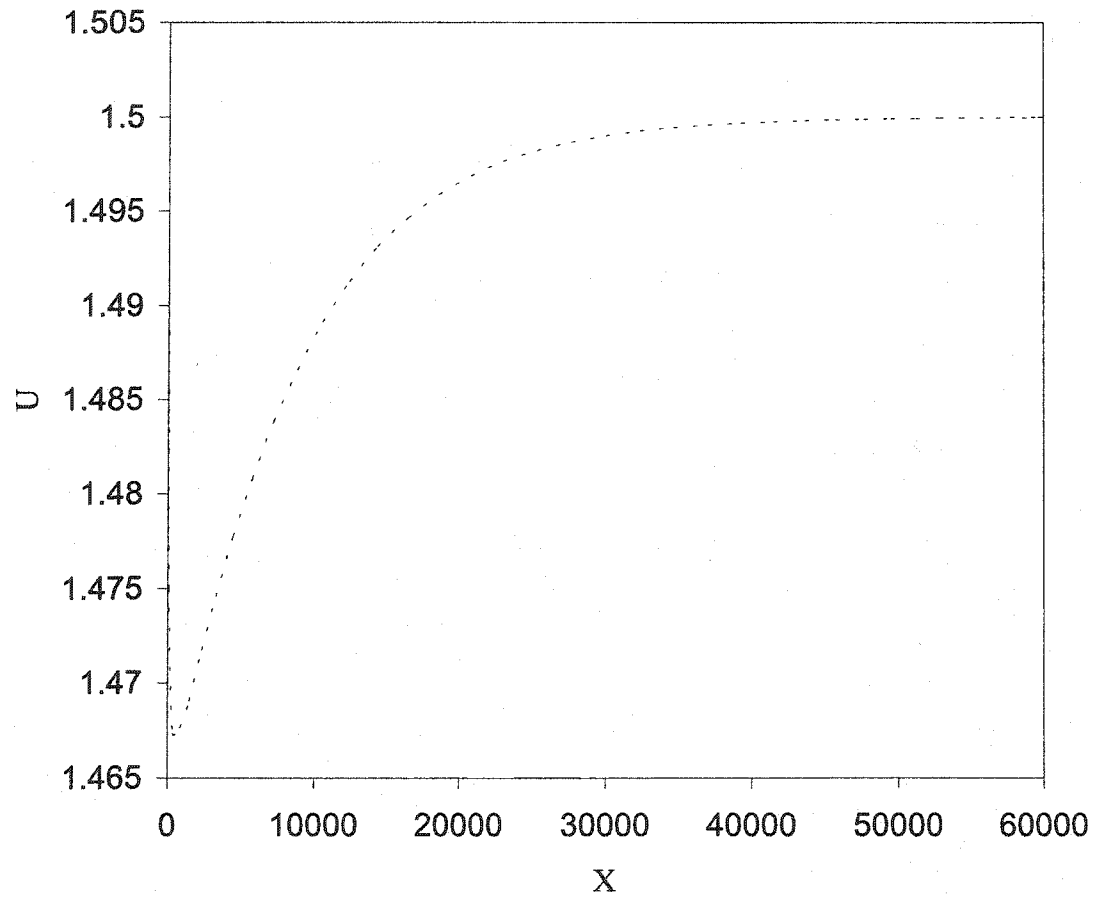


**Figure 5.16**  $U$  vs.  $X$  for variable viscosity case for ethylene glycol at  $Y = 0$  (physical properties are given in Table 5.2,  $Re = 200$ ,  $\Delta T = 10$  K and  $T_0 = 300$  K).

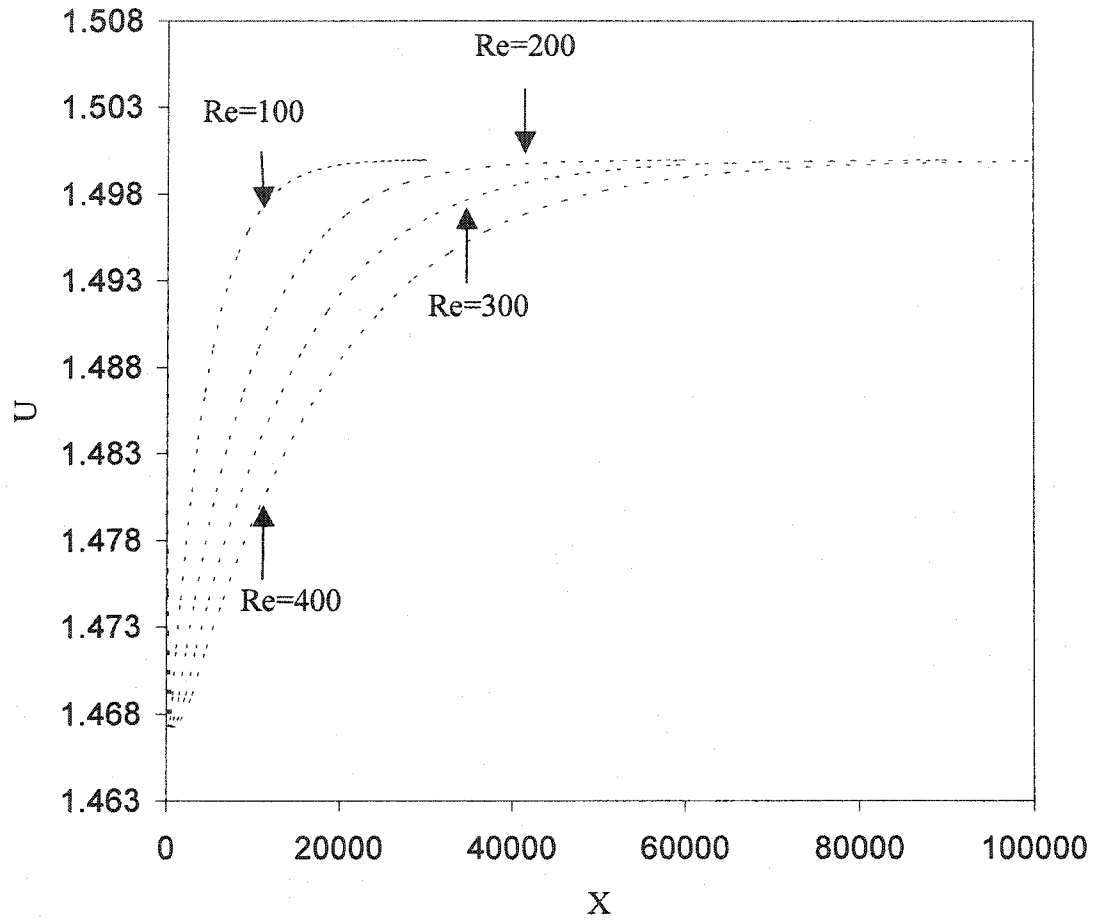


**Figure 5.17**  $U$  vs.  $X$  for variable viscosity case for ethylene glycol at  $Y = 0$  (physical properties are given in Table 5.2,  $Re = 100, 200, 300, 400$ ,  $T_0 = 300$  K,  $\Delta T = 10$  K).

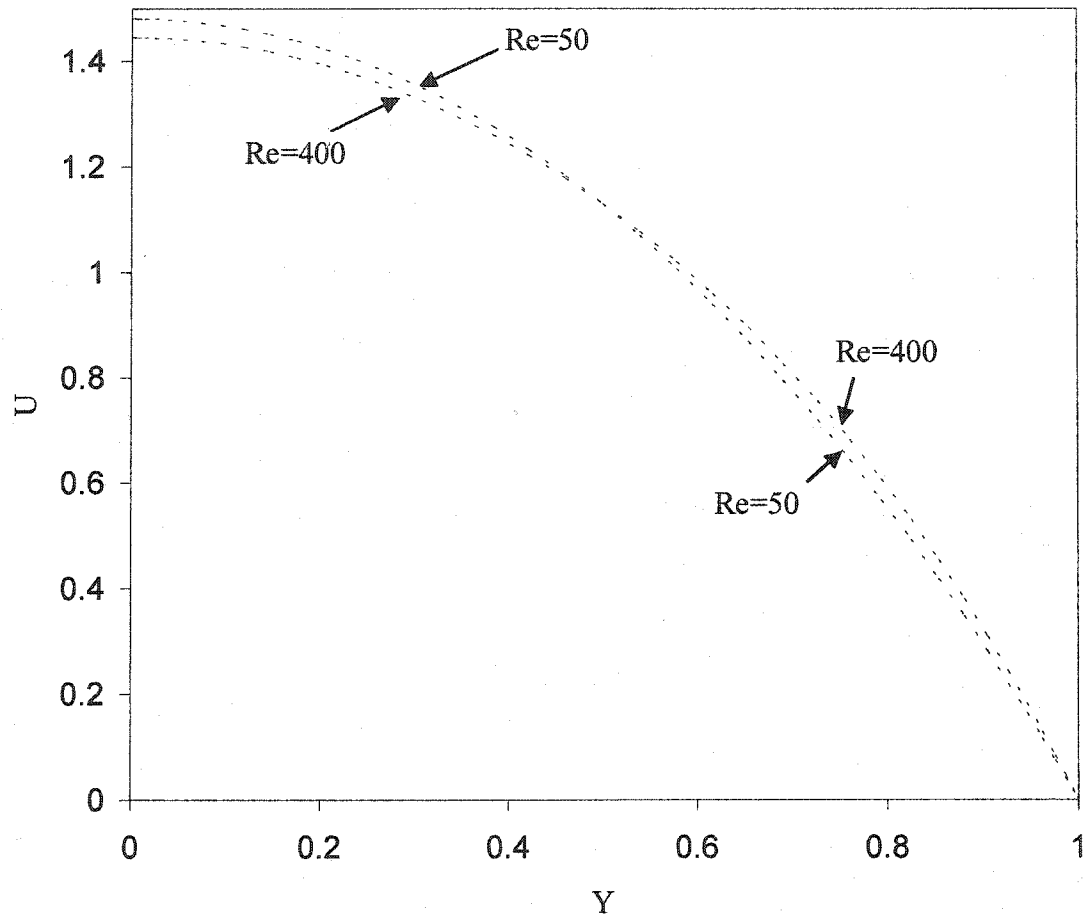


**Figure 5.18**  $U$  vs.  $Y$  for variable viscosity case for ethylene glycol at  $X = 1105$  (physical properties are given in Table 5.2,  $Re = 50$  and  $400$ ,  $T_o = 300$  K and  $\Delta T = 30$  K).



### 5.3.2.3 Effect of Liquid Type

In this study, two Newtonian liquids are chosen as one liquid is less viscous while the other is more viscous. These liquids are water that represents the less viscous liquid and ethylene glycol that represents the more viscous liquid. In Figure 5.19,  $U$  vs.  $X$  is plotted for both water and ethylene glycol at  $Y = 0$  ( $Re = 400$   $T_o = 300$  K and  $\Delta T = 30$  K). It is clear that water, being less sensitive to temperature than ethylene glycol, develops faster because water's Prandtl number is smaller than ethylene's.  $U$  vs.  $Y$  for both water and ethylene glycol is also plotted at  $X = 825$ . At the center, it is clear that water has higher velocity than that of ethylene glycol which is more viscous and therefore needs longer distance to reach the fully developed value. Therefore, we can conclude that the more sensitive the fluid to temperature, the more the heat effects are pronounced.

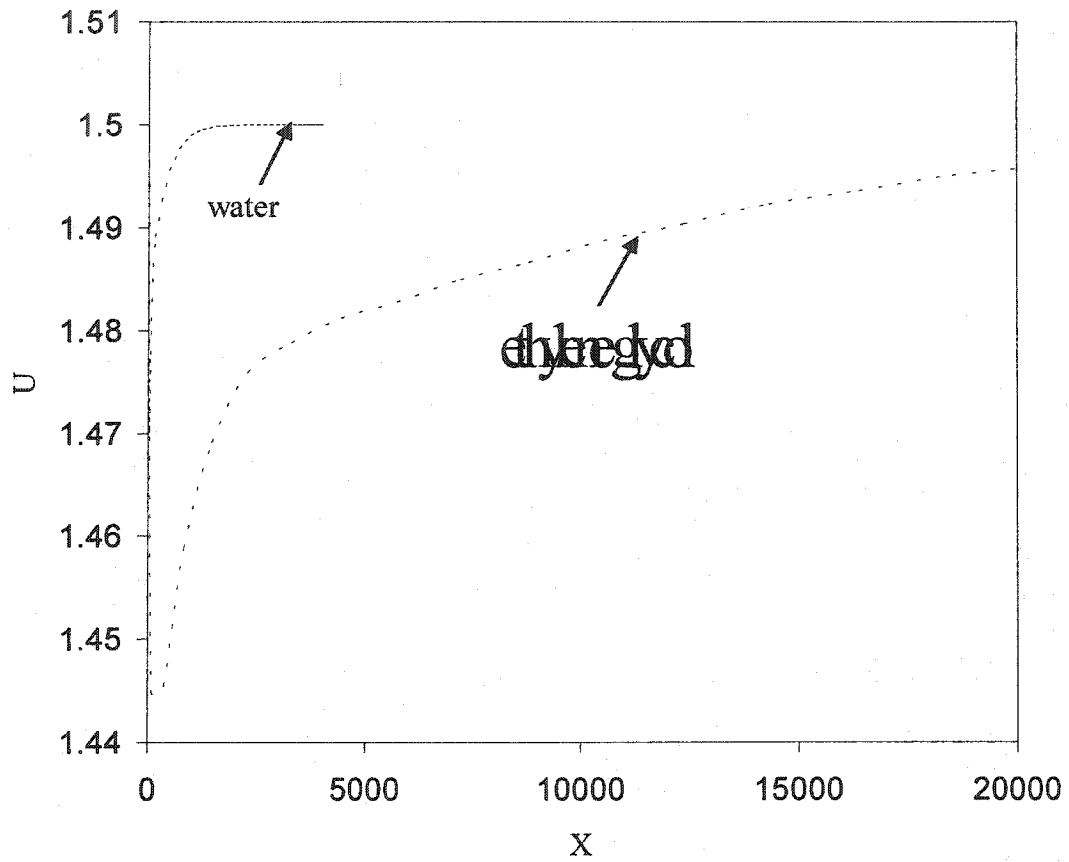


**Figure 5.19**  $U$  vs.  $X$  for variable viscosity case for ethylene glycol and water at  $Y = 0$  (physical properties are given in Table 5.2,  $Re = 200$ ,  $T_0 = 300$  K and  $\Delta T = 30$  K).

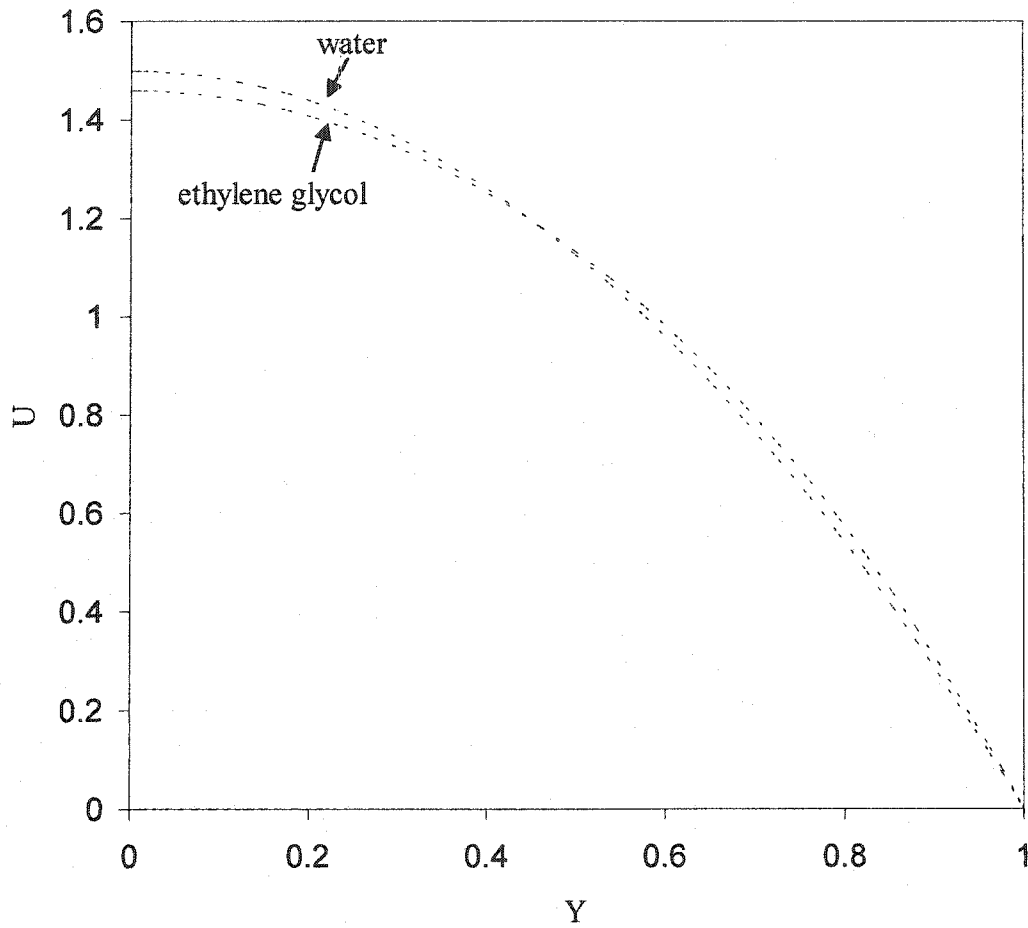


**Figure 5.20**  $U$  vs.  $Y$  for variable viscosity case for ethylene glycol and water at  $X = 825$  (physical properties are given in Table 5.2,  $Re = 200$ ,  $T_0 = 300$  K and  $\Delta T = 30$  K).

### 5.3.3 Temperature Profiles

Temperature profiles are obtained from the energy equation. The fluid enters with temperature = 300 K and it is subjected to heat transfer from the wall that is higher than the inlet fluid by 10 K for the first run, 20 K for the second run and 30 K for the third run. The heat transfer continues until the temperature difference between the fluid and the wall equals zero. Figures 5.21 and 5.22 present  $\Theta$  vs.  $X$  at various  $Y$  values for variable viscosity case ( $Re = 400$ ,  $T_o = 300$  K and  $\Delta T = 30$  K). In Figure 5.21, as is expected, the ethylene glycol gains heat from the walls of the parallel plates and the dimensionless temperature gradually increases with  $X$  till it reaches 1 at which there is no heat transfer from the wall. The temperature near the wall reaches 1 faster than that in the center.  $\Theta$  vs.  $Y$  at various  $X$  values is shown in Figure 5.22 and it is clear that the liquid gains more heat as it flows downstream because of heat transfer from the wall. This heat transfer makes the temperature gradient in the normal direction lower as  $X$  increases. Moreover, the temperature dependent viscosity influences the pattern of temperature profiles. Figure 5.23 compares the temperature profiles for the constant and variable cases.  $\Theta$  is plotted vs.  $X$  at  $Y = 0.8$  and  $0.9$  and it is clear that the temperature dependent viscosity affects the temperature profiles. In the figure, the temperature profile for the constant viscosity is higher than that of the variable viscosity because the velocity in the variable viscosity case is less than that of constant viscosity at  $Y = 0.8$  and  $0.9$  and the relation between velocity and temperature can be seen in the convection term in energy equation (3.21).

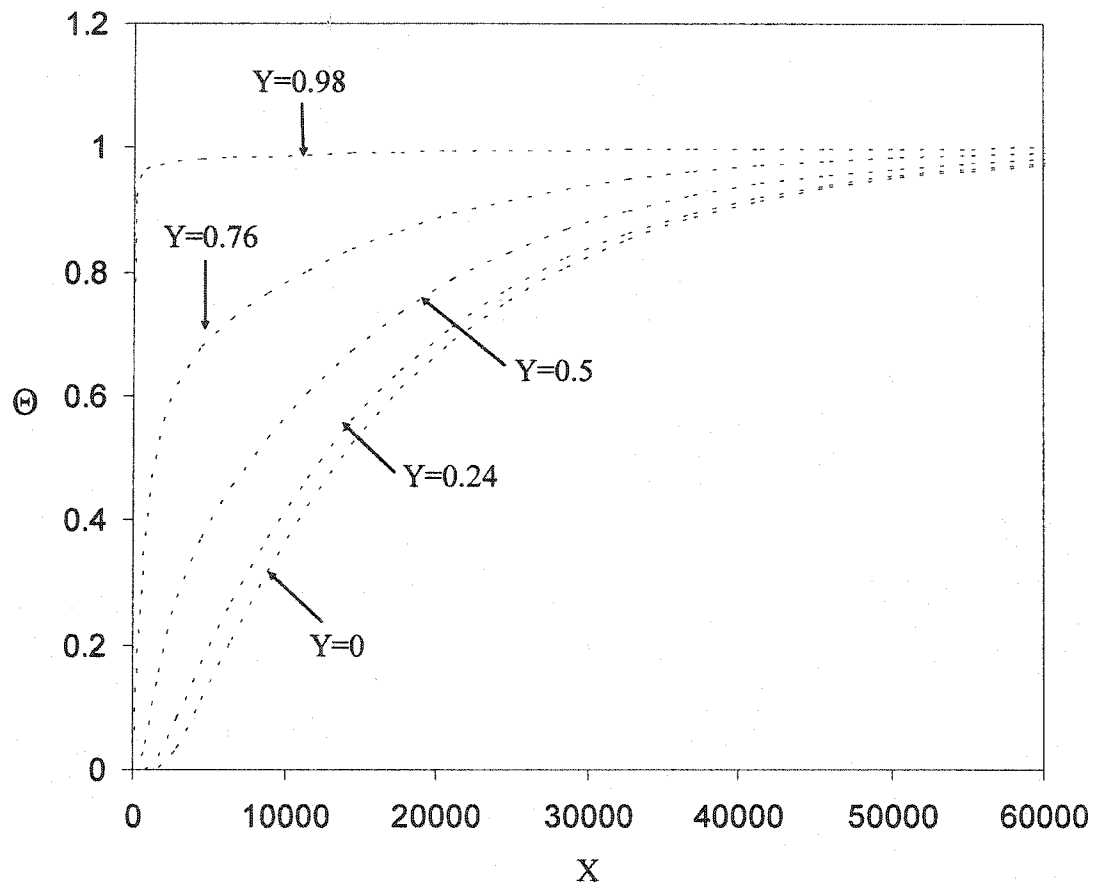


**Figure 5.21**  $\Theta$  vs.  $X$  for variable viscosity case for ethylene glycol at various  $Y$  values (physical properties are given in Table 5.2,  $Re = 400$ ,  $T_0 = 300$  K and  $\Delta T = 30$  K).

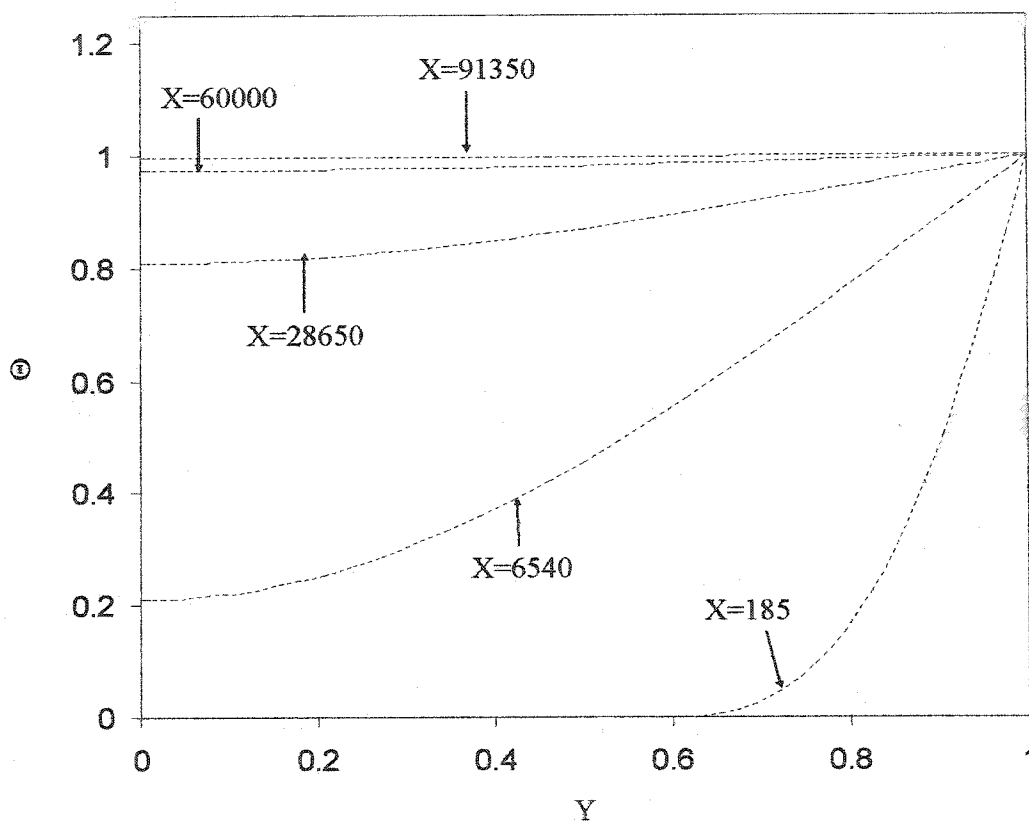


**Figure 5.22**  $\theta$  vs.  $Y$  for variable viscosity case for ethylene glycol at various  $X$  values (physical properties are given in Table 5.2,  $Re = 400$ ,  $T_o = 300$  K and  $\Delta T = 30$  K).

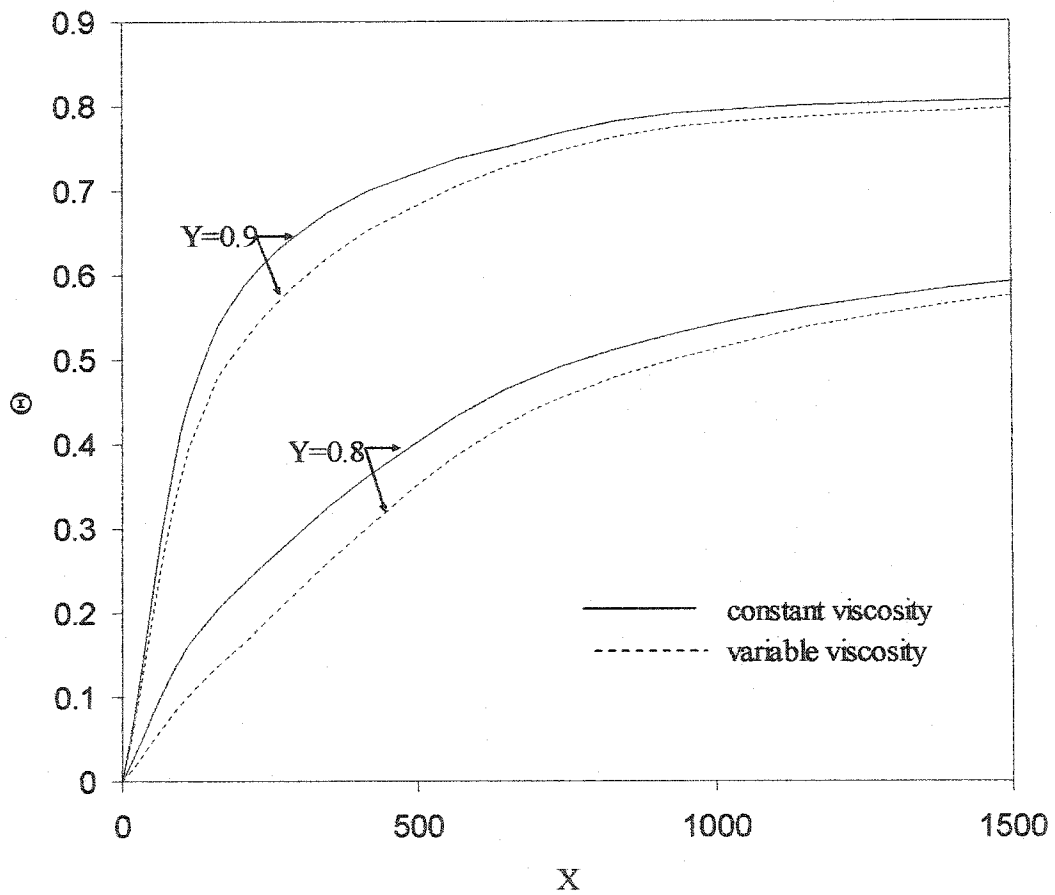


**Figure 5.23**  $\theta$  vs.  $X$  for constant and variable viscosity cases for ethylene glycol at  $Y = 0.8$  and  $0.9$  (physical properties are given in Table 5.2,  $Re = 400$ ,  $T_o = 300$  K and  $\Delta T = 30$  K).

### 5.3.4 Effect of Reynolds Number and Liquid Type on Temperature Profiles

Temperature distribution can be influenced by different parameters including the Reynolds number and the liquid types. The discussion of this section will evidently show that flow phenomena and thermal phenomena interact to a great extent.

#### 5.3.4.1 Effect of Reynolds Number

Reynolds number is a parameter that affects the velocity as well as the temperature. In the previous discussion, the effect of Reynolds number on the velocity profiles was elaborated. Similarly, Reynolds number shifts and extends the temperature profiles downstream when the Reynolds number increases.  $\Theta$  vs.  $X$  at  $Y = 0$  is plotted for ethylene glycol in Figure 5.24 for different Reynolds numbers ( $T_o=300$  K and  $\Delta T = 30$  °C). From the figure, it is clear that uniform temperature in the fluid is achieved earlier (at shorter distance) at low Reynolds numbers than at higher Reynolds numbers.

#### 5.3.4.2 Effect of Liquid Type

In Figure 5.25,  $\Theta$  vs.  $X$  at  $Y=0$  is plotted for ethylene glycol and water ( $Re=400$ ,  $T_o=300$  K and  $\Delta T = 30$  °C). Water, which is the less sensitive to temperature liquid, is heated faster than ethylene glycol. This is because the heat diffuses in water easier than in ethylene glycol and this can be explained by the comparison of the magnitude of the Prandtl number for water and ethylene glycol where the water's Prandtl number is much smaller than ethylene glycol's.



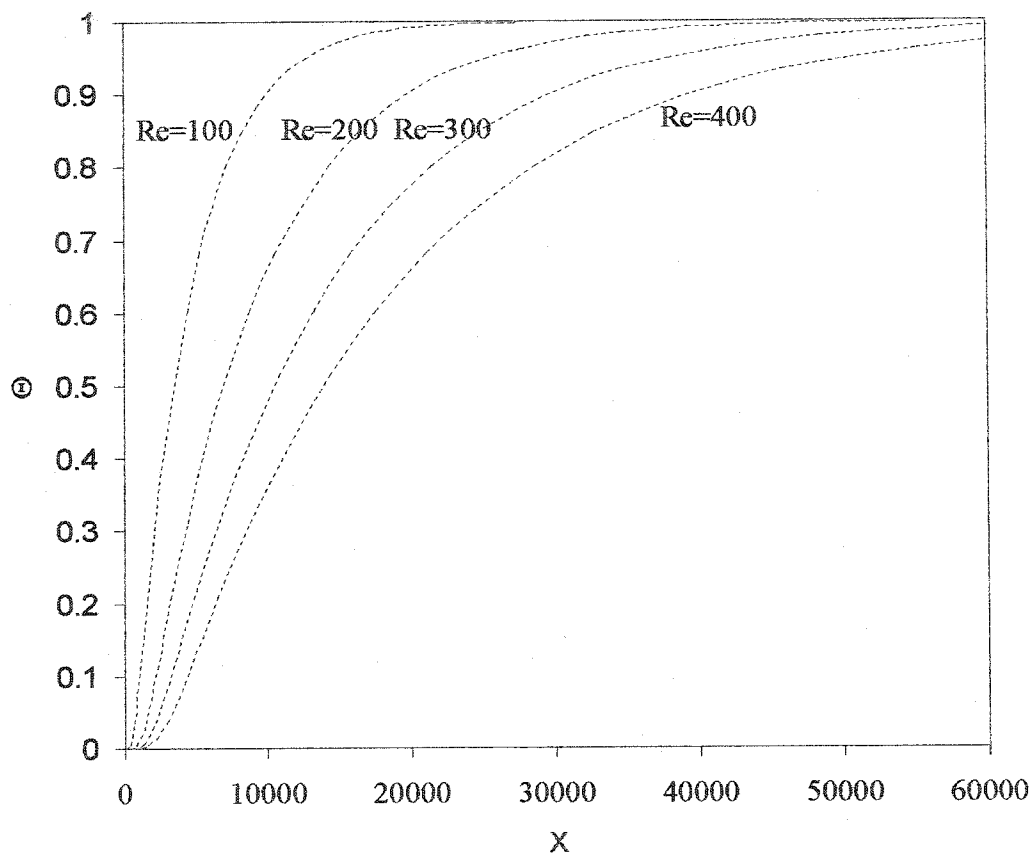


**Figure 5.24**  $\Theta$  vs.  $X$  for variable viscosity case for ethylene glycol at  $Y = 0$  (physical properties are given in Table 5.2,  $Re = 100, 200, 300$  and  $400$ ,  $T_o = 300$  K and  $\Delta T = 30$  K).

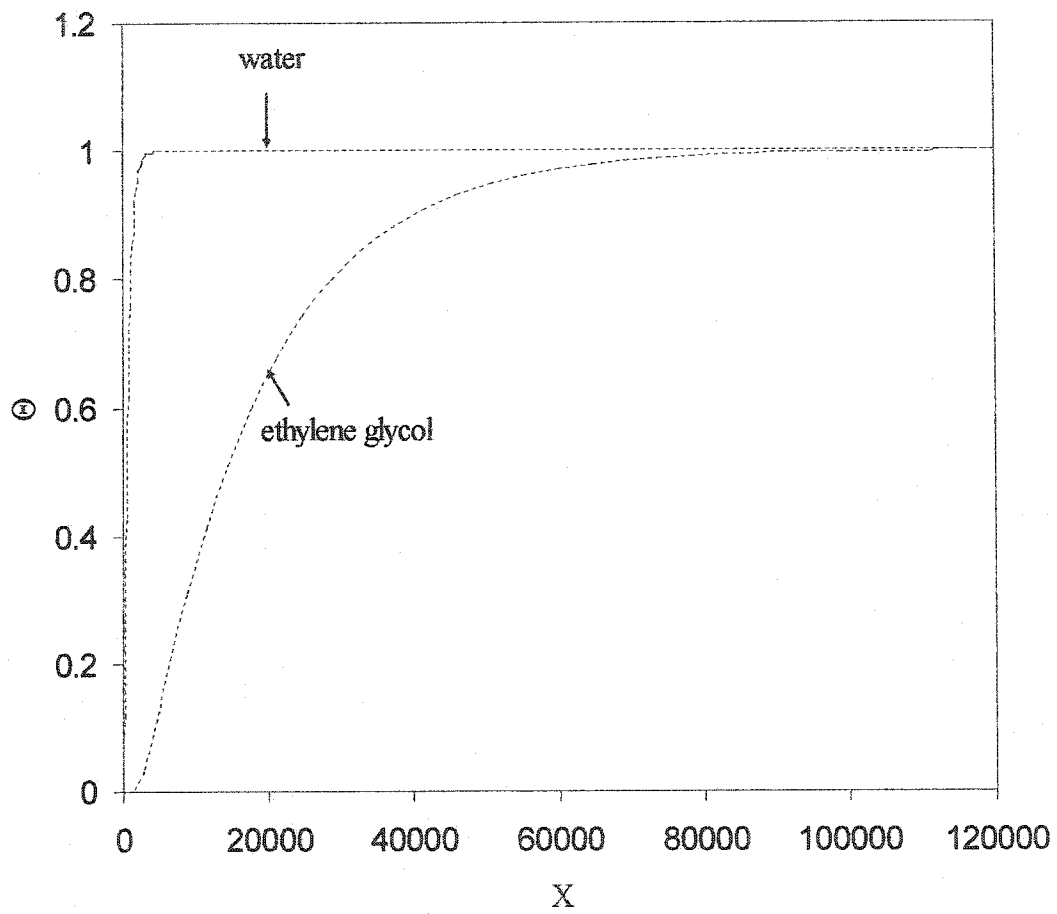


**Figure 5.25**  $\Theta$  vs.  $X$  for variable viscosity case for water and ethylene glycol at  $Y = 0$  (physical properties are given in Table 5.2,  $Re = 400$ ,  $T_o = 300$  K and  $\Delta T = 30$  K).

### 5.3.5 Entropy Generation Profiles

Entropy generation calculated from temperature and velocity data will be presented and discussed after the previous discussions of velocity and temperature profiles. Entropy generation arises from fluid friction. As a result, the entropy generation profiles depend on the behavior of both velocity and temperature profiles. To investigate and gain insight of the behavior of entropy generation profiles, this section is divided into four parts. The first part is to investigate entropy generation per unit volume ( $\dot{S}_{gen}^m$ ) profiles from fluid friction perspective only whereas the second part is to investigate  $\dot{S}_{gen}^m$  from heat transfer perspective. The third part is to investigate the  $\dot{S}_{gen}^m$  under the effect of several parameters, namely,  $\Delta T$ , Reynolds number and liquid type. The fourth part is to estimate the total entropy generation along Y for a specified X-location,  $\dot{S}_{\Delta Y}$ , where  $\Delta Y$  represents the distance from the center to the wall. Further, the fourth part includes total entropy generation along Y and X from inlet to a specified X-location,  $\dot{S}_{\Delta Y \Delta X}$ , where  $\Delta X$  represents the distance from inlet to the selected specified X-location.

#### 5.3.5.1 Entropy Generation from Fluid Friction Effect

Friction is one source of irreversibility in a flowing fluid in a channel. Fluid friction arises from the friction between the liquid and the plate walls and from the friction between liquid molecules themselves. Viscous dissipation represents this friction effect. Viscous dissipation function ( $\Phi$ ) appears in the second part of the entropy generation equation:

$$\dot{S}_{gen}^m = -\frac{1}{T^2}(\nabla T)^2 + \frac{\mu}{T}\Phi \quad 3.11$$

At low Reynolds number, viscous dissipation function is not significant and a small effect of viscous dissipation on entropy generation is expected. Even though the effect of fluid friction is not significant, it is worth to see the patterns of entropy generation profiles arising from fluid friction (considering only the second part of Equation 3.11).  $\dot{S}_{gen}^m$  vs. X is plotted in Figure 5.26 for ethylene glycol with Reynolds number = 400 at various Y values.  $\dot{S}_{gen}^m$  increases as the value of Y increases. This is expected since the shear stress increases towards the wall.

$\dot{S}_{gen}^m$  vs. Y is plotted for various X values in Figure 5.27 for fluid friction effect. This figure shows that as the flow proceeds downstream,  $\dot{S}_{gen}^m$  decreases at any Y. This is related to the minimizing of the velocity gradient as the flow proceeds further. Furthermore, entropy generation arising from fluid friction effect can also be influenced by the increase of the Reynolds number because the viscous dissipation function increases as the Reynolds number increases. To examine this effect,  $\dot{S}_{gen}^m$  arising from fluid friction effect is plotted vs. X for different Reynolds numbers in Figure 5.28. The selected Reynolds numbers are 100, 200, 300 and 400.  $Re = 400$  provides the highest viscous dissipation among the other Reynolds number values. As a result, the entropy generation arising from fluid friction effect increases if the Reynolds number increases.

To conclude this section, it is evident that the entropy generation arising from fluid friction effect is of order  $10^{-8}$  which is  $\ll 1$ . As a result, the entropy generation arising from fluid friction is negligible and viscous dissipation function can be neglected in solving the governing equation in this study.

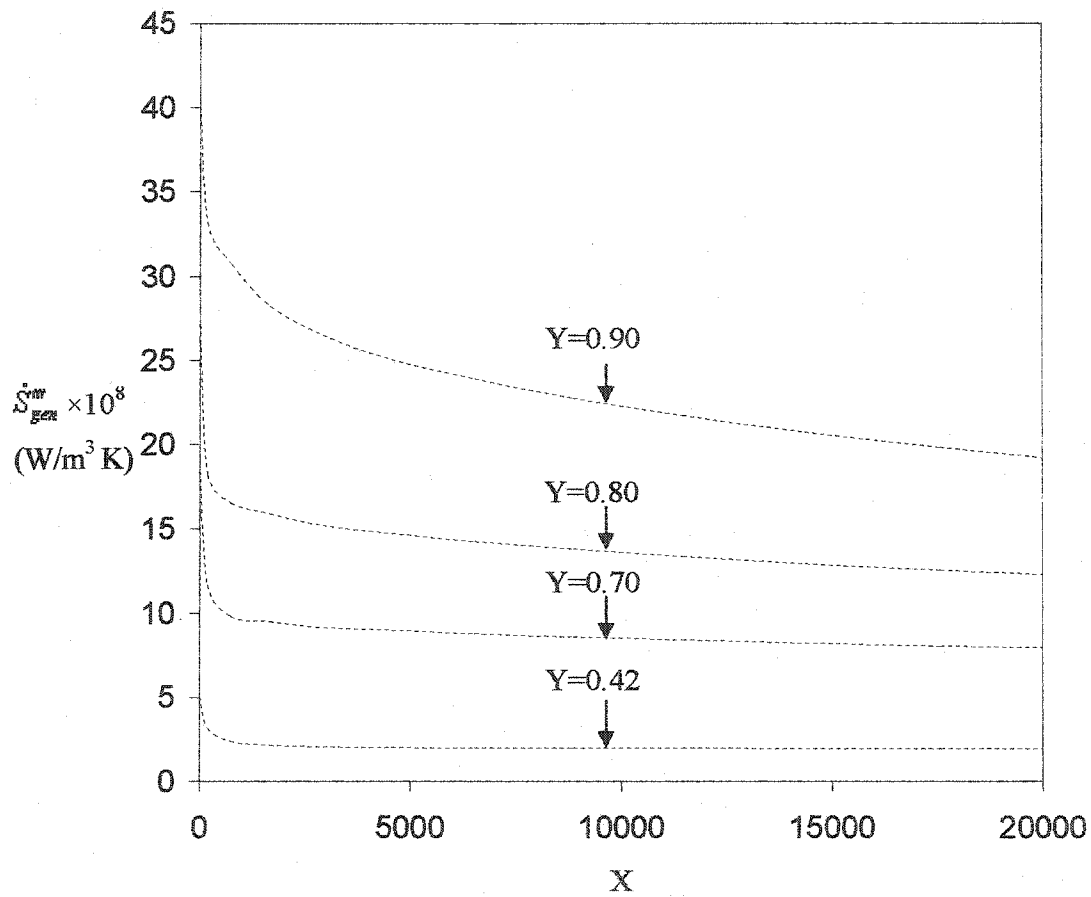


**Figure 5.26**  $\dot{S}_{gen}''$  (fluid friction effect) vs.  $X$  for variable viscosity case for ethylene glycol at various  $Y$  values (physical properties are given in Table 5.2,  $Re = 400$ ,  $T_o = 300$  K and  $\Delta T = 30$  K).

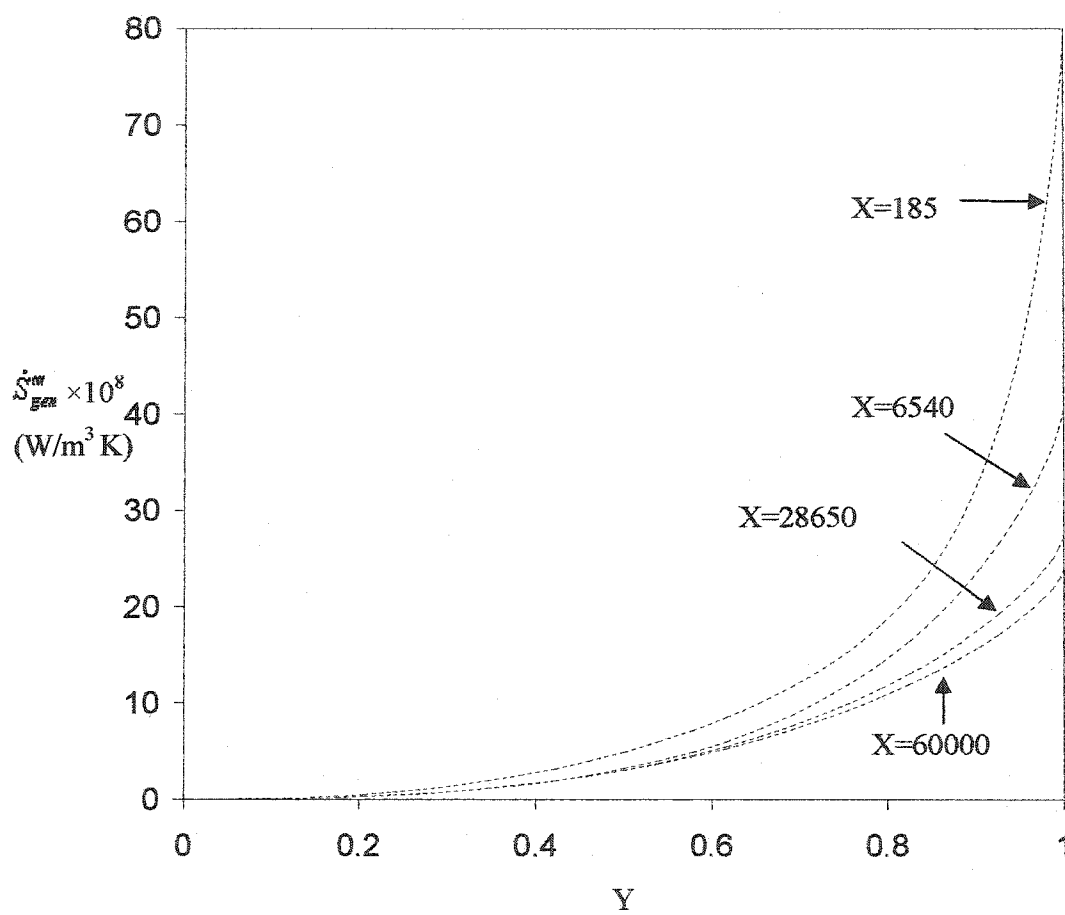


**Figure 5.27**  $\dot{S}_{gen}^m$  (fluid friction) vs. Y for variable viscosity case for ethylene glycol at various Y values (physical properties are given in Table 5.2,  $Re = 400$ ,  $T_o = 300$  K and  $\Delta T = 30$  K).

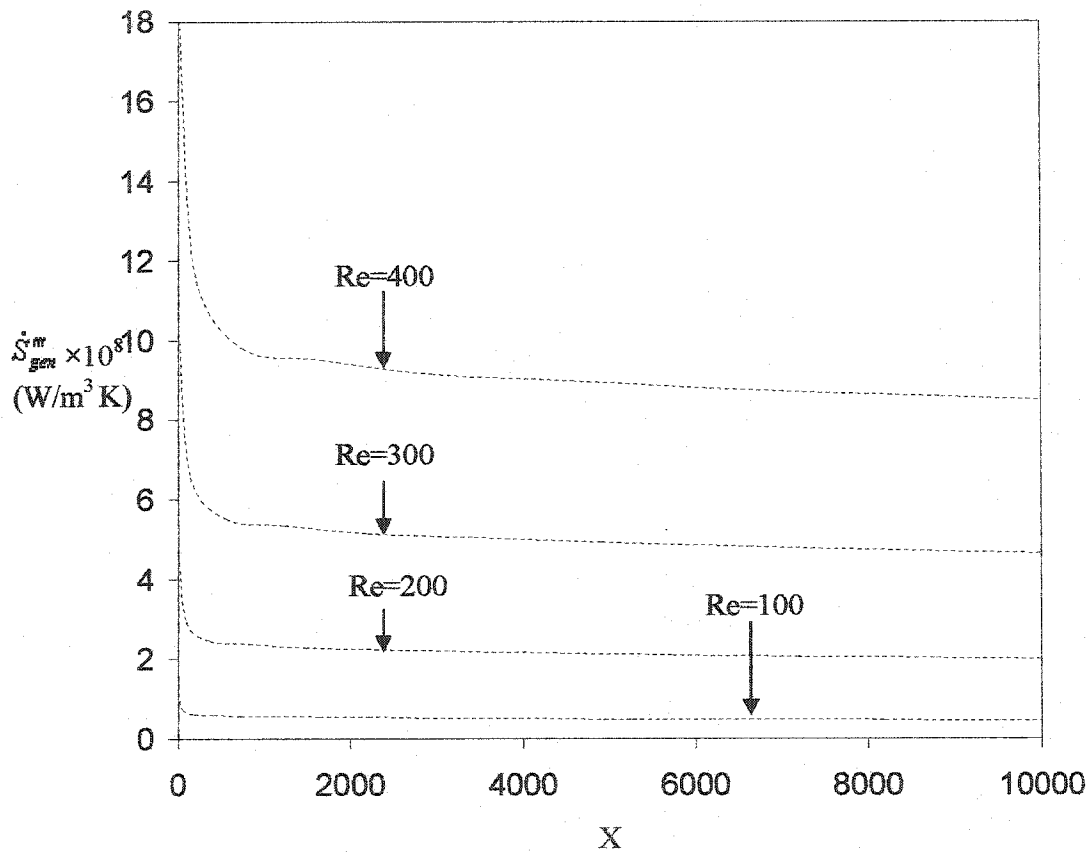


**Figure 5.28**  $\dot{S}_{gen}^m$  (fluid friction) vs.  $X$  for variable viscosity case for ethylene glycol at  $Y = 0.70$  ( physical properties are given in Table 5.2,  $Re = 100, 200, 300$  and  $400$ ,  $T_o = 300 \text{ K}$  and  $\Delta T = 30 \text{ K}$ ).

### 5.3.5.2 Entropy Generation from Heat Transfer Effect

Entropy generated from heat transfer is dominant between the parallel plates. In this section, the entropy generation arising from heat transfer effect (the first term of equation 3.11) will be investigated. Figure 5.29, 5.30 and 5.31 are plotted for  $\dot{S}_{gen}^m$  vs. X for different Y values. The profiles for  $\dot{S}_{gen}^m$  vs. X are divided into three figures in order to illustrate their behavior clearly. Figure 5.29 covers the range of Y from 0.12 to 0.31 while Figure 5.30 covers the range from 0.42 to 0.82. Furthermore, Figure 5.31 investigates  $\dot{S}_{gen}^m$  at Y = 0.92 and 1. All these figures correspond to Reynolds number = 400 and  $\Delta T = 30$  K. In the vicinity of the wall, the heat transfer is significant and the generation of entropy is expected to be higher than that at the center. Therefore,  $\dot{S}_{gen}^m$  increases towards the wall due to the significant effect of high temperature gradients near wall. Furthermore, as the Y value increases, the maximum entropy generations shifted to the left of the diagram (towards the entrance of the parallel plates). This is related to the effect of the shift of the velocity that was explained in Figure 5.10. The maximum entropy generation is located at the same X-location of the maximum velocity and this is can be established if Figure 5.9 is compared to Figure 5.30 at Y=0.82. In both figures, the location of the maximum velocity and entropy is approximately at X = 185.  $\dot{S}_{gen}^m$  in Figures 5.29, 5.30, 5.31 start from zero at the inlet of the parallel plates then increases to a maximum and subsequently decreasing back to zero. This is due to the temperature gradient which undergoes the same behavior from the inlet to the end.

On the other hand, the preceding discussion of velocity and temperature profiles showed that the velocity and temperature profiles in the variable viscosity case deviate



from those of the constant viscosity case. As a result, the entropy generation profiles from the variable viscosity case should also deviate from those of constant viscosity case since the entropy generation consists of velocity and temperature data. This can be shown in Figure 5.32 which is a comparison of  $\dot{S}_{gen}^m$  from variable and constant viscosity cases. The effect of consideration of temperature dependent viscosity can also be noticed in Figure 5.33 which is a plot of  $\dot{S}_{gen}^m$  vs.  $Y$  at  $X = 185$ . In this figure, it is clear that the entropy generation from variable viscosity is higher than that of constant viscosity at location close to the wall. On the other hand, the entropy generation from the variable viscosity is less than that of the constant viscosity at a location close to the center. This behavior is a result of the behavior of the velocity profile in Figure 5.3 that was explained in the preceding discussion of velocity profiles. To sum up this section, the investigation of the entropy generation arising from heat transfer effects equals to the total entropy since the entropy generation from fluid friction effects can be neglected.

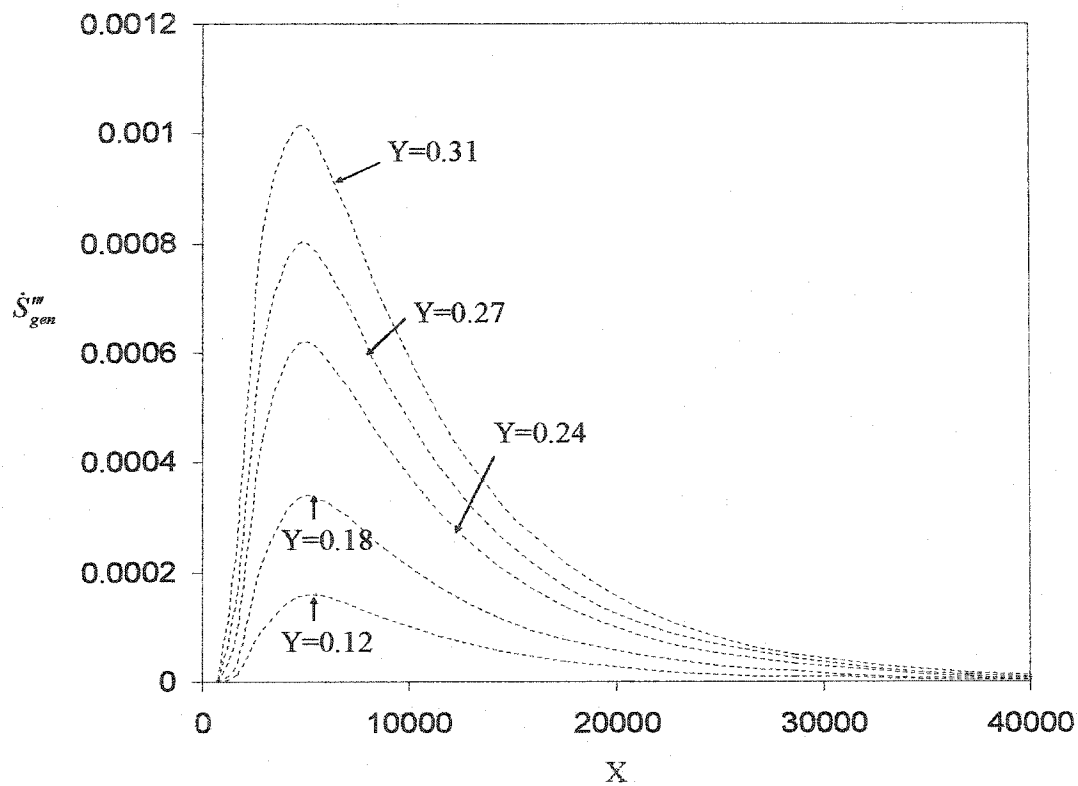
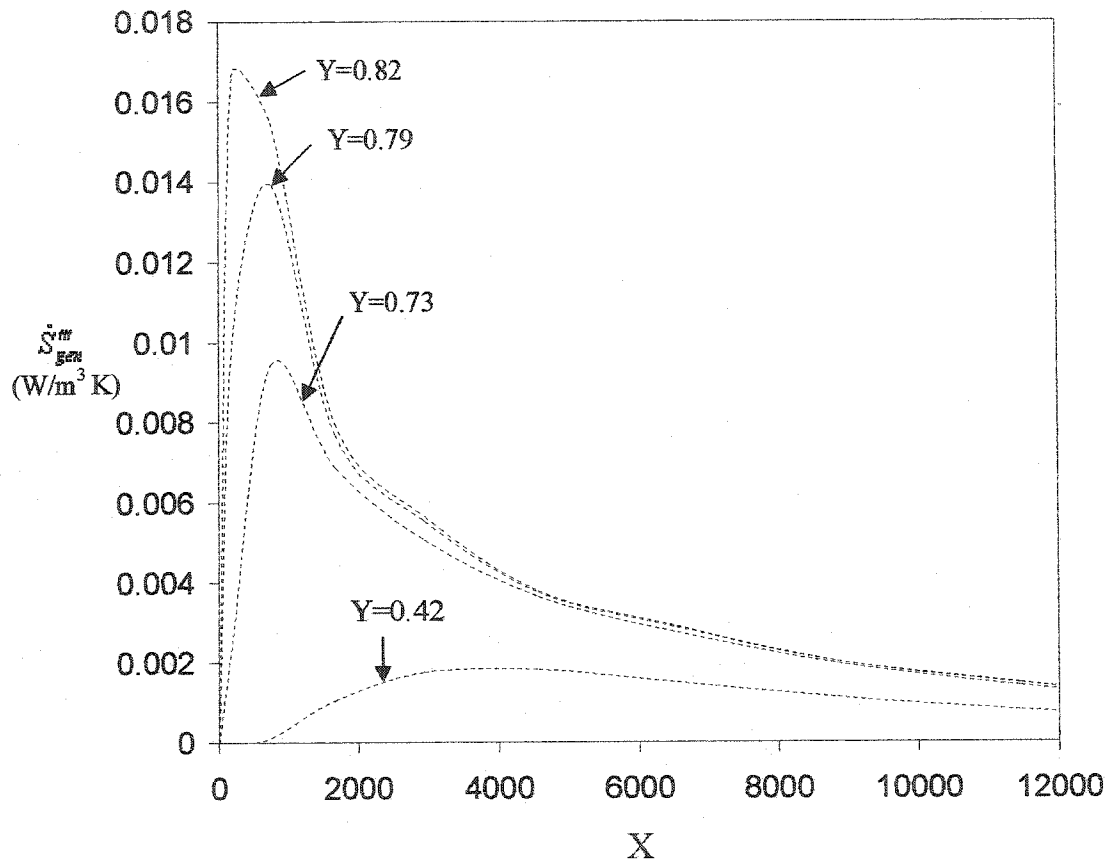
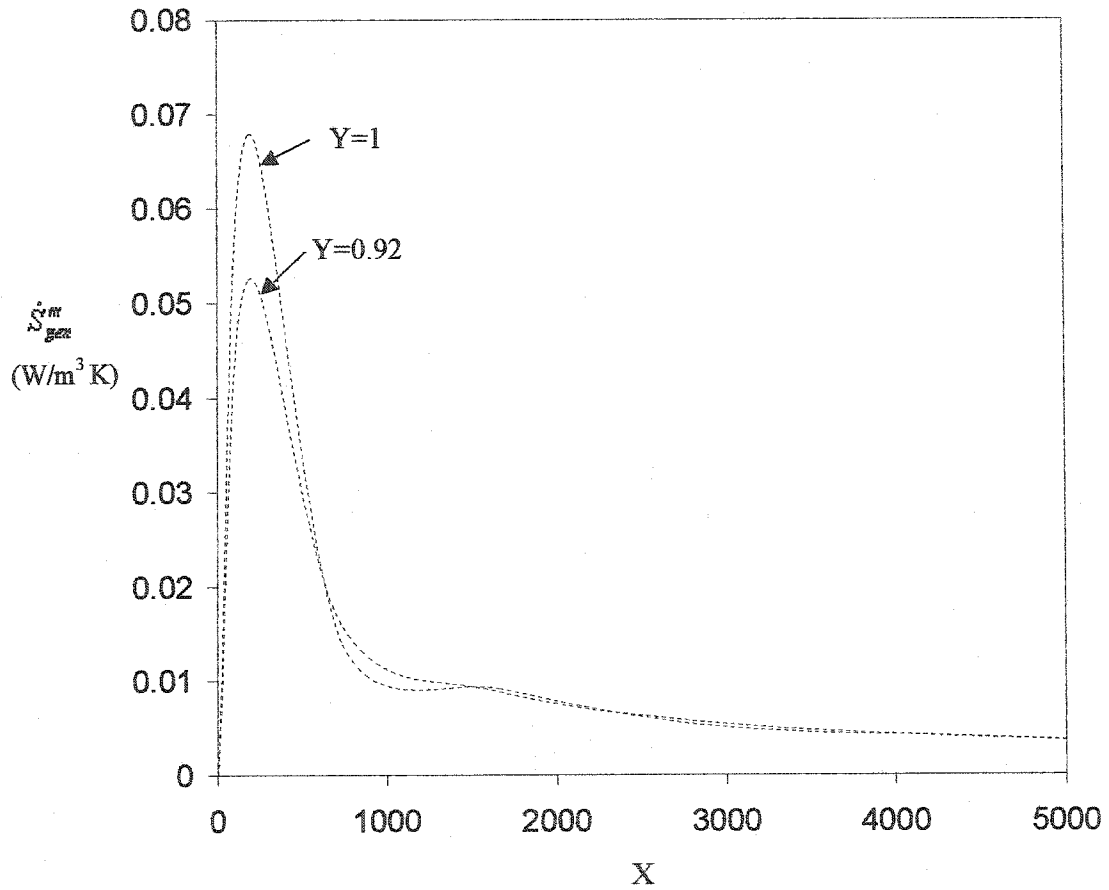


Figure 5.29  $\dot{S}_{gen}^m$  (heat transfer effect) vs.  $X$  for variable viscosity case for ethylene glycol at various  $Y$  values (physical properties are given in Table 5.2,  $Re = 400$ ,  $T_o = 300$  K and  $\Delta T = 30$  K).



**Figure 5.30**  $\dot{S}_{gen}^m$  vs.  $X$  for variable viscosity case for ethylene glycol at various  $Y$  values (physical properties are given in Table 5.2,  $Re = 400$ ,  $T_o = 300$  K and  $\Delta T = 30$  K).



**Figure 5.31**  $\dot{S}_{gen}''$  (heat transfer effect) vs.  $X$  for variable viscosity case for ethylene glycol at  $Y = 0.91$  and  $1$  (physical properties are given in Table 5.2,  $Re = 400$ ,  $T_o = 300$  K and  $\Delta T = 30$  K).

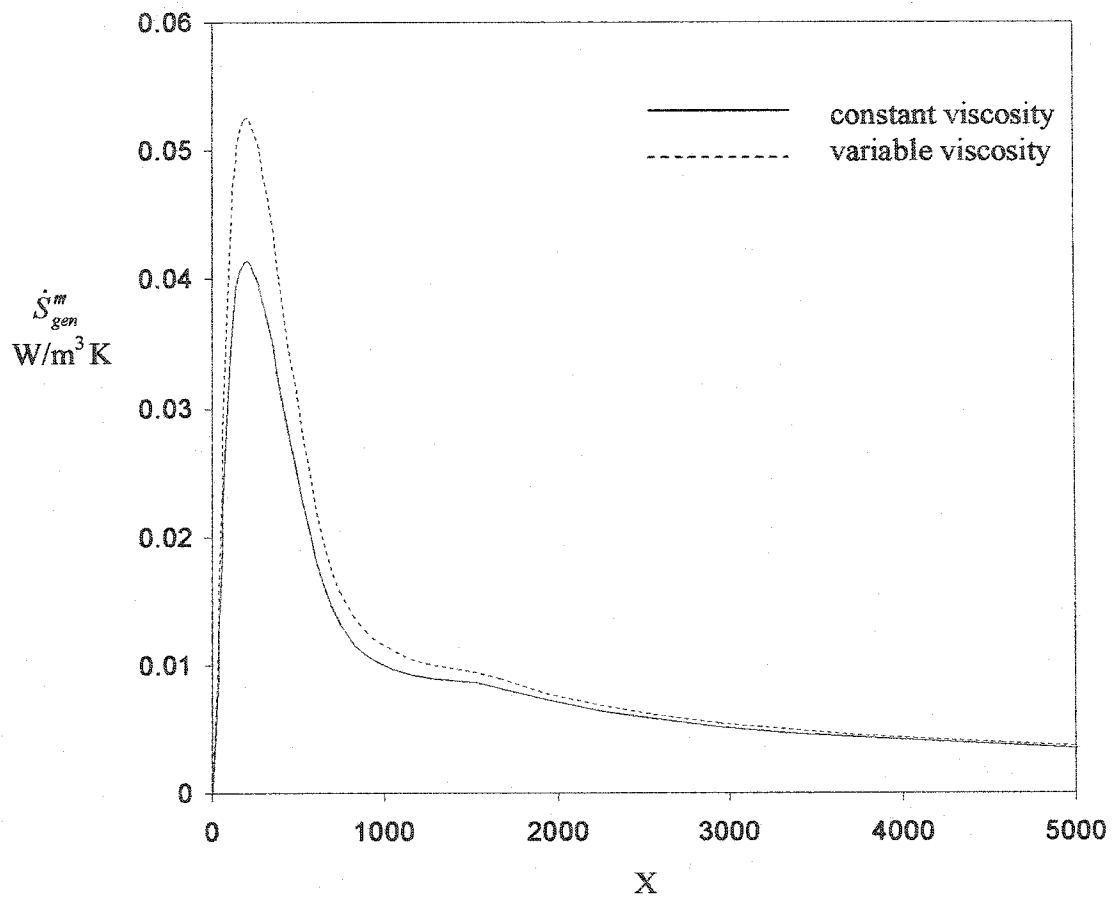


**Figure 5.32**  $\dot{S}_{gen}^m$  vs.  $X$  for constant and variable viscosity cases for ethylene glycol at  $Y = 0.92$  (physical properties are given in Table 5.2,  $Re = 400$ ,  $T_o = 300$  K and  $\Delta T = 30$  K).

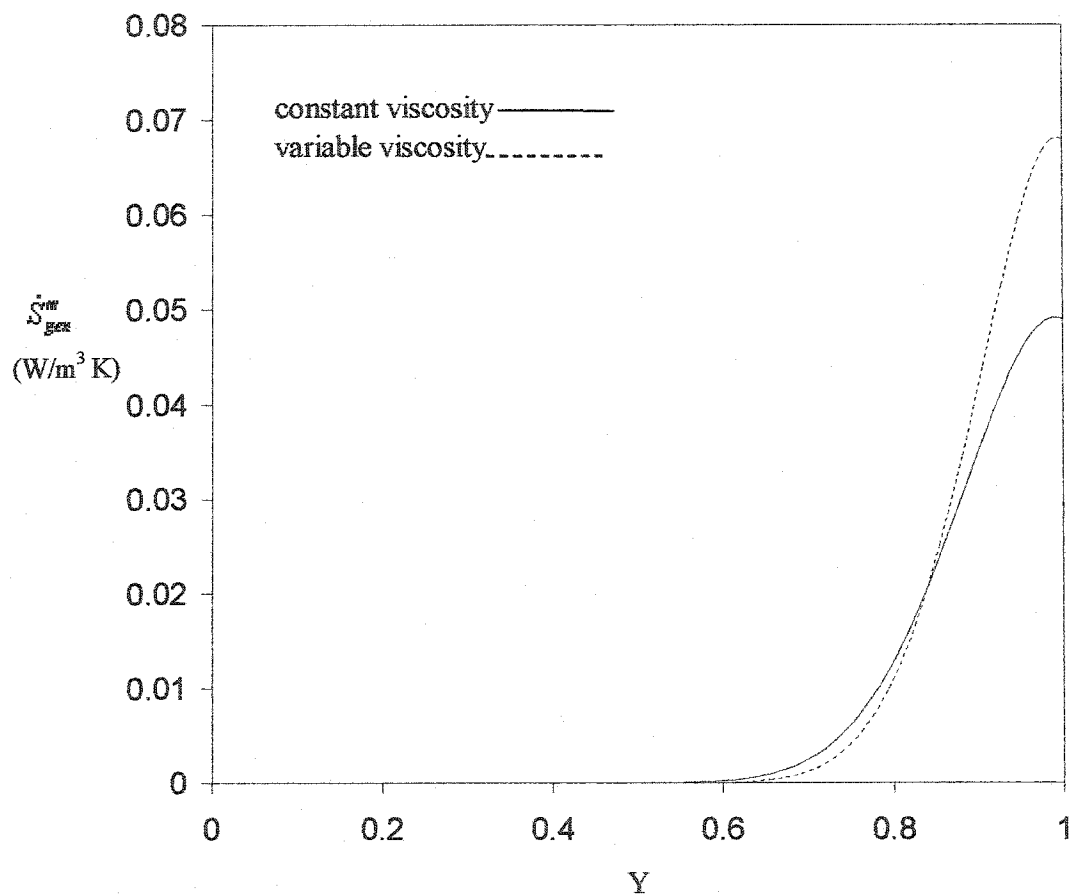


**Figure 5.33**  $\dot{S}_{gen}'''$  (heat transfer effect) vs. Y for constant and variable viscosity cases for ethylene glycol at  $X = 185$  (physical properties are given in Table 5.2,  $Re = 400$ ,  $T_0 = 300$  K and  $\Delta T = 30$  K).

### 5.3.5.3 Effect of Reynolds Number, Liquid Type and $\Delta T$ on Entropy Generation

One of the main objectives of this study is to investigate the effect of some parameters on local entropy generation of viscous fluid flow between parallel plates. This section will elaborate the effect of some of these parameters on the local entropy generation, namely, Reynolds number, inlet-wall temperature difference and liquid type.

#### 5.3.5.3.1 Effect of Reynolds Number

Reynolds number effect has been discussed on the behavior of the velocity (Figure 5.17) and temperature (Figure 5.24) profiles. Similar behavior can be expected for the local entropy generation since the entropy generation consists of velocity and temperature data. Figure 5.34 shows plots  $\dot{S}_{gen}'''$  vs.  $X$  at  $Y = 0.90$  for ethylene glycol for  $Re = 200$  and  $400$  ( $T_0 = 300$  K and  $\Delta T = 30$  K). Similar to the behavior observed in Figures 5.17 and 5.24, increasing Reynolds number shifts and extends the entropy generation profiles downstream. Furthermore, the area under these profiles increases as the Reynolds number increases and this indicates that as the Reynolds number increases the total entropy generation between the parallel plates increases. Same behavior can be observed in Figure 5.35 but at  $Y = 0.5$ . The difference between Figure 5.34 and Figure 5.35 is that the profile in Figure 5.35 extends more downstream because the profile in Figure 5.34 is closer to the heating plate and it develops faster.

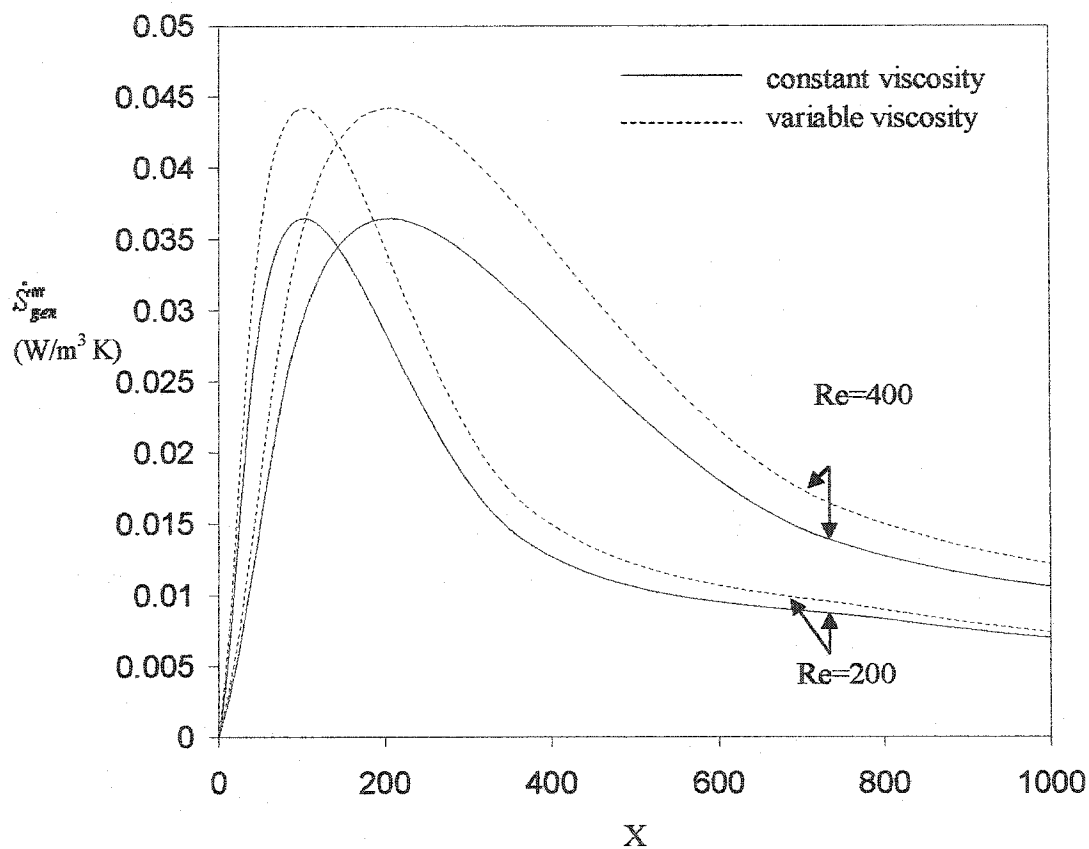


**Figure 5.34**  $\dot{S}_{gen}^m$  (heat transfer effect) vs.  $X$  at  $Y = 0.90$  for constant and variable viscosity cases for ethylene glycol for two  $Re$  values (physical properties are given in Table 5.2,  $T_o = 300$  K and  $\Delta T = 30$  K).



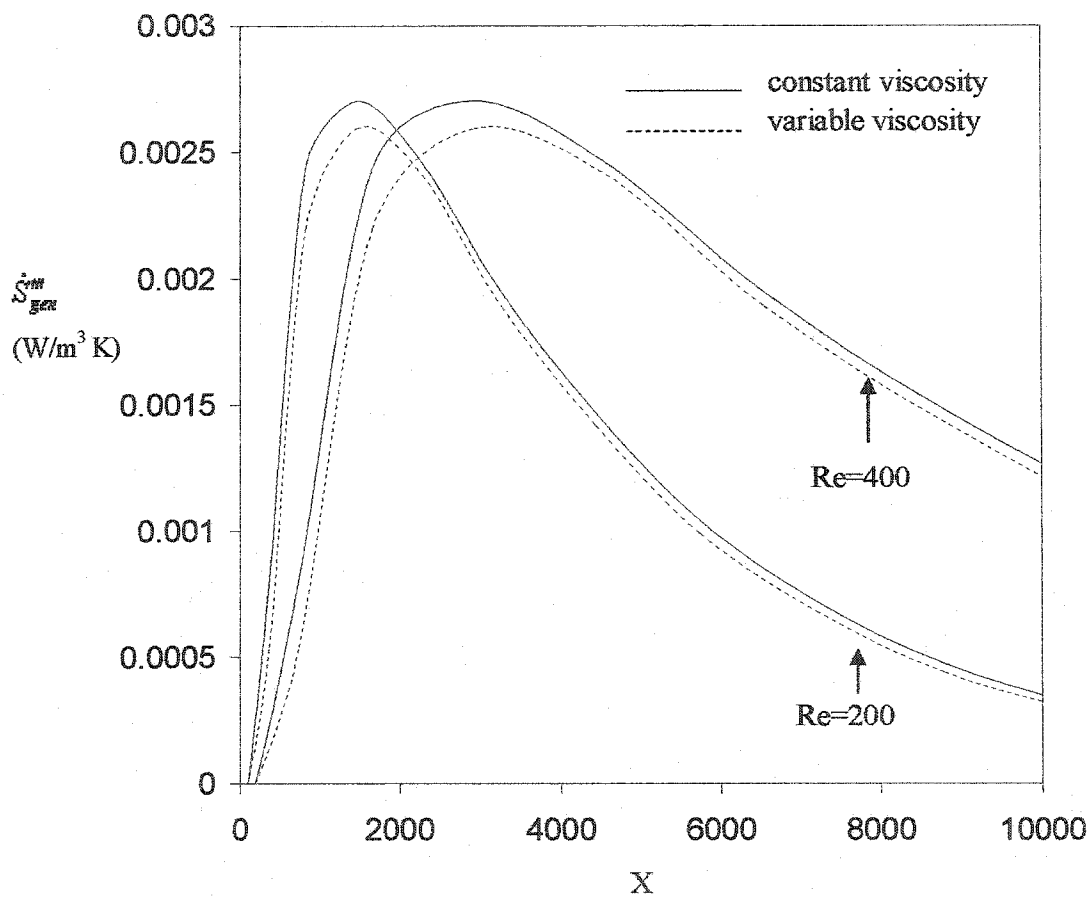


**Figure 5.35**  $\dot{S}_{gen}^m$  (heat transfer effect) vs.  $X$  at  $Y = 0.5$  for constant and variable viscosity cases for two  $Re$  values (physical properties are given in Table 5.2,  $T_0 = 300$  K and  $\Delta T = 30$  K).

### 5.3.5.3.2 Effect of Liquid Type

The liquid type can influence the amount of entropy generation. In the discussion of velocity and temperature, it was shown that the liquid type can influence the behavior of velocity and temperature profiles as shown in Figures 5.19 and 5.25. The discussion of the liquid type is based on ethylene glycol and water. When water flows between parallel plates, the fully developed profile establishes after a short distance because viscous resistance of water is weak. However, the viscous resistance in ethylene glycol is very strong and the ethylene glycol needs longer distance to develop. As a result, heat diffuses into water faster than that of ethylene glycol. In terms of entropy generation, this behavior can be demonstrated by examining Figures 5.36 and 5.37. In Figure 5.36,  $\dot{S}_{gen}^m$  vs.  $X$  is plotted for ethylene glycol and water ( $Re = 400$ ,  $T_0 = 300$  K,  $\Delta T = 30$  K and  $Y = 0.90$ ). At  $X = 600$ , it is clear that the entropy generation for water approaches zero because the temperature gradient almost equals to zero, the no jump temperature condition. But, from this figure, it is clear that the ethylene glycol needs longer distance to reach fully developed condition since at  $X = 600$  the temperature gradient is still significant. Furthermore, the quick response to temperature gradient causes the area under the water curve to be smaller. On the other hand, the area under the curve in the case of ethylene glycol is larger since it does not respond to the applied temperature difference as quickly as water. As a result, the total entropy generation for ethylene glycol will be more than that of water. This conclusion demonstrates that the total entropy generation increases as the viscosity of the liquid increases when liquid flows downstream till it develops. Figure 5.37 which represents entropy generation vs.  $Y$  at  $X = 185$  shows the influence of liquid

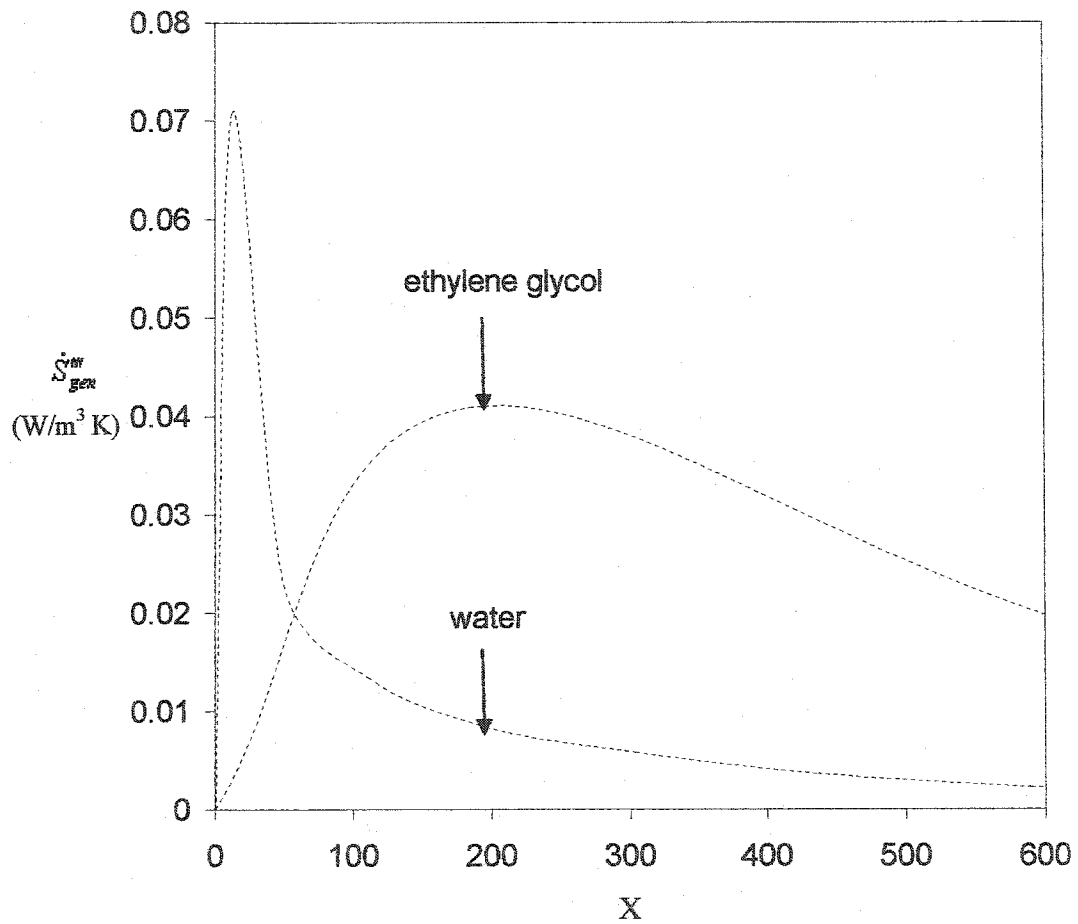


**Figure 5.36**  $\dot{S}_{gen}^m$  (heat transfer effect) vs. X for variable viscosity case for water and ethylene glycol at  $Y = 0.90$  (physical properties are given in Table 5.2,  $Re = 400$ ,  $T_0 = 300$  K and  $\Delta T = 30$  K).

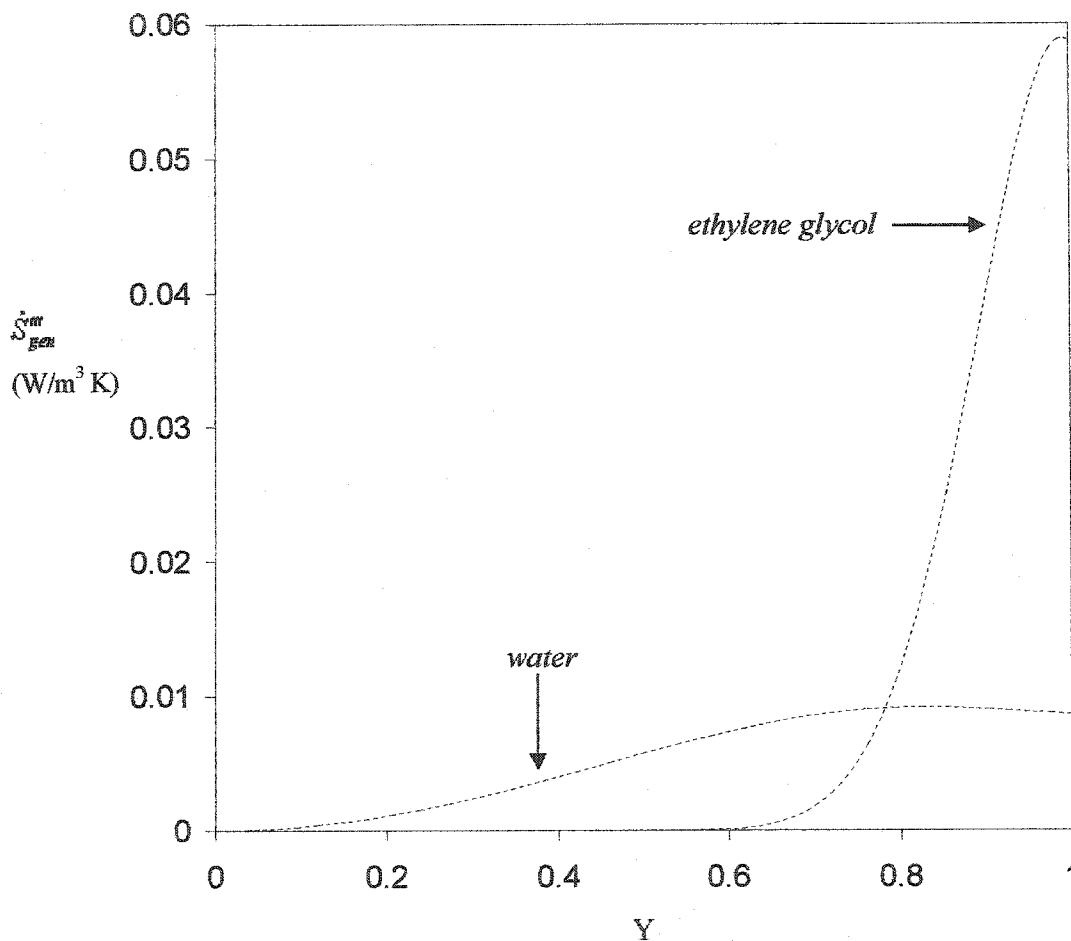


**Figure 5.37**  $\dot{S}_{gen}^m$  (heat transfer effect) vs. Y for variable viscosity case for ethylene glycol and water at  $X = 185$  (physical properties are given in Table 5.2,  $Re = 400$ ,  $T_0 = 300$  K and  $\Delta T = 30$  K).

type on entropy generation from different angle. At the wall, where  $Y = 1$ , the entropy generation in ethylene glycol is higher than that of water. At this specified  $X$  location, the temperature gradient of water is less than that of ethylene glycol. As a result, the entropy generation for ethylene glycol will be higher.

#### **5.3.5.3.3 Effect of Inlet-Wall Temperature Difference**

Heat transfer is dominant effect for entropy generation in forced fluid flow between parallel plates.  $\Delta T$  represents the heat transfer driving force. In this section, the investigation of entropy generation will be highlighted by using different  $\Delta T$  values. Here, it must be emphasized that  $T_o$  is fixed to be 300 K during each run while the wall temperature controls  $\Delta T$ . Figure 5.38 presents  $\dot{S}_{gen}''$  vs.  $X$  at  $Y = 0.90$  for ethylene glycol for  $\Delta T = 10, 20$  and  $30$  K ( $Re = 400$  and  $T_o = 300$  K). The effect of increasing  $\Delta T$  on the entropy generation is demonstrated and, as expected, it is clear that as  $\Delta T$  increases, the entropy generation increases.

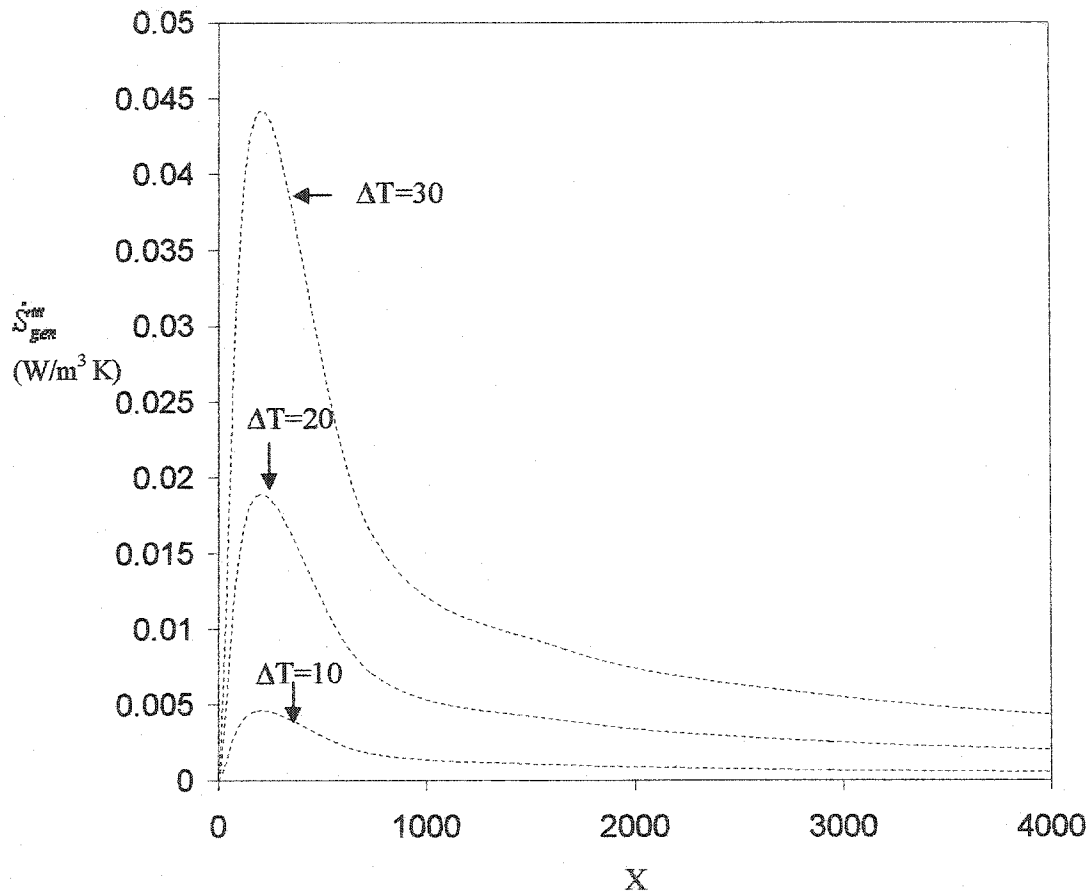


**Figure 5.38**  $\dot{S}_{gen}^m$  vs.  $X$  at  $Y = 0.90$  for variable viscosity case for ethylene glycol at different  $\Delta T$  values (physical properties are given in Table 5.2,  $Re = 400$  and  $T_0 = 300$  K).

### 5.3.5.4 $\dot{S}_{\Delta Y}$ and $\dot{S}_{\Delta Y \Delta X}$

In the analysis of the entropy generation, entropy generation must be minimized in order to avoid the loss of the available work in any system. In order to achieve this minimization of the entropy generation, the analyzer needs to discover the parameters that influence the entropy generation as well as the locations as the quantity of the entropy generation can be enormous. Although this study introduced entropy generation profiles and the parameters that affect these profiles, the optimum parameters that satisfy the minimum entropy generation conditions is out of the scope of this study. Thus, this section will cover important figures that can help in achieving the minimization of the entropy generation. The first figure, Figure 5.39, is the plot of total entropy generation along Y between the parallel plates at specified X-locations,  $\dot{S}_{\Delta Y}$ , for different Reynolds numbers.  $\dot{S}_{\Delta Y}$  was obtained by averaging the entropy generation data along y-direction using Simpson rule. This figure illustrates that  $\dot{S}_{\Delta Y}$  initially increases in X-direction reaching a maximum value then it decreases as the uniform temperature is reached between the parallel plates. This increase and decrease is related to the behavior of  $\dot{S}_{gen}^m$  vs. X that was explained in Figures 5.29, 5.30 and 5.31. Increasing the Reynolds number shifts and extends these profiles and this is related to the shifting and extending of velocity and temperature profiles that were explained earlier.

Figure 5.40 is a plot of total entropy generation from the inlet to  $X = 7500$ ,  $\dot{S}_{\Delta Y \Delta X}$ , vs. Reynolds number. The total entropy generation  $\dot{S}_{\Delta Y \Delta X}$ , represents the overall average of entropy in the X and Y-directions between the parallel plates. As the Reynolds number increases,  $\dot{S}_{\Delta Y \Delta X}$  increases. An inspection of Figure 5.34 explains this behavior. In Figure

5.34, the comparison was between Reynolds number = 200 and 400. As it was discussed earlier, the increase of the Reynolds number shifts and extends the entropy generation profile and that is related to the extending and shifting of velocity and temperature profiles. The extension of the entropy generation profile creates more area under the curve of the entropy generation. As a result, as the Reynolds number increases, the total entropy generation increases due to the increase of the area under the curves.



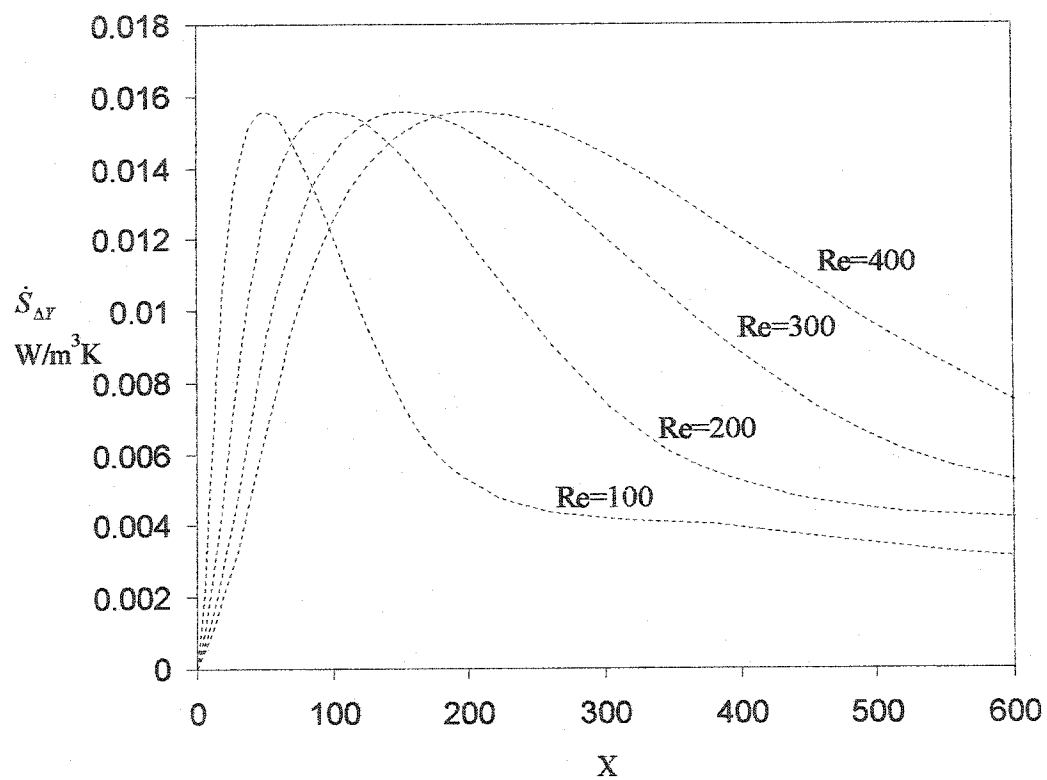


**Figure 5.39**  $\dot{S}_{\Delta T}$  vs.  $X$  for variable viscosity case for ethylene glycol for different  $Re$  numbers (physical properties are given in Table 5.2,  $T_0 = 300$  K,  $\Delta T = 30$  K).

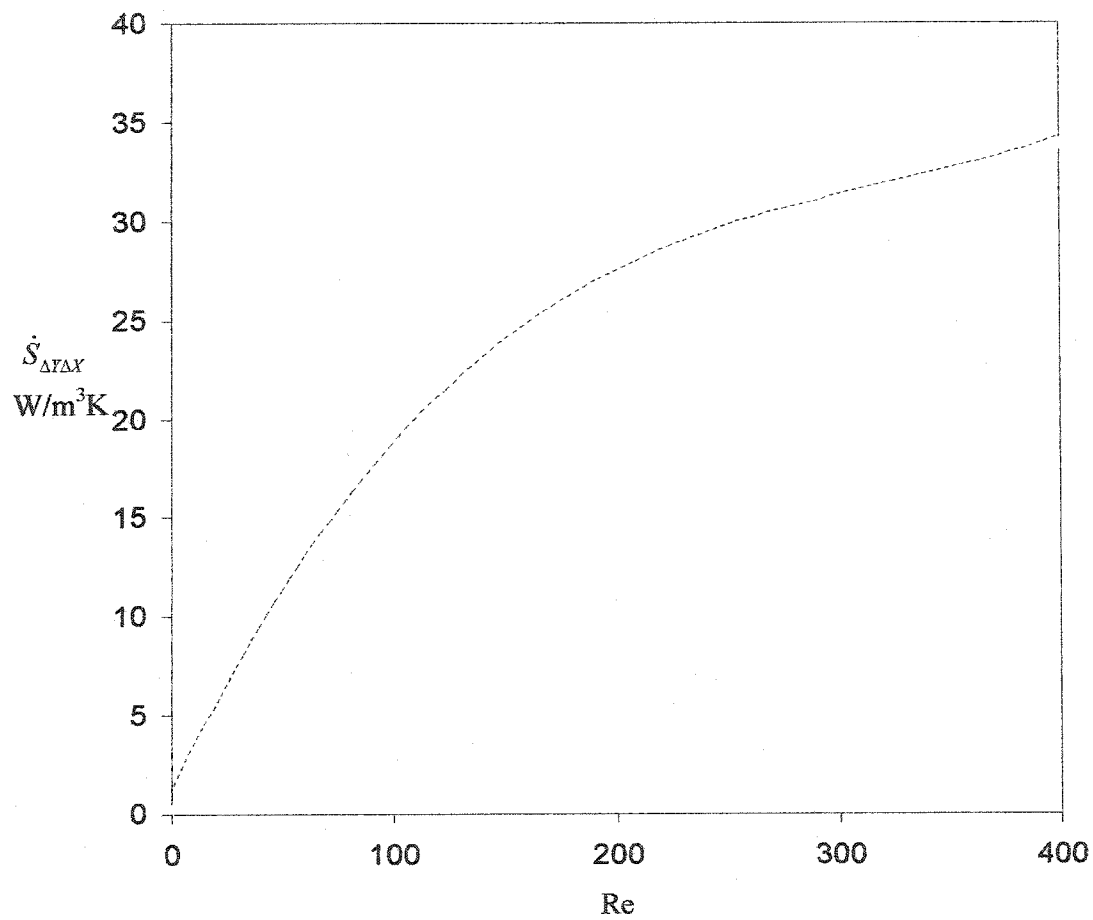


**Figure 5.40**  $\dot{S}_{\Delta T_{\Delta X}}$  vs. Re for variable viscosity case for ethylene glycol between  $X = 0$  and  $X = 7500$  (physical properties are given in Table 5.2,  $T_0 = 300$  K,  $\Delta T = 30$  K).

## 5.4 Constant Heat Flux:

### 5.4.1 Velocity Profiles

In a similar manner to the constant wall temperature case, velocity distributions can be obtained in the case of constant heat flux by solving vorticity, stream function and energy equations iteratively. After that, Equations 3.15 and 3.16 are utilized to obtain velocity distributions. Both plates are subjected to the same constant heat flux which equals to  $10 \text{ W/m}^2$ . The viscosity linear relationship is also applied in this case and the inlet liquid temperature ( $T_o$ ) equals to 300 K. The applicability of the linear relationship is valid to maximum temperature difference equals to  $30 \text{ }^\circ\text{C}$  (330 K). The liquid is continuously heated and its temperature increases. Therefore, the length of the parallel plates is carefully chosen in order to make sure that the liquid temperature does not exceed 330 K in any point throughout the liquid in the duct.

In order to investigate the velocity profiles clearly,  $U$  vs.  $X$  is plotted for ethylene glycol at various  $Y$  values in Figures 5.41, 5.42, 5.43 and 5.44 (physical properties are given in Table 5.2,  $Re = 400$ ,  $T_o = 300 \text{ K}$ ,  $Q = 10 \text{ W/m}^2$ ). Further, the velocity profiles obtained from variable viscosity case are compared to those of constant viscosity. Figure 5.41 represents  $U$  vs.  $X$  at  $Y=0$  for constant and variable viscosity. The velocity decreases as the liquid proceeds downstream due to the temperature gradient. The liquid is heated until the liquid temperature becomes 330 K and this temperature occurs at  $X= 10000$ . The same velocity behavior appears in Figure 5.42 which presents  $U$  vs.  $X$  at  $Y = 0.43$ . The only difference between the two figures is that Figure 5.41 shows more deviation than Figure 5.42 from the constant viscosity profile because the temperature gradient is higher in Figure 5.42 (see the difference in the  $U$  values in both figures). Further, Figure 5.43

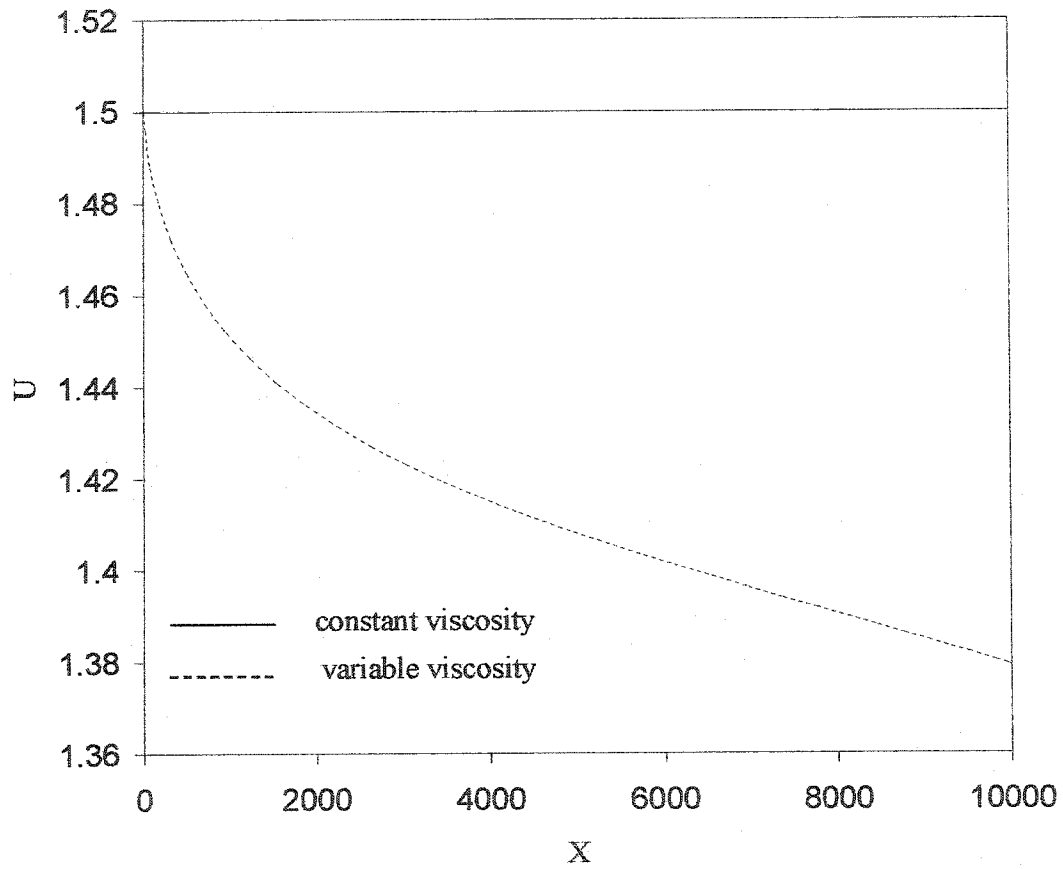


**Figure 5.41**  $U$  vs.  $X$  for constant and variable viscosity cases for ethylene glycol at  $Y = 0$  (physical properties are given in Table 5.2,  $Re = 400$ ,  $T_o = 300$  K and  $Q'' = 10$  W/m<sup>2</sup>).

represents  $U$  vs.  $X$  at  $Y = 0.95$ . Here, the velocity profile increases as the liquid proceeds downstream because the liquid viscosity decreases due to the effect of heating which causes a decrease in the shear stresses between liquid molecules and therefore an increase in the velocity. Moreover, Figure 5.44 represents  $U$  vs.  $X$  at  $Y = 0.5$ . It represents a combination between Figure 5.43 and Figure 5.42. At a distance close to the entrance, the velocity profile shows a decrease then an increase as the flow proceeds downstream.

Now, the change of axial velocity in the normal direction will be investigated. Figure 5.45 is a plot of  $U$  vs.  $Y$  for ethylene glycol at  $X = 4400$  (physical properties are given in Table 5.2,  $Re = 400$ ,  $T_o = 300$  K,  $Q = 10$  W/m<sup>2</sup>). The figure is similar to Figure 5.3 and it was discussed in detail in Section 5.3.1.2.

Furthermore, the change of the normal velocity in normal direction will be discussed. Figure 5.46 represents this change.  $V$  vs.  $Y$  is plotted for ethylene glycol at various  $X$  values for variable viscosity (physical properties are given in Table 5.2,  $Re = 400$ ,  $T_o = 300$  K,  $Q = 10$  W/m<sup>2</sup>). Here, the continuous heating changes the axial velocity as the flow goes downstream. Therefore, the change of the normal velocity in the normal direction does not equal to zero. At the entrance the normal velocity equal to zero. It is clear that from the figure the magnitude of the normal velocity decreases as the  $X$  value increases.

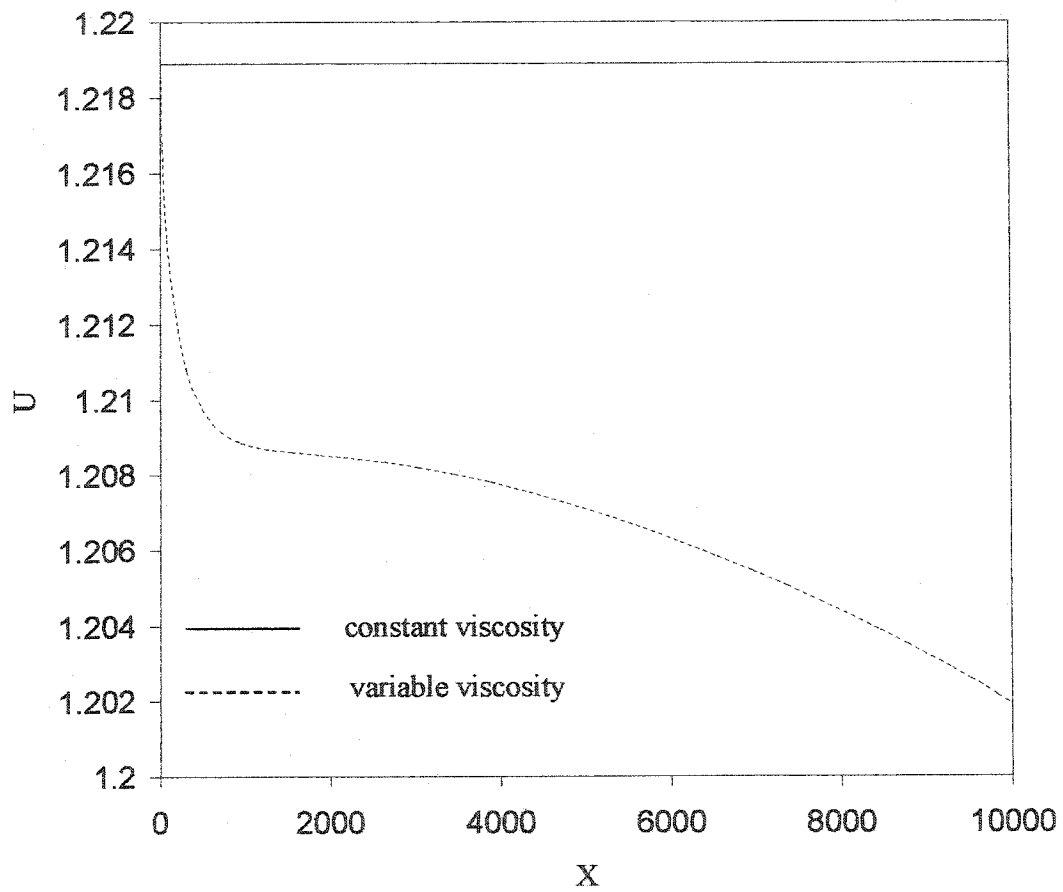


**Figure 5.42**  $U$  vs.  $X$  for constant and variable viscosity cases for ethylene glycol at  $Y = 0.43$  (physical properties are given in Table 5.2,  $Re = 400$ ,  $T_o = 300$  K and  $Q'' = 10$  W/m<sup>2</sup>).

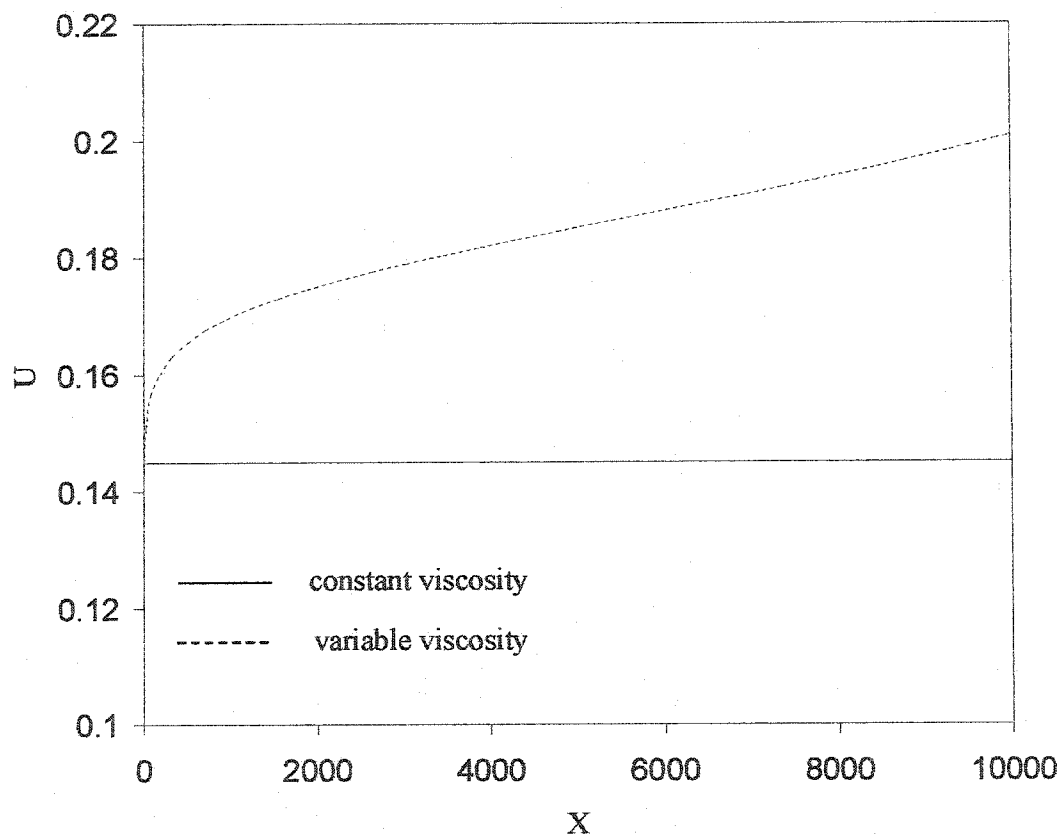


**Figure 5.43**  $U$  vs.  $X$  for constant and variable viscosity cases for ethylene glycol at  $Y = 0.95$  (physical properties are given in Table 5.2,  $Re = 400$ ,  $T_o = 300$  K and  $Q'' = 10$  W/m<sup>2</sup>).

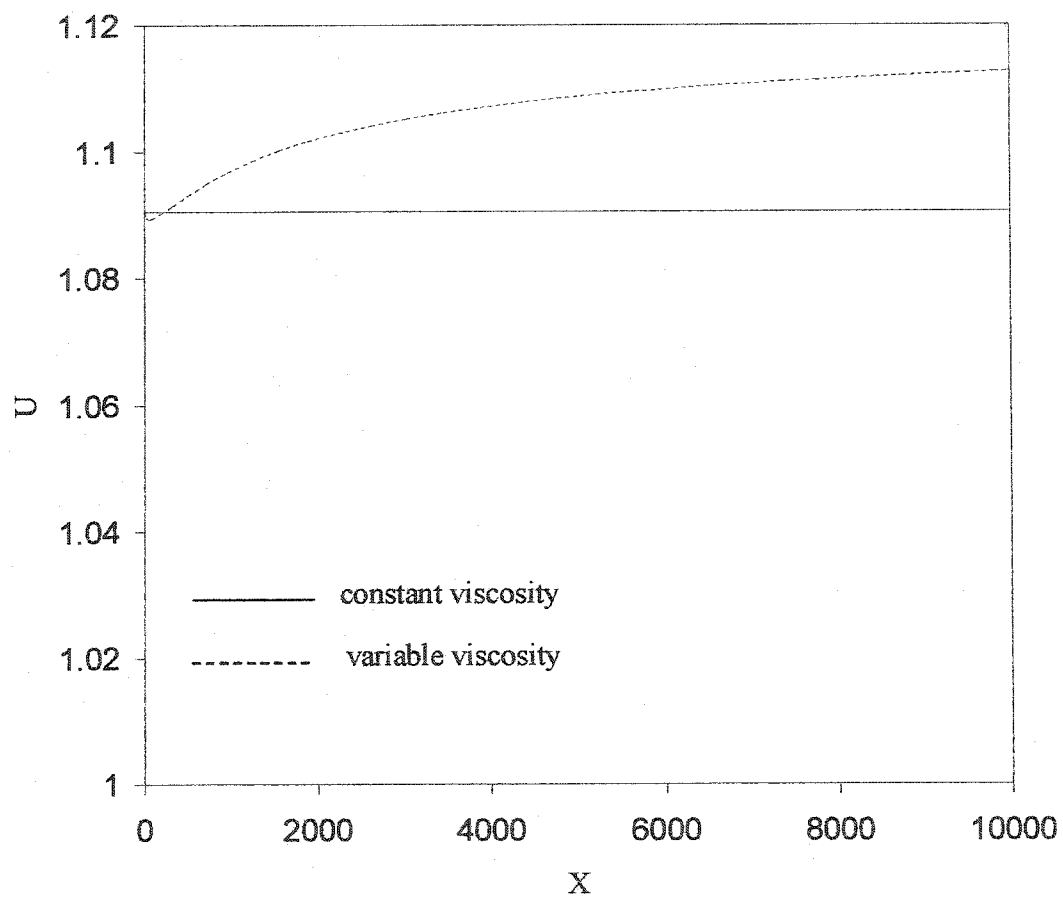


**Figure 5.44**  $U$  vs.  $X$  for constant and variable viscosity cases for ethylene glycol at  $Y = 0.5$  (physical properties are given in Table 5.2,  $Re = 400$ ,  $T_o = 300$  K and  $Q'' = 10$  W/m<sup>2</sup>).



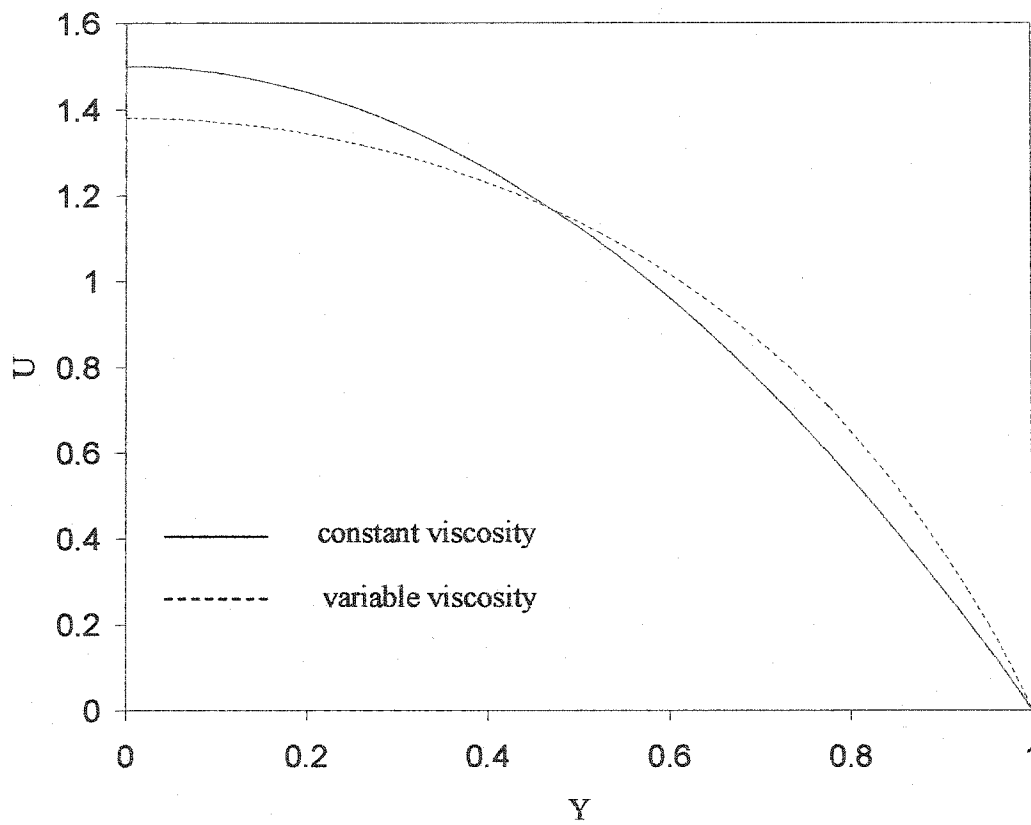


**Figure 5.45**  $U$  vs.  $Y$  for constant and variable viscosity cases for ethylene glycol at  $X = 10000$  (physical properties are given in Table 5.2,  $Re = 400$ ,  $T_o = 300$  K,  $Q'' = 10$  W/m<sup>2</sup>).

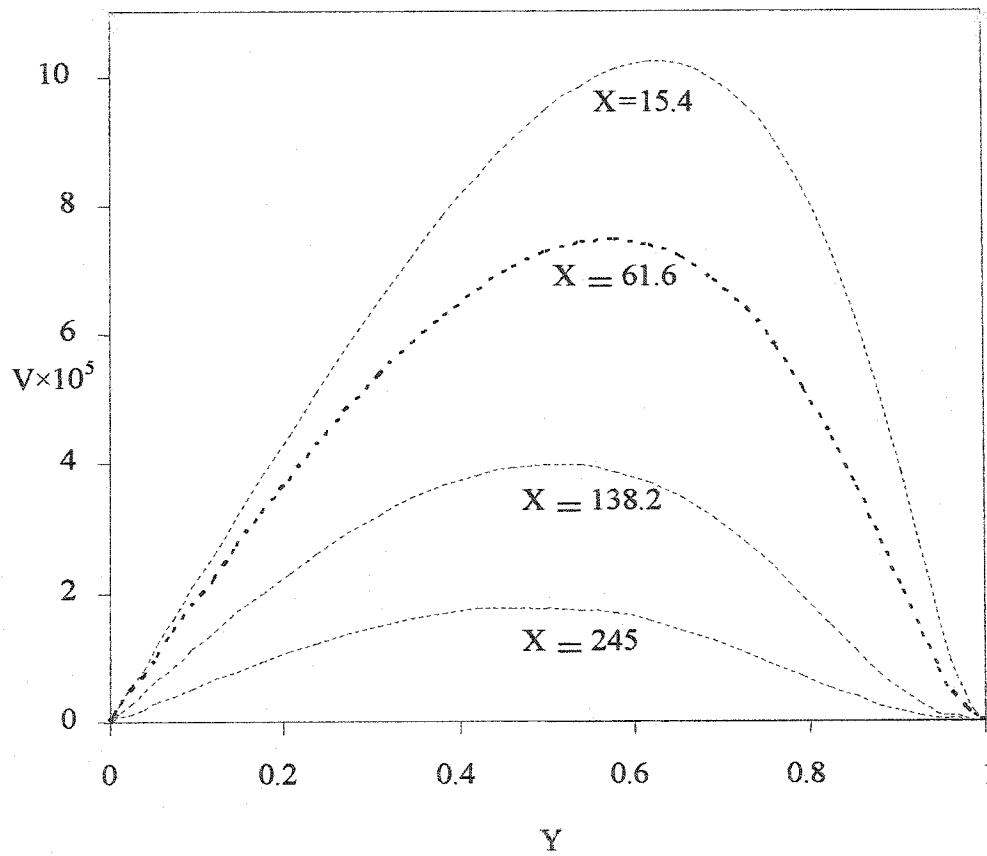


**Figure 5.46**  $V$  vs.  $Y$  for variable viscosity case for ethylene glycol at various  $X$  values (physical properties are given in Table 5.2,  $Re = 400$ ,  $T_o = 300$  K and  $Q'' = 10$  W/m<sup>2</sup>).

## 5.4.2 Effect of Reynolds Number and the Liquid type on Velocity Profile

### 5.4.2.1 Effect of Reynolds Number

Reynolds number as it was shown is one of the parameters that affect the velocity profiles as well as temperature profiles. The change of the temperature boundary condition does not eliminate the effect of the Reynolds number on velocity and temperature profiles. To see the effect of the Reynolds number on velocity profile, Figure 5.47 is plotted for  $U$  vs.  $X$  for ethylene glycol at  $Y = 0.52$  for various Reynolds numbers. (physical properties are given in Table 5.2,  $T_o = 300$  K,  $Q = 10$  W/m<sup>2</sup>). For the constant wall temperature, the velocity profile becomes fully developed at the end of the parallel plates where the inlet-wall temperature difference equals to zero. However, for constant heat flux, the inlet liquid is heated until the temperature becomes 330 K since the linear viscosity relation is not valid beyond 330 K. The length of the parallel plates is chosen based on satisfying this temperature. So, the profiles in Figure 5.47 demonstrate the velocity profile up to the length at which liquid temperature equals to 330 K. As the Reynolds number increases, the required length of the parallel plates increases. In the figure, when  $Re = 400, 300, 200$  and  $100$ , the required length at which the temperature equals 330 K are 10000, 7500, 5000 and 2500, respectively.

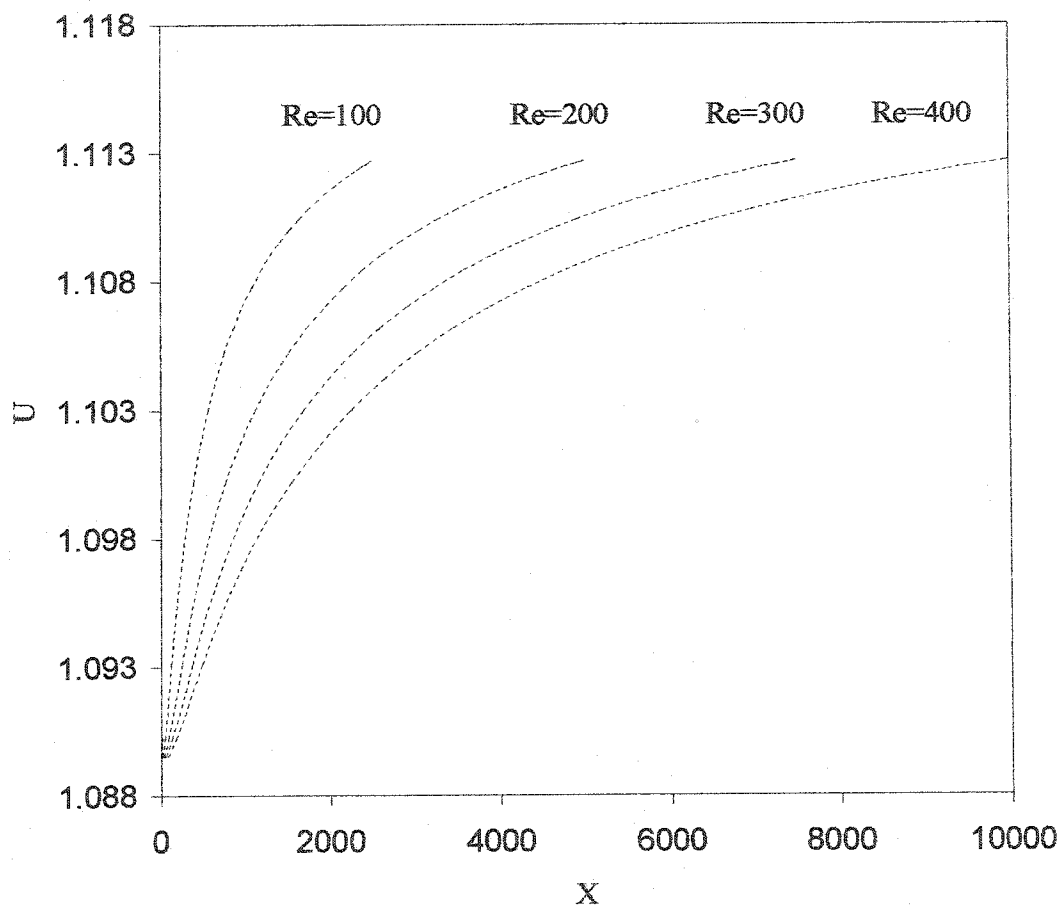


**Figure 5.47**  $U$  vs.  $X$  at  $Y = 0.52$  for variable viscosity case for ethylene glycol (physical properties are given in Table 5.2,  $Re = 100, 200, 300, 400$ ,  $T_o = 300$  K and  $Q'' = 10$  W/m<sup>2</sup>).

#### 5.4.2.2 Effect of Liquid Type

The effect of temperature dependent viscosity appears clearly in the more viscous liquids such as ethylene glycol. On the other hand, the less viscous liquids such as water do not show strong temperature dependency effect on viscosity. This is demonstrated in Figure 5.48 which is a plot of  $U$  vs.  $X$  at  $Y = 0$  for variable viscosity of ethylene glycol and water (physical properties are given in Table 5.2,  $Re = 400$ ,  $T_o = 300$  K and  $Q = 10$  W/m<sup>2</sup>). In this figure, the ethylene glycol responds to the effect of the heating higher than that of water. Moreover, the required length of the parallel plates at which the liquid temperature equals to 330 K for water is smaller than that of ethylene glycol. The length of the parallel plates when the liquid is water equals to 1500 whereas the length of the parallel plates when the liquid is ethylene glycol equals to 10000. This is because the Prandtl number of ethylene glycol is higher than that of water.

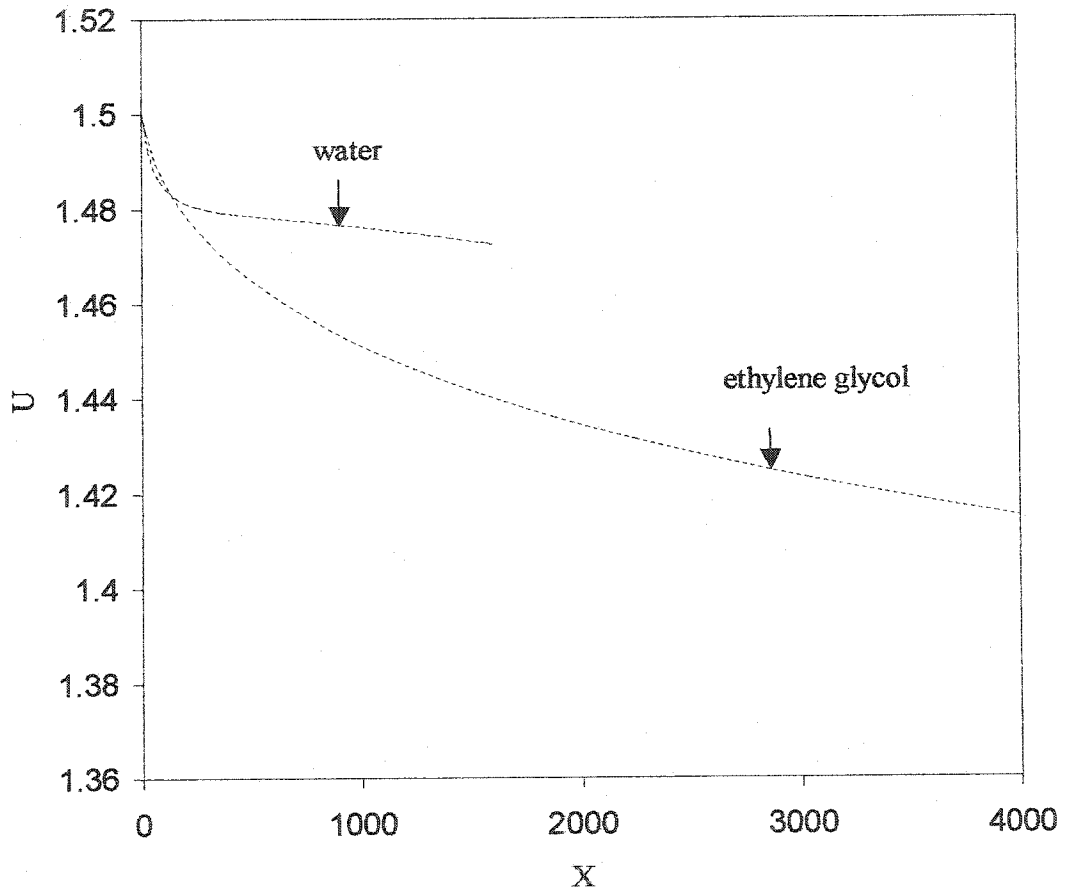


**Figure 5.48**  $U$  vs.  $X$  for variable viscosity case for ethylene glycol and water at  $Y = 0$  (physical properties are given in Table 5.2,  $Re = 400$ ,  $T_o = 300$  K and  $Q'' = 10$  W/m<sup>2</sup>).

### 5.4.3 Temperature Profiles

To investigate temperature profiles, temperature behavior in axial and normal directions needs to be demonstrated. Figures 5.49, 5.50, 5.51 are plotted for  $\Theta$  vs.  $X$  at various  $Y$  values. The three figures are plotted for  $Y$ -values equal to 0, 1 and 0.52, respectively. For Figure 5.49, the temperature gradually increases because it is not located close to the source of heating while in Figure 5.50 the temperature increases sharply since it is located at the source of heating. The temperature profile at  $Y = 0.52$  increases almost in linear fashion.

To examine the temperature profiles in  $Y$ -direction, Figure 5.52 is plotted for  $\Theta$  vs.  $Y$  for different  $X$  values. In this figure, it is clear that as the  $X$  increases the temperature increases and this is due to the increase of the amount of heating for the liquid from the constant heat flux.

### 5.4.4 Effect of Reynolds Number and Liquid Type on Temperature Profiles

#### 5.4.4.1 Effect of Reynolds Number

It was demonstrated that Reynolds number influences the velocity profiles as well as the temperature profiles in the case of constant wall temperature. Likewise, the Reynolds number can influence the temperature profile in the constant heat flux case. This can be figured out from Figure 5.53 which is plotted for  $\Theta$  vs.  $X$  at  $Y = 0$  for different Reynolds number values. Here, as the Reynolds number increases, the temperature profiles shifts downstream.

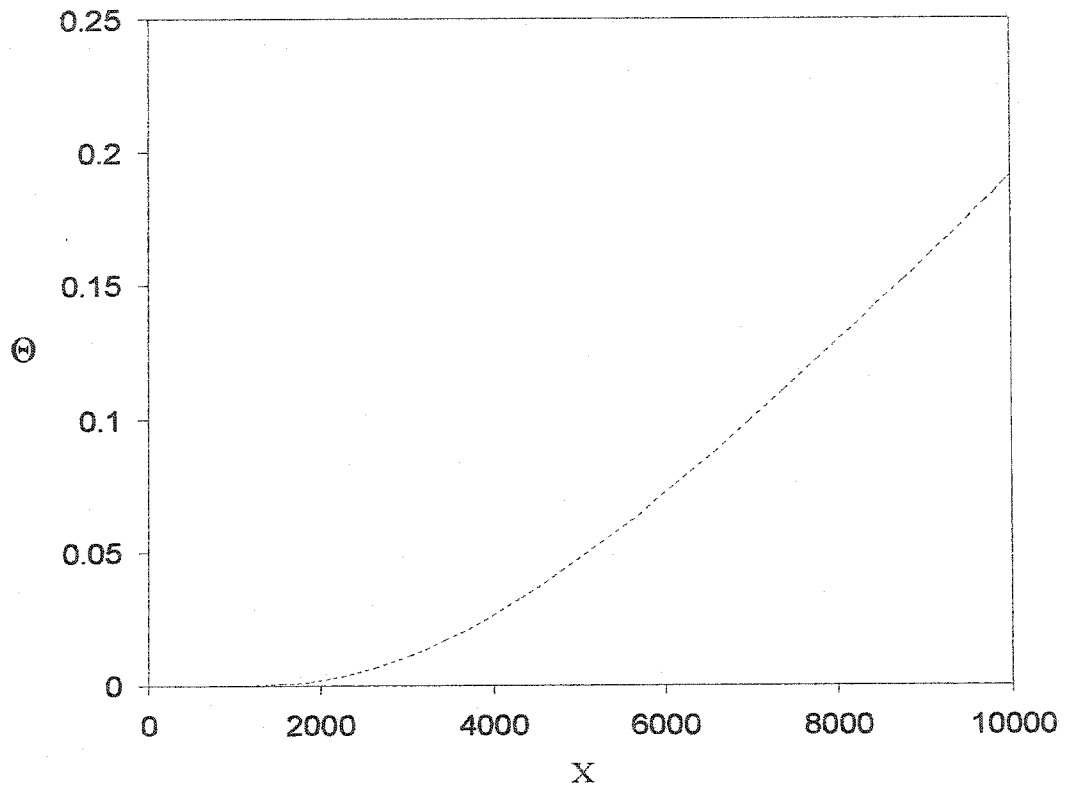


**Figure 5.49**  $\Theta$  vs.  $X$  for variable viscosity case for ethylene glycol at  $Y = 0$  (physical properties are given in Table 5.2,  $Re = 400$ ,  $T_o = 300$  K and  $Q'' = 10$  W/m<sup>2</sup>).



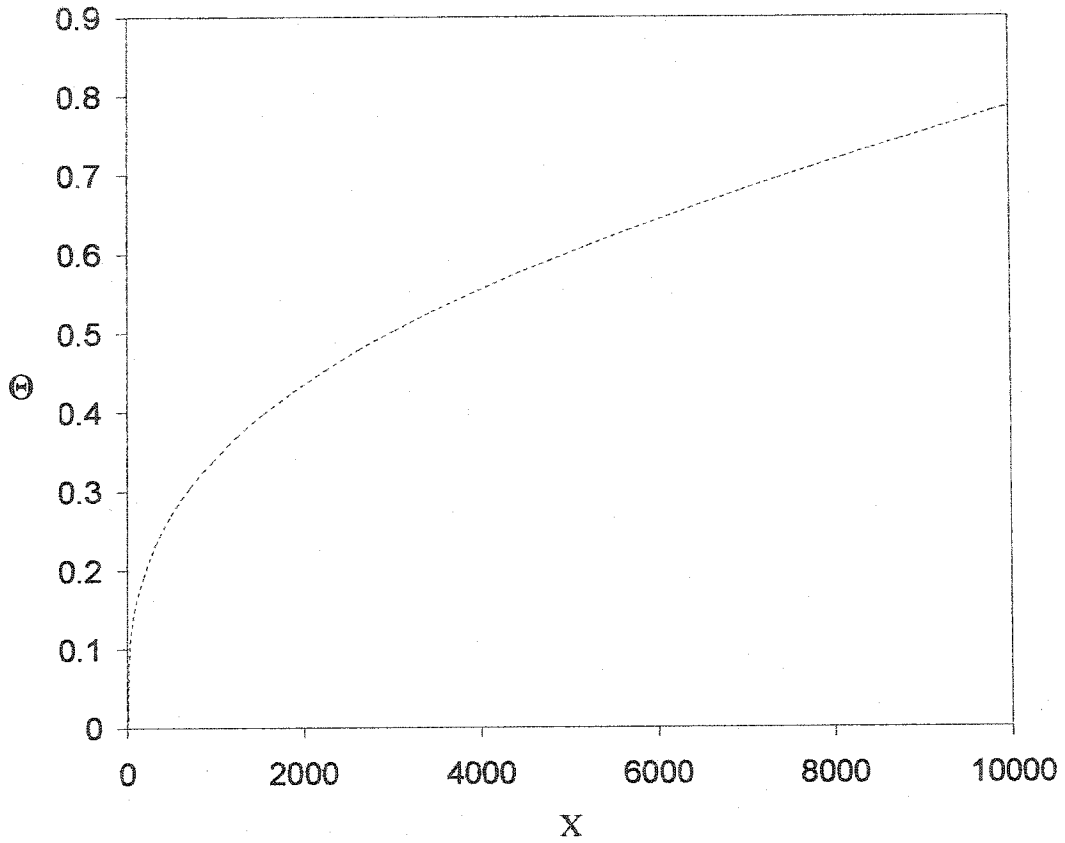


**Figure 5.50**  $\Theta$  vs.  $X$  for variable viscosity case for ethylene glycol at  $Y = 1$  (physical properties are given in Table 5.2,  $Re = 400$ ,  $T_o = 300$  K and  $Q'' = 10$   $W/m^2$ ).

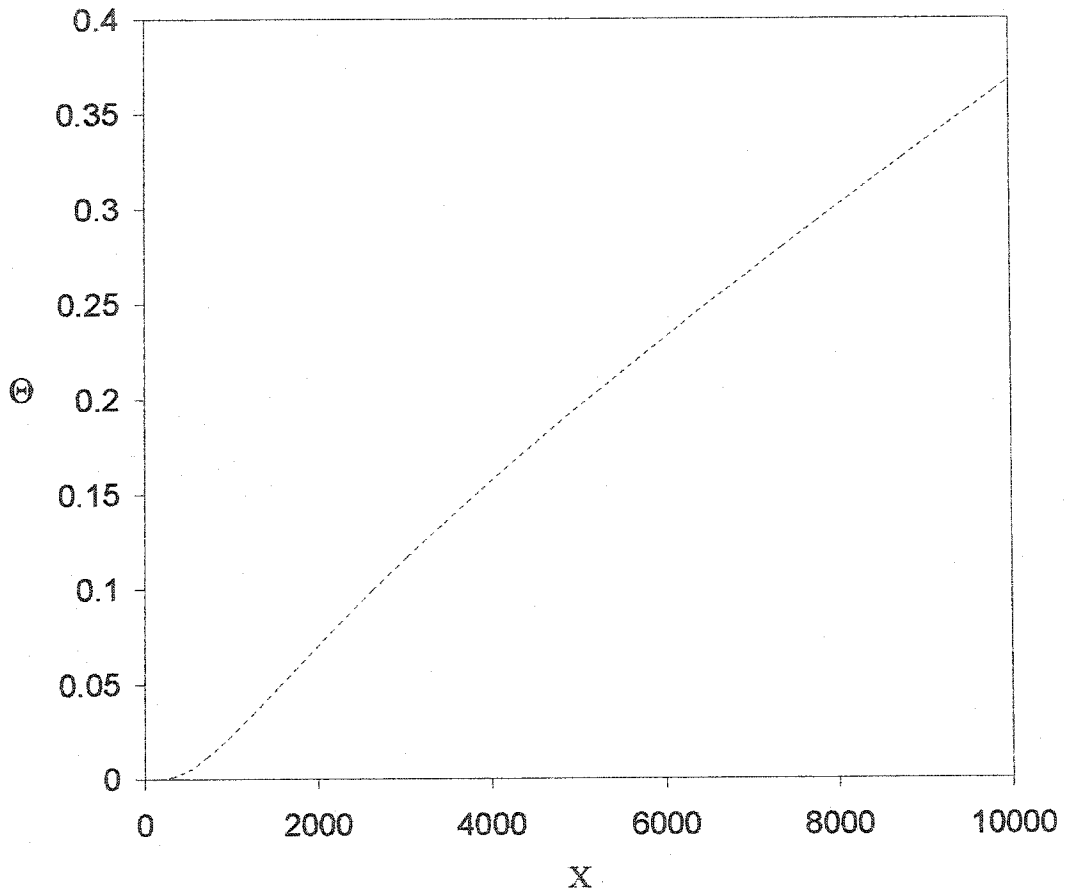


**Figure 5.51**  $\Theta$  vs.  $X$  for variable viscosity case for ethylene glycol at  $Y = 0.52$  (physical properties are given in Table 5.2,  $Re = 400$ ,  $T_o = 300$  K and  $Q'' = 10$  W/m<sup>2</sup>).

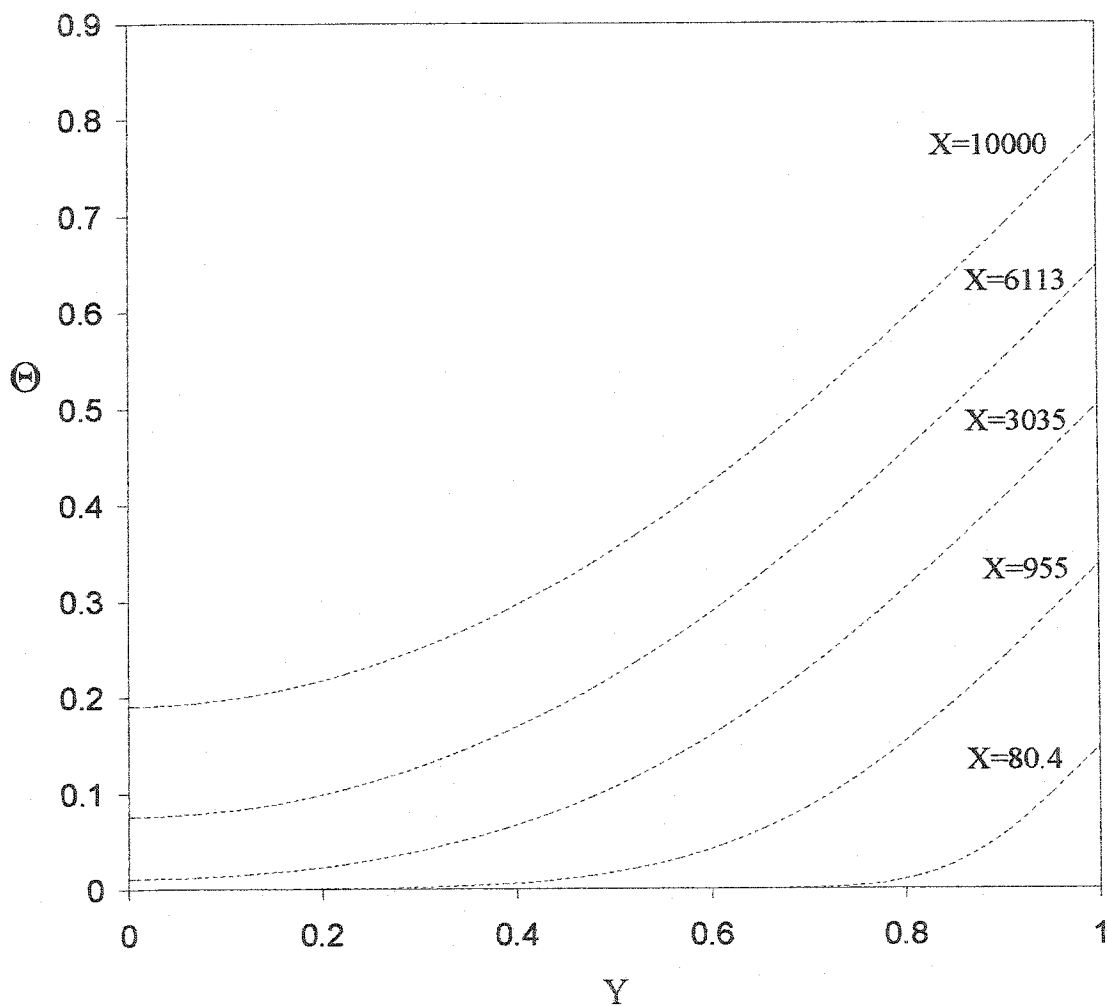


**Figure 5.52**  $\Theta$  vs.  $Y$  for variable viscosity for ethylene glycol at various  $X$  values (physical properties are given in Table 5.2,  $Re = 400$ ,  $T_o = 300$  K and  $Q'' = 10$  W/m<sup>2</sup>).

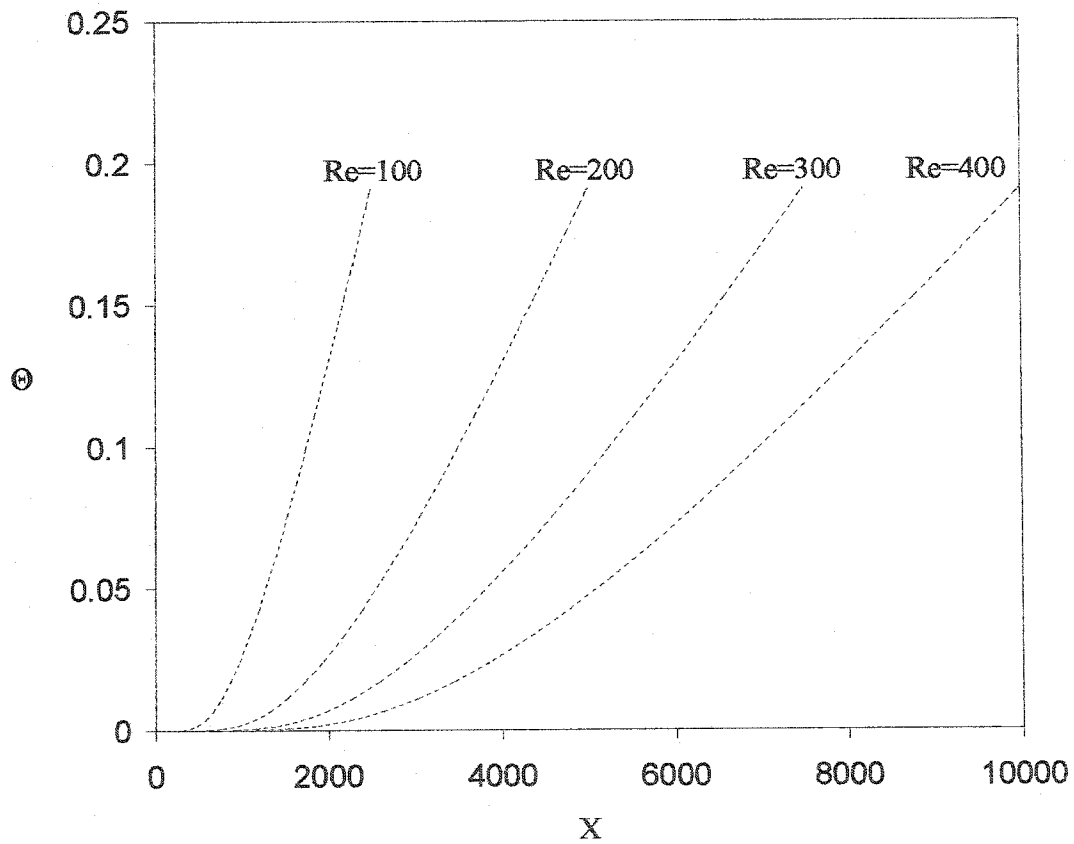


**Figure 5.53**  $\theta$  vs.  $X$  for variable viscosity case for ethylene glycol at  $Y = 0$  (physical properties are given in Table 5.2,  $Re = 100, 200, 300, 400$ ,  $T_o = 300$  K and  $Q'' = 10$  W/m<sup>2</sup>).

#### 5.4.4.2 Effect of Liquid Type

The two liquids, ethylene glycol and water, are compared to show the effect of heating on the liquid behavior. Figure 5.54 is plotted for  $\Theta$  vs.  $X$  for ethylene and water at  $Y=0$  (physical properties are given in Table 5.2,  $Re = 400$ ,  $T_o = 300$  K and  $Q = 10$  W/m<sup>2</sup>). In this figure, the length of the parallel plates at which the liquid becomes 330 K in the case of water is smaller than that of ethylene glycol. This is because heat diffuses quickly in water and slowly in ethylene glycol and that can be figured out from the magnitude of Prandtl number.

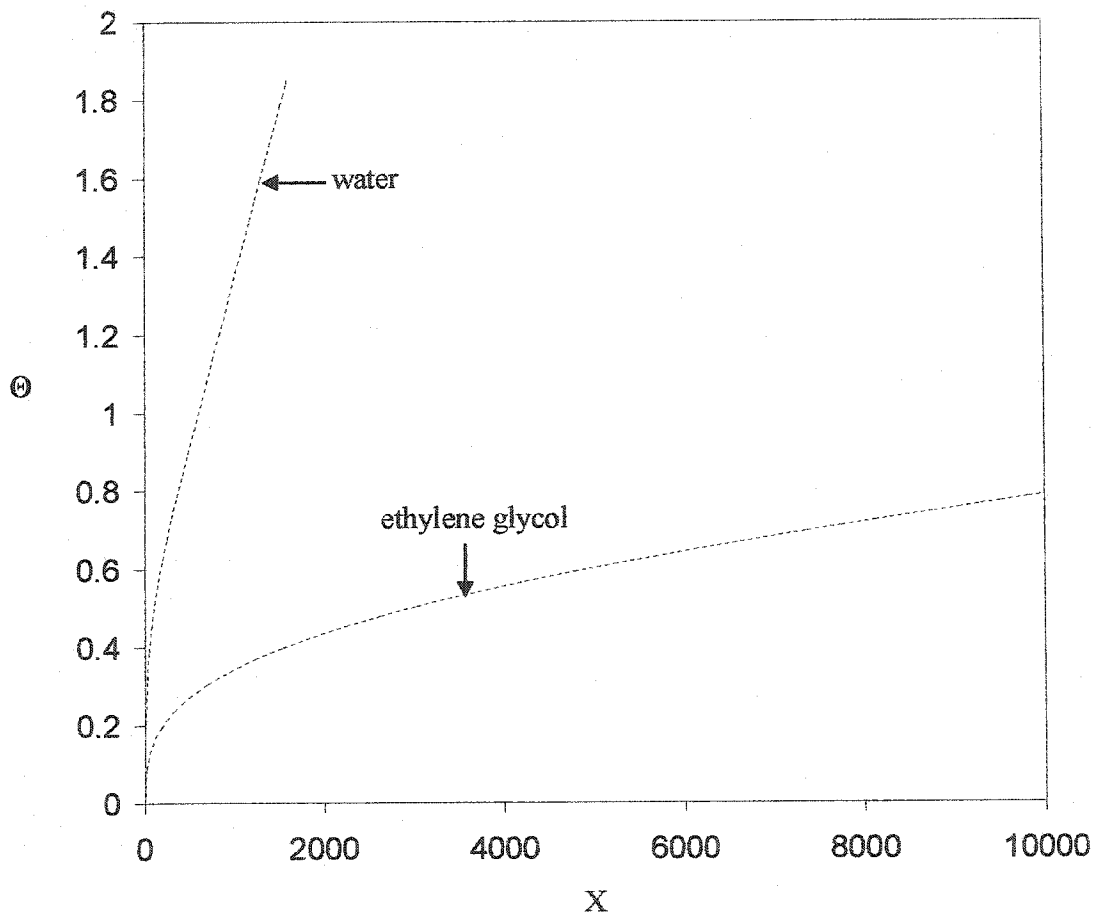


**Figure 5.54**  $\theta$  vs.  $X$  for variable viscosity case for ethylene glycol and water at  $Y = 1$  (physical properties are given in Table 5.2  $Re = 400$ ,  $T_o = 300$  K and  $Q'' = 10$   $W/m^2$ ).

### 5.4.5 Entropy Generation Profiles

The source of entropy generation between the heated parallel plates comes from heat transfer effect and fluid friction effect. It was found that the entropy generation from fluid friction effects could be neglected. Thus, the total entropy generation is a result of the heat transfer effect. In this section, the discussions of the entropy generation profiles are divided into three parts. The first part is to discuss the patterns and the behavior of the  $\dot{S}_{gen}^m$  while the second part is to discuss the effect of some parameters on  $\dot{S}_{gen}^m$  profiles. The third part is to discuss  $\dot{S}_{\Delta Y}$  and  $\dot{S}_{\Delta Y \Delta X}$  for the constant heat flux case.

#### 5.4.5.1 Patterns of Entropy Generation Profiles

To investigate the entropy generation profiles in the constant heat flux case, the patterns of the profiles should be demonstrated. As the fluid flows downstream, it is subjected to heat transfer that increases entropy generation in the fluid. To show this effect, Figure 5.55 is plotted for  $\dot{S}_{gen}^m$  vs. X for different Y-values. At a location very close to the wall, the entropy generation is expected to be higher than any location in the parallel plates. That is related to the significant effect of heating near the wall since the source of heat flux comes from the wall. To complete the investigation of entropy generation, the entropy generation obtained from the variable viscosity should be compared to those obtained from constant viscosity. For this purpose, Figure 5.56 is plotted for  $\dot{S}_{gen}^m$  vs. X at Y-values equals to 0.52 and 0.74. From the figure, the generation of the entropy at Y = 0.74 is higher than the generation of entropy at Y = 0.52 since at Y = 0.74 is closer to the heating wall. Furthermore, these two profiles are compared to profiles that are obtained from constant viscosity. It is clear that the deviation between the

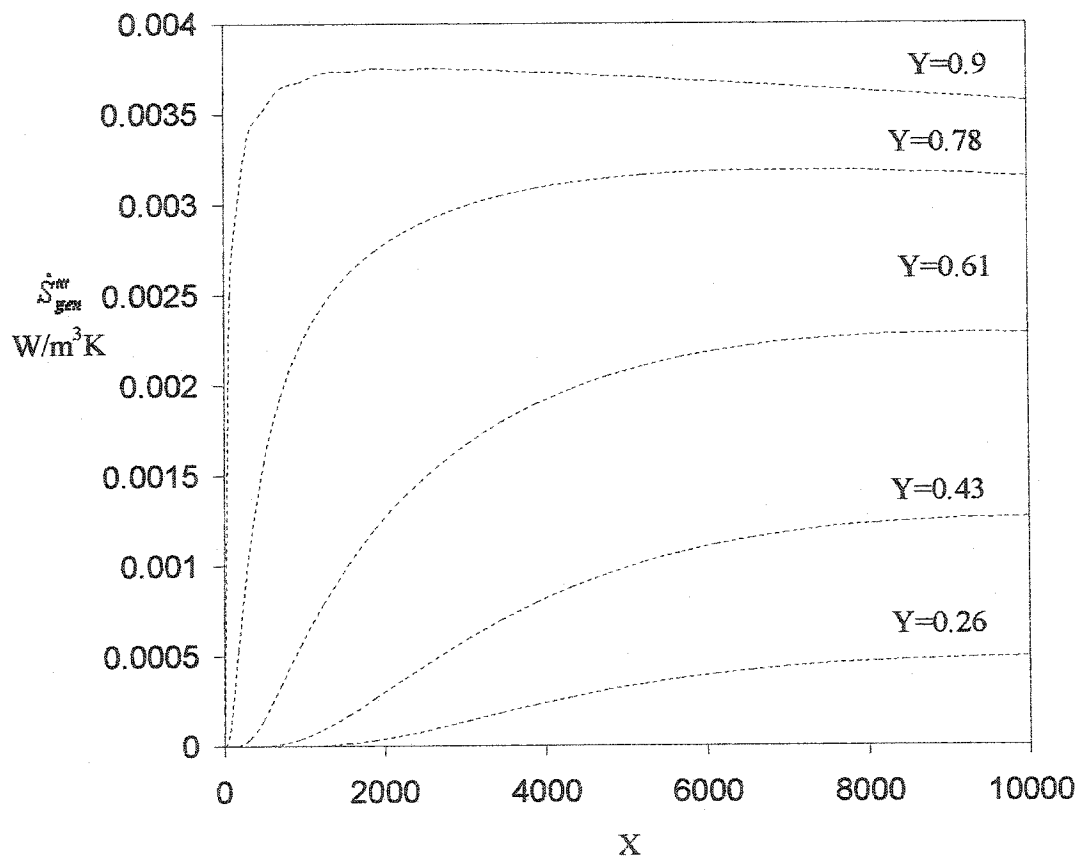


**Figure 5.55**  $\dot{S}_{gen}^m$  vs.  $X$  for variable viscosity case for ethylene glycol at various  $Y$  values (physical properties are given in Table 5.2,  $Re = 400$ ,  $T_o = 300$  K and  $Q'' = 10$   $W/m^2$ ).



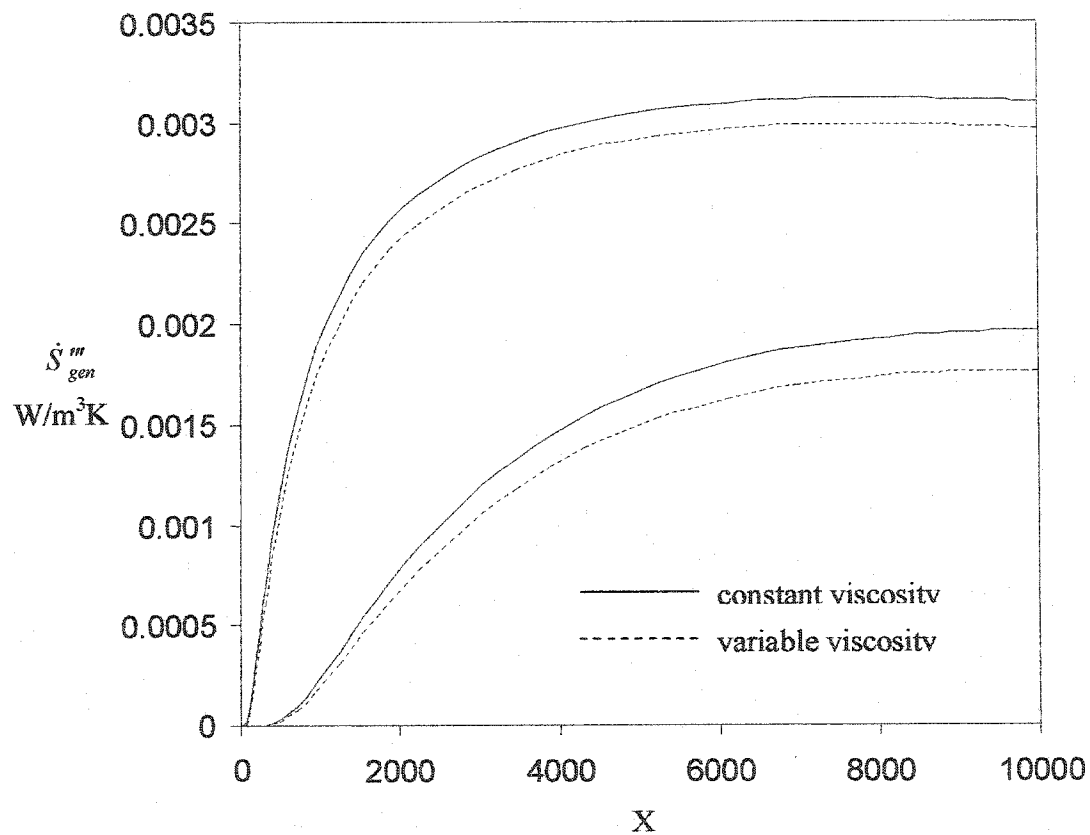


**Figure 5.56**  $\dot{S}_{gen}'''$  vs.  $X$  for constant and variable viscosity cases for ethylene glycol at  $Y = 0.52$  and  $0.74$  (physical properties are given in Table 5.2,  $Re = 400$ ,  $T_o = 300$  K and  $Q'' = 10$   $W/m^2$ ).

constant viscosity profile and the variable viscosity profile increases as the flow proceeds downstream because the fluid receives more heat as it moves downstream and the effect of temperature dependent viscosity increases. In order to investigate the entropy generation profiles from different angle, Figure 5.57 is plotted for  $\dot{S}_{gen}^m$  vs. Y for different X values. This figure shows that the entropy generation increases in the X-direction and that is due to the increase of the amount of heating in the ethylene glycol as the flow proceeds downstream.

#### **5.4.5.2 Effect of Reynolds Number and the Liquid Type on Entropy Generation**

The effect of various parameters was demonstrated for velocity and temperature profiles. These parameters are the effect of Reynolds number and the type of the fluid. In this section, the effect of the two parameters on entropy generation profiles are discussed which are effect of Reynolds number and effect of liquid type.

##### **5.4.5.2.1 Effect of Reynolds Number**

The main effect of the Reynolds number in the previous discussions was the shifting and extension of the profiles downstream as the Reynolds number increases. This effect was also noticed in entropy generation profiles as shown in Figure 5.58. In this figure,  $\dot{S}_{gen}^m$  vs. X is plotted for different Reynolds numbers values at Y=0.52. It is clear that the entropy generation profiles extend and shift downstream as the Reynolds number increases. Furthermore,  $\dot{S}_{gen}^m$  vs. Y is plotted for different Reynolds number values at X=80.4. From Figure 5.59, it is clear that as the Reynolds number increases, the entropy generation profile shifts towards the wall.

#### 5.4.5.2.2 Liquid Type

Entropy generation for ethylene glycol and water will be tested in one figure to show the difference in behavior between more and less viscous liquids. Figure 5.60 is plotted for  $\dot{S}_{gen}^m$  vs. X for ethylene glycol and water at the same condition. It is clear that water reaches the final X-location, 1800, faster than the final X-location, 10000, of ethylene glycol. This is because heat diffuses quickly in water while the heat diffuses very slowly in ethylene glycol. Therefore, substantial amount of heat is needed in ethylene glycol case and this explains why the entropy generation is larger in ethylene glycol case in comparison to water. Moreover,  $\dot{S}_{gen}^m$  vs. Y is plotted in Figure 5.61 to complete the discussion of the effect of the liquid type on the entropy generation. This figure is plotted at  $X = 100$  and  $Re = 400$ . At a distance very close to the wall, it is clear from the figure that  $\dot{S}_{gen}^m$  for the ethylene glycol is higher than that of water. This is related to the temperature gradient in the Y-direction for the ethylene glycol that is longer than that for water because the temperature difference between the wall and the ethylene glycol is higher. That is because the ethylene glycol responds slower to the effect of heating.

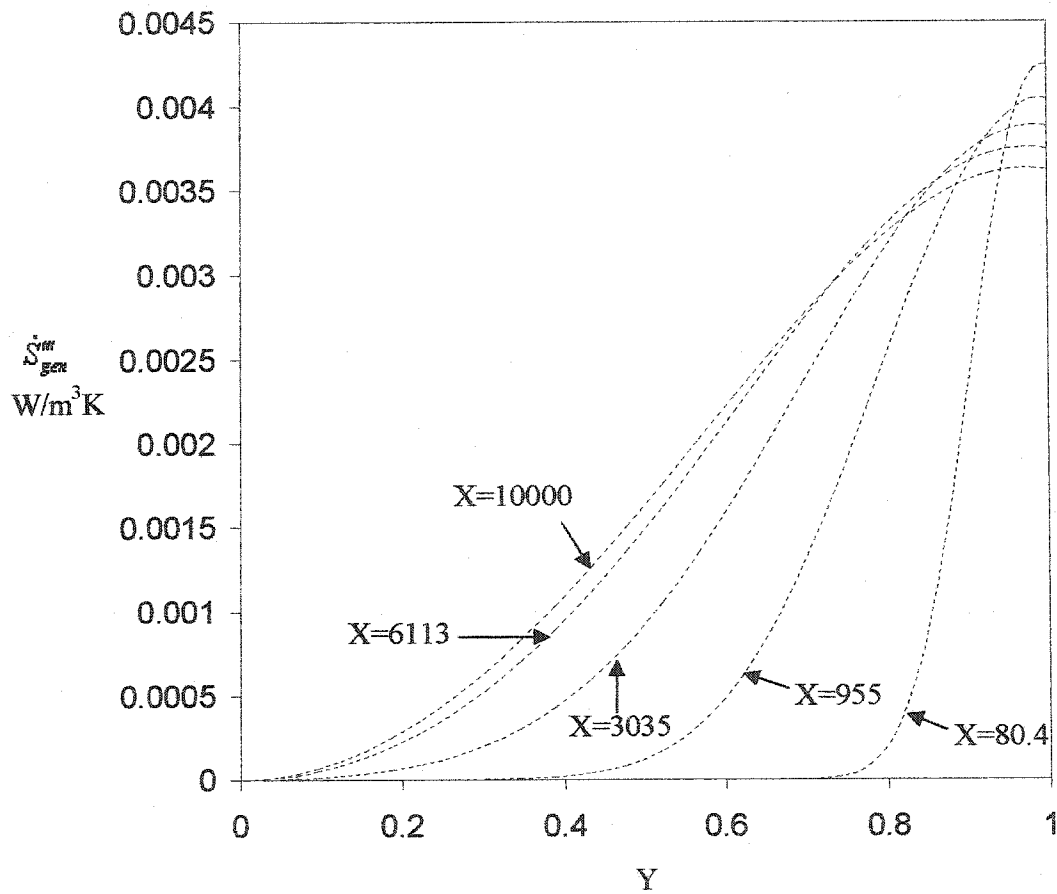


**Figure 5.57**  $\dot{S}_{gen}^m$  vs.  $Y$  for variable viscosity case for ethylene glycol at various  $X$  values (physical properties are given in Table 5.2,  $Re = 400$ ,  $T_o = 300$  K and  $Q'' = 10$  W/m<sup>2</sup>).

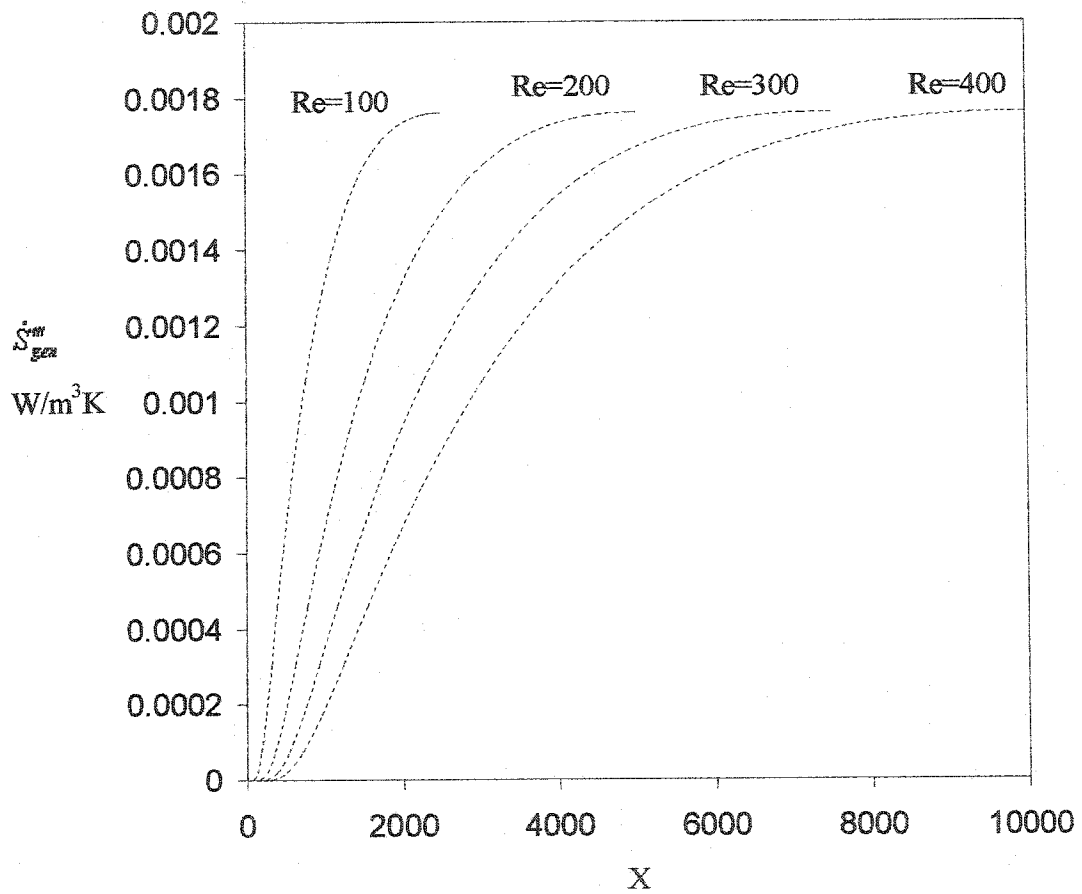


**Figure 5.58**  $\dot{S}_{gen}^m$  vs.  $X$  for variable viscosity case for ethylene glycol at  $Y = 0.52$  (physical properties are given in Table 5.2,  $Re = 100, 200, 300, 400$ ,  $T_o = 300$  K and  $Q'' = 10$   $W/m^2$ ).

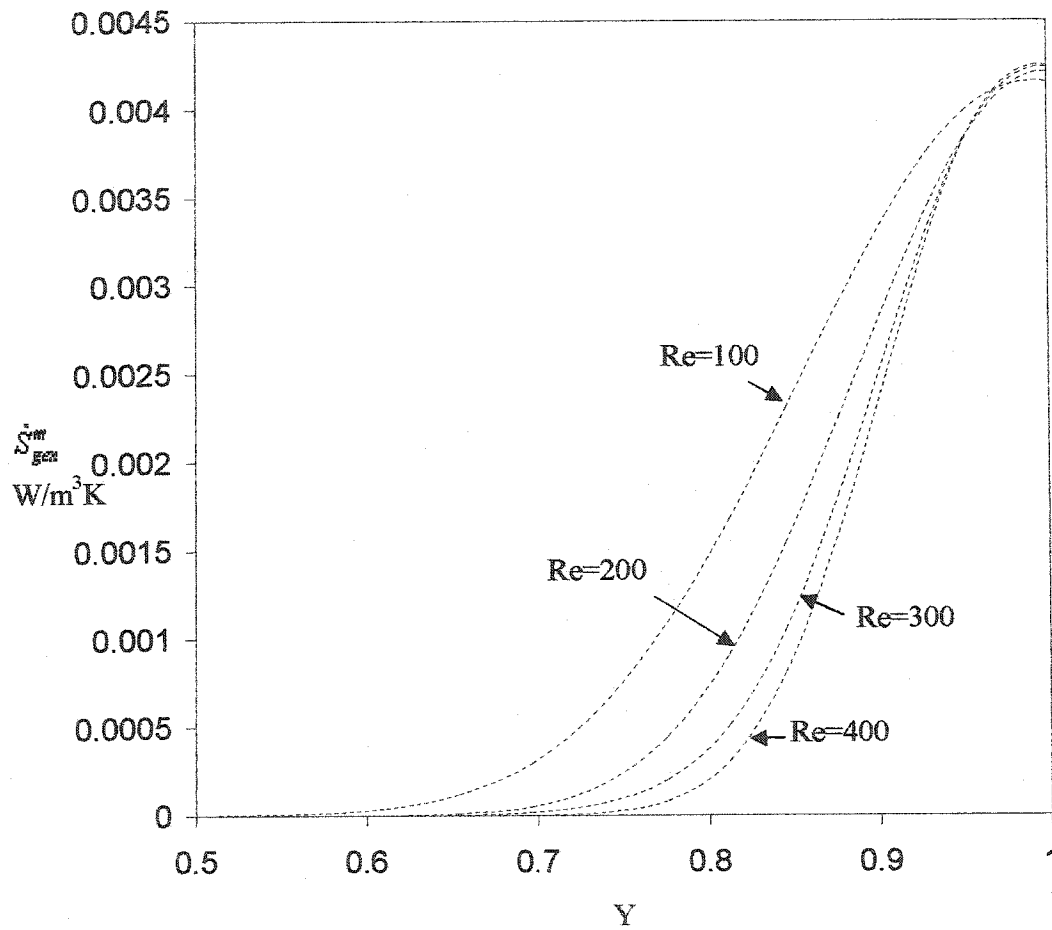


**Figure 5.59**  $S_{gen}^m$  vs.  $Y$  for variable viscosity case for ethylene glycol at  $X = 80.4$  (physical properties are given in Table 5.2,  $Re = 100, 200, 300, 400$ ,  $T_o = 300$  K and  $Q'' = 10$   $W/m^2$ ).

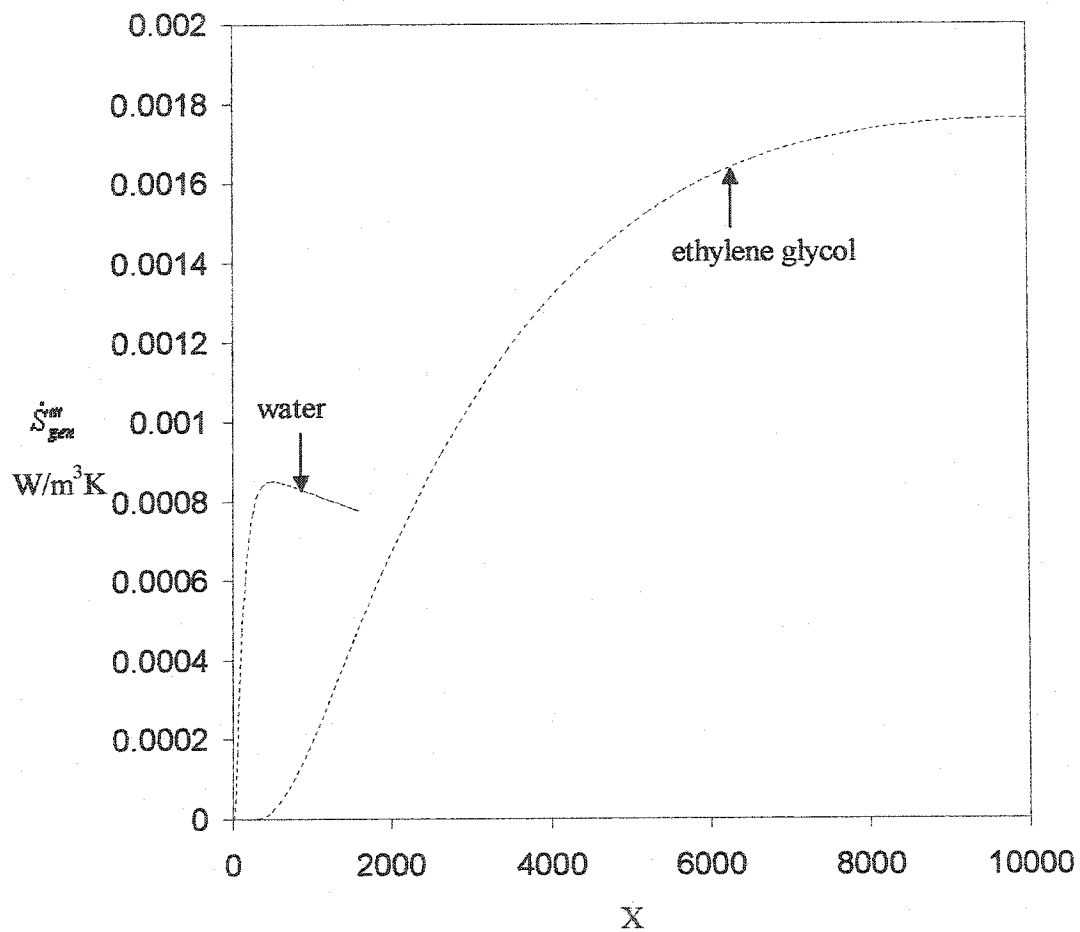


**Figure 5.60**  $\dot{S}_{gen}^m$  vs.  $X$  for variable viscosity case for ethylene glycol and water at  $Y = 0.52$  (physical properties are given in Table 5.2,  $Re = 400$ ,  $T_o = 300$  K and  $Q'' = 10$   $W/m^2$ ).

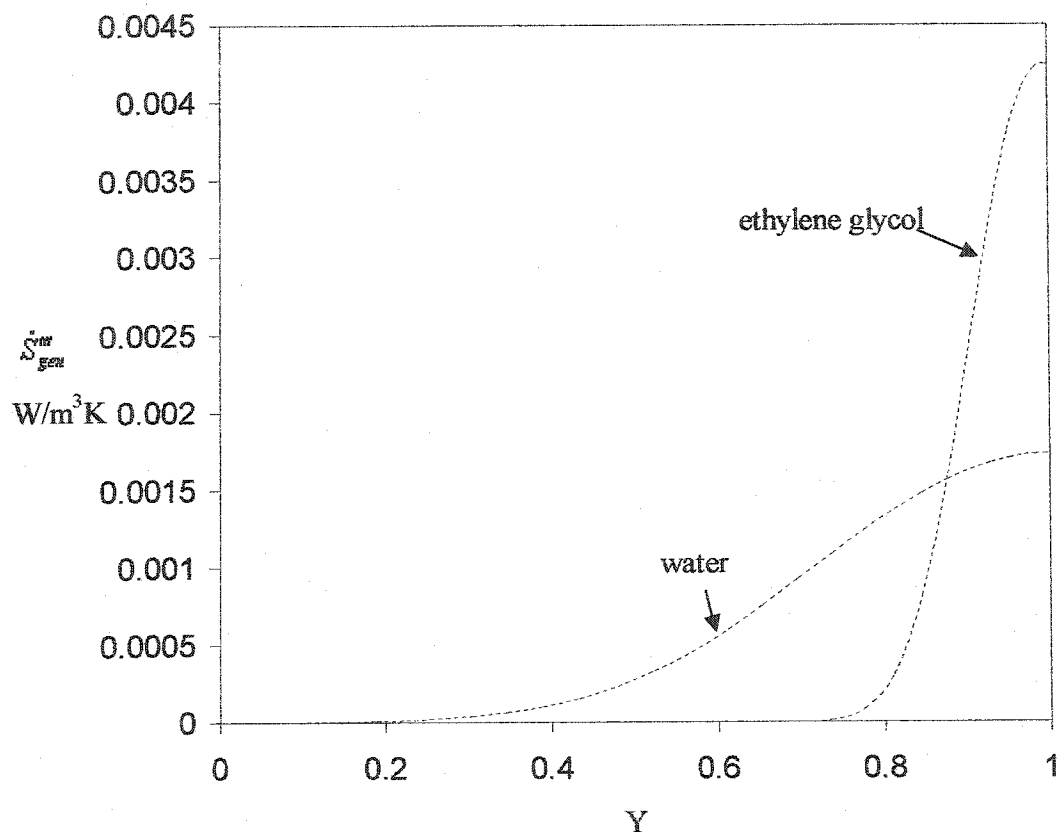


**Figure 5.61**  $\dot{S}_{gen}''$  vs.  $Y$  for variable viscosity case for ethylene glycol and water at  $X = 100$  (physical properties are given in Table 5.2,  $Re = 400$ ,  $T_o = 300$  K and  $Q'' = 10$   $\text{W/m}^2$ ).



### 5.4.5.3 $\dot{S}_{\Delta Y}$ and $\dot{S}_{\Delta Y \Delta X}$

In the constant wall temperature case, the importance of total entropy generation in Y-direction at a specified X-location,  $\dot{S}_{\Delta Y}$ , and total entropy generation in Y-direction from inlet to a specified X-location,  $\dot{S}_{\Delta Y \Delta X}$ , were explained and two figures were shown and discussed. In this section, the same two figures are discussed for the constant heat flux. Figure 5.62 is plotted for  $\dot{S}_{\Delta Y}$  vs. X for different Reynolds numbers. In this figure, it is demonstrated that as the flow goes downstream,  $\dot{S}_{\Delta Y}$  increases due to the increasing amount of heat coming from the wall into the liquid.

Finally,  $\dot{S}_{\Delta Y \Delta X}$  vs. Reynolds number is plotted in Figure 5.63 for ethylene glycol where X starts from inlet to 1250.  $\dot{S}_{\Delta Y \Delta X}$  increases from Re = 0 to 100. After this point,  $\dot{S}_{\Delta Y \Delta X}$  decreases as the Reynolds number increases. To explain why  $\dot{S}_{\Delta Y \Delta X}$  decreases as the Reynolds number increases after 100, two points must be emphasized to understand this behavior. The first point is related to the final length of the parallel plates at which these calculations are ended. The final length of the parallel plates was limited due to the linear viscosity relation that should not exceed 30 °C difference. The second point is related to the length of the X at which this figure is plotted. These two points can be noticed clearly in Figure 5.58. In this figure, the first point specifies the shape and the limit of these profiles. Furthermore, the X length is taken at 1250 and the location of this point on Figure 5.58 shows that the area under these curves explains why the entropy generation decreases. It is clear that the area for Re = 100 is the largest at X = 1250 while the area for Re = 400 is the smallest.

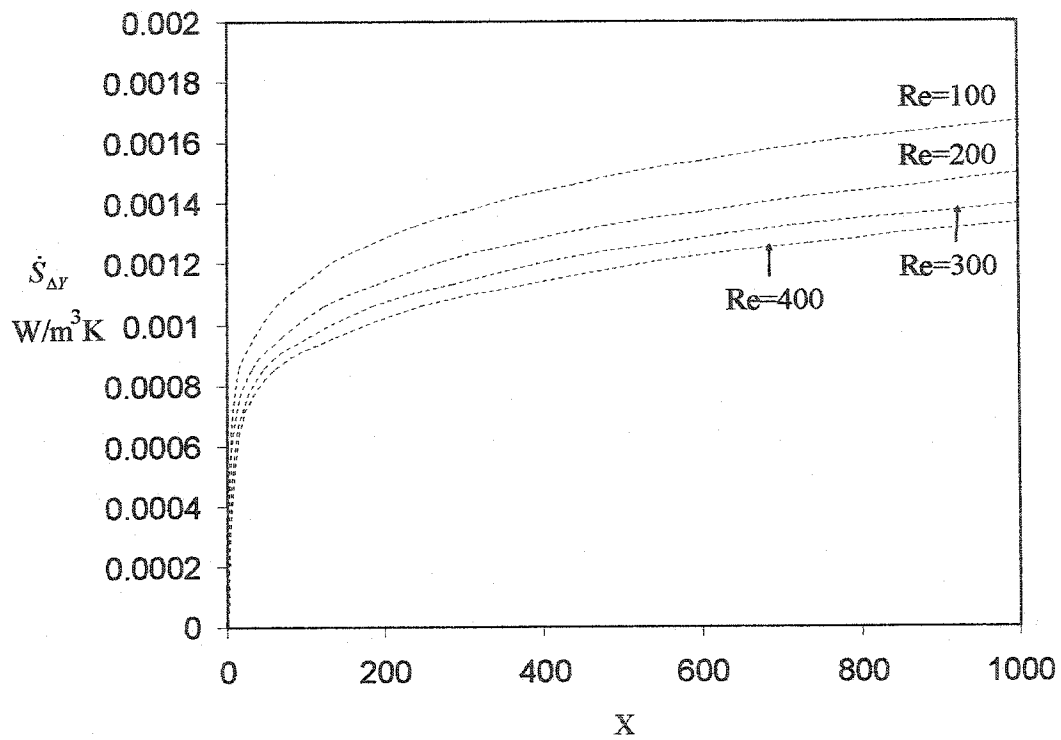


**Figure 5.62**  $\dot{S}_{\Delta Y}$  vs.  $X$  for variable viscosity case for ethylene glycol for different  $Re$  numbers (physical properties are given in Table 5.2,  $T_o = 300$  K and  $Q'' = 10$   $\text{W/m}^2$ ).

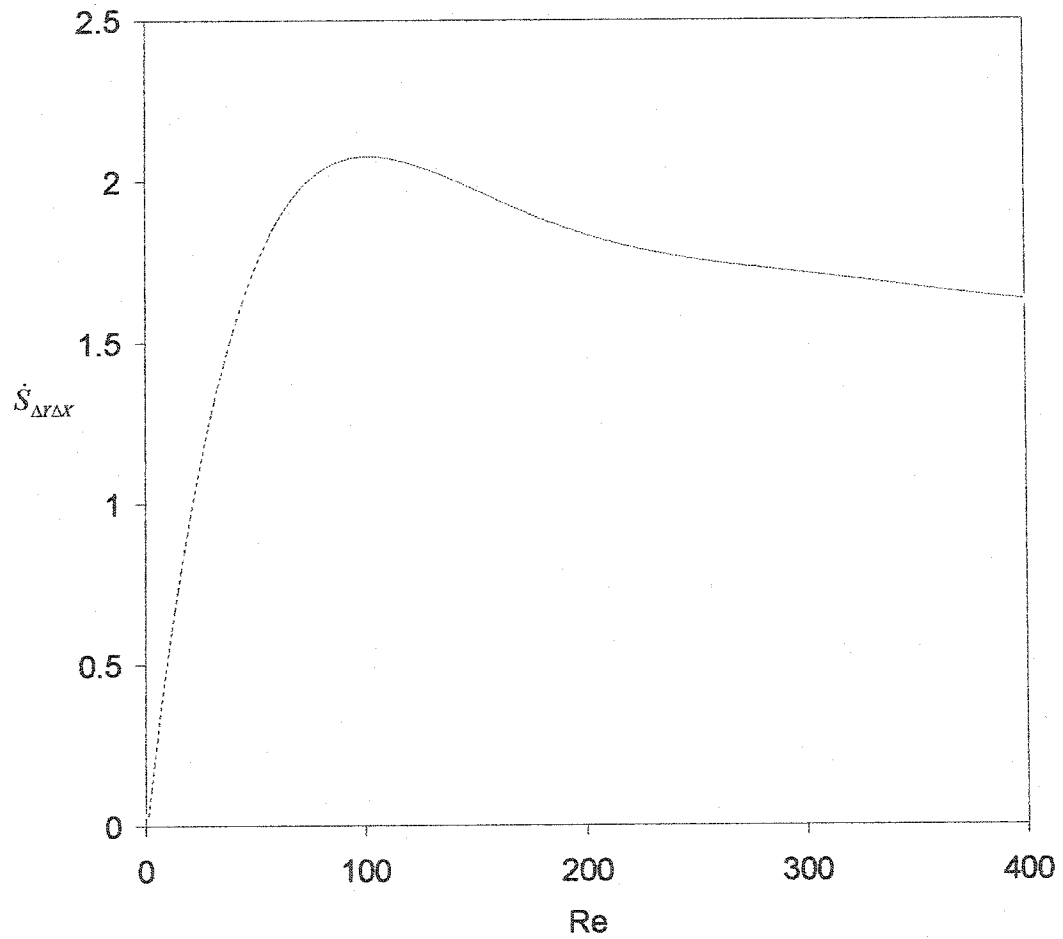


**Figure 5.63**  $\dot{S}_{\Delta T_{MAX}}$  vs.  $Re$  for variable viscosity case for ethylene glycol between  $X = 0$  and  $X = 1250$  (physical properties are given in Table 5.2,  $T_o = 300$  K and  $Q'' = 10$  W/m<sup>2</sup>).

## CHAPTER 6

### CONCLUSIONS AND RECOMMENDATIONS

Entropy generation has been investigated for forced laminar flow between parallel plates subjected to constant wall temperature and constant heat flux. The effect of temperature dependency of the viscosity has been taken into consideration. The investigation has been approached by determining temperature and velocity data and inserting them into the entropy generation equation. Different parameters have been investigated to show their effect on entropy generation. These parameters include the Reynolds number, inlet-wall temperature difference and liquid type.

The influence of Reynolds number is remarkable on the entropy generation profiles. It has been shown that increasing the Reynolds number results in shifting and extending velocity, temperature and therefore entropy generation profiles downstream the parallel plates. It has been shown for constant wall temperature case that increasing the Reynolds number leads to an increase in the total entropy generation because the entropy generation profiles are shifted downstream as shown in Figure 5.40. However, for the constant heat flux case, it has been shown that the total entropy generation increases at low Reynolds number and then it decreases as the Reynolds number increases as shown in Figure 5.63. For both cases, these behaviors can be changed if various lengths of the parallel plates are chosen. For example, in Figure 5.35 which represents the entropy generation per unit volume vs. axial length for Reynolds numbers = 200 and 400, the total

entropy generation can be determined from the area under the curve. The area under the curve for  $Re = 400$  is greater than that of  $Re = 200$  when the axial length is long. However, it is smaller when the axial length is short. Therefore, the length of the parallel plates is a critical parameter when the total entropy generation of different Reynolds number is compared. Thus, it is recommended to include the length of the parallel plates as a parameter in studying the entropy generation. Further, for the constant wall temperature case,  $\dot{S}_{\Delta T}$  increases downstream until it reaches a maximum at a specific length. Then, it decreases since the temperature gradient diminishes as the fluid moves downstream. Before that length,  $\dot{S}_{\Delta T}$  increases as Reynolds number decreases while beyond that length  $\dot{S}_{\Delta T}$  increases as the Reynolds number increases. This is related the shape of temperature and velocity profiles when Reynolds number is increased. In constant heat flux, however, as the Reynolds number increases,  $\dot{S}_{\Delta T}$  increases downstream because the heating continues as the flow proceeds downstream.

The influence of liquid type has been investigated in this study by using two different liquids, ethylene glycol and water. It has been shown that in the constant wall temperature case, the entropy generation in ethylene glycol to be higher than that of water because heat transfer develops faster for water than ethylene glycol since water has smaller Prandtl number. However, in the case of constant heat flux, the same conclusion is true but here the temperature profile does not develop (i.e. it continues to increase). In general, the total entropy generation between parallel plates increases as the Prandtl number increases.

The effect of the temperature difference between the wall and the inlet is considered in constant wall temperature case. As expected, increasing the temperature difference leads to an increase in the entropy of the flowing liquid.

In this study, the two sources of the entropy generation which are heat transfer and fluid friction are compared. It has been shown that the effect of heat transfer is dominant and the effect of fluid friction could be neglected without a significant effect on the total entropy generation.

Furthermore, when temperature dependent viscosity is considered, velocity and temperature profiles deviate from those of constant viscosity and therefore entropy generation obtained from variable viscosity deviates from that obtained from constant viscosity. For constant wall temperature case, this deviation increases as the inlet-wall temperature difference increases because entropy increases when temperature increases. In heat flux case, the deviation increases as the flow proceeds downstream because the continuous heating to the fluid changes the viscosity and therefore changes the velocity since the momentum and energy equations are coupled through viscosity. This behavior is noticed clearly in ethylene glycol which is thermally more sensitive than water.

To sum up, determining the entropy generation profiles and studying the effective parameters in this study is a first step to the minimization of the entropy generation which is beyond this study. The two cases of heating (constant wall temperature and constant heat flux) have not been compared since the outlet temperature does not provide valuable information in determining the entropy generation profiles. However, if the minimization of entropy generation is to be included, it is an essential task to compare not only the two case of heating but also to include several configurations of heating. Therefore, it is

recommended to extend this study to include various configurations of heating and consider that as an additive parameter. Also, it is recommended to include the length of parallel plates as a parameter in order to investigate its effect on entropy generation. Further, it is recommended to obtain the optimum conditions that satisfy the minimum entropy generation. The investigation of the parallel plates can be extended to include rectangular duct since this study serves as a stepping-stone to more complex situations.

## NOMENCLATURE

$b$ (N s/m <sup>2</sup> K)	Fluid dependent constant
$Br$	Brinkman number
$Br'$	Suggested Brinkman number for heat flux
$C_p$ (J/kg.K)	Specific heat
$D_h$ (m)	Hydraulic diameter
$H$ (m)	Width of the parallel plates
$k$ (W/m.K)	Thermal conductivity
$\dot{m}$ (kg/s)	Mass flow rate
$P$ (Pa)	Pressure
$Pe$	Peclet number
$Pr$	Prandtl number
$Q''$ (W)	Heat flux
$q_x$ (W)	Heat flux in X-direction
$q_y$ (W)	Heat flux in Y-direction
$Re$	Reynolds number
$s$ (J/kg.K)	Specific entropy
$\dot{S}_{gen}^m$ (W/m <sup>3</sup> K)	Entropy generation per unit volume
$\dot{S}_{\Delta T}$ (W/m <sup>2</sup> K)	Total entropy generation averaged over Y-direction for a specified X
$\dot{S}_{\Delta T \Delta X}$ (W/m <sup>3</sup> K)	Total entropy generation in Y-direction for $\Delta X$



$T$ (K)	Temperature
$\Theta$	Dimensionless temperature
$T_o$ (K)	Inlet temperature
$T_w$ (K)	Wall temperature
$u$ (J/kg)	Internal energy
$u_m$ (m/sec)	Average velocity
$v_x$ (m/sec)	Axial velocity
$U$	Dimensionless axial velocity
$v_y$ (m/sec)	Velocity in Y-direction
$V$	Dimensionless velocity in Y-direction
$x$ (m)	Axial direction
$X$	Dimensionless axial direction
$y$ (m)	y-direction
$Y$	Dimensionless y-direction
$\Delta T$ (K)	Inlet-wall temperature difference

#### Greek Symbols

$\beta_i$ (1/sec)	Vorticity boundary condition at the wall
$\rho$ (kg/m <sup>3</sup> )	Density
$\mu$ (N s/m <sup>2</sup> )	Viscosity
$\mu_o$ (N s/m <sup>2</sup> )	Reference viscosity

$\bar{\mu}$	Dimensionless viscosity
$\omega$ (1/sec)	Vorticity
$\bar{\omega}$	Dimensionless vorticity
$\psi$ (m <sup>2</sup> /sec)	Stream function
$\bar{\psi}$	Dimensionless stream function
$\Phi$	Viscous dissipation function

## Bibliography

Abu-Hijleh, B., Entropy Generation in Laminar Convection from an Isothermal Cylinder in Cross Flow, *Energy*, **23**, 851-857 (1998).

Arpaci, V., A Thermal Microscale via Lost Heat into Entropy, *ASME, HTD* **80**, 21-25 (1989).

Badar, M., Zubair, S. and Al-Farayedhi, A., Second-Law-Based Thermoeconomic Optimization of A Sensible Heat Thermal Energy Storage System, *Energy*, **18**, 641-649 (1993).

Baytas, A., Entropy Generation for Natural Convection in an Inclined Porous Cavity, *International Journal of Heat and Mass Transfer*, **43**, 2089-2099 (2000).

Bejan, A., A Study of Entropy Generation in Fundamental Convective Heat Transfer, *Journal of Heat Transfer*, **101**, 718 -725(1979).

Bejan, A., Second Law Analysis in Heat Transfer, *Energy*, **5**, 721-728(1980).

Bejan, A, Entropy Generation through Heat and Fluid Flow, Wiley, 1<sup>st</sup> ed., New York, (1982)

Bejan, A., Advanced Engineering Thermodynamics, Wiley, 1<sup>st</sup> ed., New York, (1988).

Bejan, A., Entropy Generation Minimization, 1<sup>st</sup> ed., Wiley, New York, (1995).

Bird, R., Stewart, W. and Lightfoot, E., Transport Phenomena, 3<sup>rd</sup> ed., McGraw-Hill, New York, (1977).

Blanco, H., Irreversibility in Heat Transfer Enhancement, *ASME, HTD* **33**, 19-26 (1984).

Butler, H. and McKee, D., An Exact Solution for the Flow of Temperature-Dependent Viscous Fluids in Heated Rectangular Ducts, *Journal of Heat Transfer*, 555 -557(1973).

Cervantes, J. and Solorio F., Entropy Generation in a Plane Turbulent Oscillating Jet, *International Journal of Heat and Mass Transfer*, **45**, 3125-3129 (2002).

Chang, P., Chou, F. and Tung, C., Heat Transfer Mechanism for Newtonian and non-Newtonian Fluids in 2:1 Rectangular Ducts, *International Journal of Heat and Mass Transfer*, **41**, 3841-3856 (1998).

Chang, C. and Huang, W., Numerical Prediction for Laminar Forced Convection in Parallel Plate Channels with Transverse Arrays, *International Journal of Heat and Mass Transfer*, **34**, 2739-2749 (1991).

Cheng, C., Ma, W., and Huang, W., Numerical Predictions of Entropy Generation for Mixed Convection Flows in a Vertical Channel with Transverse Fin Array, *Int. Comm. Heat Mass Transfer*, **21**, 519-530 (1994).

Chou, F. and Tung, C., The Mechanism of Heat Transfer Enhancement for Mineral Oil in 2:1 Rectangular Ducts, *International Journal of Heat and Mass Transfer*, **38**, 2863-2871 (1995).

Deavours, C., An Exact Solution for the Temperature Distribution in Parallel Plate Poiseuille Flow, *Journal of Heat Transfer*, 489-495 (1974).

Demirel, Y. and Kahraman, R., Entropy Generation in a Rectangular Packed Duct with Wall Heat Flux, *International Journal of Heat and Mass Transfer*, **42**, 2337-2344 (1999).

Drost, M. and White M., Local Entropy Generation Analysis of a Rotary Magnetic Heat Pump Regenerator, *Journal of Energy Resource and Technology*, **116**, 140-147 (1994).

Gaggioli, R., The Concept of Available Energy, *Chemical Engineering Science*, **16**, 87-90 (1960).

Gaggioli, R. and Wepfer, W., Exergy Economics, *Energy*, **5**, 823-837 (1980).

Gaggioli, R., El-Sayed, Y., El-Nashar, A. and Kamaluddin, B., Second Law Efficiency and Costing Analysis of a Combined Power and Desalination Plant, *Journal of Energy Resource Technology*, **110**, 114-118 (1988).

Gool, W., Thermodynamic Aspects of Energy Conservation, *Energy*, **5**, 783-792 (1980).

Gyftopoulos, E. and Beretta, G., Entropy Generation Rate in a Chemically Reacting System, *Journal of Energy Resource Technology*, **115**, 208-215 (1993).

Ibanez, G., Cuevas S., and Haro, M., Minimization of Entropy Generation by Asymmetric Convective Cooling, *International Journal of Heat and Mass Transfer*, **46**, 1321-1328 (2003).

Johannessen, E., Nummedal, L. and Kjelstrup, S., Minimizing the Entropy Production in Heat Exchange, *International Journal of Heat and Mass Transfer*, **45**, 2649-2657 (2002).

Kestin, J., Availability: The concept and Associated Terminology, *Energy*, **5**, 679-692 (1980).

Leidenfrost, W., Lee, K. and Korenic, B., Conservation of Energy Estimated by Second Law Analysis of A Power-Consuming Process, *Energy*, **5**, 47-61(1980).

Lin, W. and Lee D., Second-law Analysis on a Pin-fin Array under Cross flow, *International Journal of Heat and Mass Transfer*, **40**, 1937-1945 (1996).

Marcella, T., Entropy Production and Second Law of Thermodynamics: An introduction to Second Law Analysis, American Association of Physics Teachers, **60**, 888-895 (1992)

Narusawa, U., The Second-law Analysis of Convective Pattern Change in a Rectangular Cavity, *Journal of Fluid Mechanics.*, **392**, 361-377 (1999).

Nevers, N. and Seader, J., Lost Work: A Measure of Thermodynamic Efficiency, *Energy*, **5**, 757-769 (1980).

Peyret, R., Spectral Methods for Incompressible Viscous Flow, 1<sup>st</sup> ed., Springer-Verlag, New York, (2002).

Pinelli, A. and Vacca, A., Chebyshev Collocation Method and Multidomain Decomposition for the Incompressible Navier-Stokes Equation. *International Journal Numerical Mechanics Fluids*, **18**, 781-790(1994).

Plawsky, J., Transport Phenomena Fundamentals, 1<sup>st</sup> ed., McGraw-Hill, New York, (2001).

Pons, M., Second Law Analysis of Adsorption Cycles With Thermal Regeneration, *Journal Engineering Resource Technology*, **118**, 229-235 (1996).

Poulikakos, D., and Johnson, J., Second Law Analysis of Combined Heat and Mass Transfer Phenomena in External Flow, *Energy*, **14**, 67-75(1989).

Prins, M., Ptasiński, K. and Janssen F., Thermodynamics of Gas-Char Reaction: First and Law Analysis, *Chem. Eng. Science*, **58**, 1003-1011 (2003).

Ray, S and Sengupta S., Irreversibilities Analysis of a Sieve Tray in a Distillation Column, *International Journal of Heat and Mass Transfer*, **39**, 1535-1542 (1994).

Reddy, B., Ramkiran G., Kumar, K. and Nag P., Second Law Analysis of a Waste Heat Recovery Steam Generator, *International Journal of Heat and Mass Transfer*, **45**, 1807-1814 (2002).

Saboya, F. and Costa, C., Minimum Irreversibility Criteria for Heat Exchanger Configuration, *Journal of Energy Resources Technology*, **121**, 241-246 (1999).

Sahin, A., Entropy Generation in Turbulent Liquid Flow through a Smooth Duct subjected to Constant Wall Temperature, *International Journal of Heat and Mass Transfer*, **43**, 1469-1478 (2000).

Sahin, A., Irreversibilities in Various Duct Geometries with Constant Wall Heat Flux and Laminar Flow, *Energy*, **23**, 465-473 (1998).

Sahin, A.Z., Thermodynamics of Laminar Viscous Flow through a Duct Subjected to Constant Heat Flux, *Energy*, **21**, 1179-1187 (1996).

Sama, D., The use of the Second Law of Thermodynamics in Process Design, *Journal Engineering Resource Technology*, **117**, 179-185 (1995).

San, J., Worek, W. and Lavan, Z., Entropy Generation in Combined Heat and Mass Transfer, *International Journal of Heat and Mass Transfer*, **30**, 1359-1369 (1987).

Schlichting, H., Boundary Layer Theory, 7<sup>th</sup> ed., McGraw-Hill, New York, (1979).

Sekulic, D., Campo, A. and Morales, J., Irreversibility Phenomena Associated with Heat Transfer and Fluid Friction in Laminar Flows through Singly Connected Ducts, *International Journal of Heat and Mass Transfer*, **40**, 905-914 (1996).

Shah, R. and London, A., Laminar Flow Forced Convection in Ducts, 1<sup>st</sup> ed., Academic Press, New York, (1978).

Shannon, R. and Depew, C., Forced Laminar Flow Convection in a Horizontal Tube With Variable Viscosity and Free-Convection Effects, *Journal of Heat Transfer*, 251-258 (1969).

Shin, S., Cho, Y., Gringrich, W. and Shyy, W., Numerical Study of Laminar Heat Transfer with Temperature Dependent Fluid Viscosity in a 2:1 Rectangular Duct, *International Journal of Heat and Mass Transfer*, **36**, 4365-4374 (1993).

Shome, B. and Jensen, M., Mixed Convection Laminar Flow and Heat Transfer of Liquids in Isothermal Horizontal Circular Ducts, *International Journal of Heat and Mass Transfer*, **38**, 1945-1956 (1995).

Sotiropoulos, F., and Abdullah, S., Coupled Fully Implicit Solution Procedure for the Steady Incompressible Navier-Stokes Equations, *Journal of Computational Physics* **87**, 328-348 (1990).

Sun, Z., and Carrington, C., Application of Nonequilibrium Thermodynamics in Second Law Analysis, *Journal of Energy Resources Technology*, **113**, 33-39 (1991).

Syrjala, S., Laminar Flow of Viscoelastic Fluids in Rectangular Ducts With Heat Transfer: A Finite Element Analysis, *International Communication of Heat and Mass Transfer*, **25**, 191-204 (1998).

Teng, H., Kinoshita, C., Masutani, S. and Zhou, J., Entropy Generation in Multicomponent Reacting Flows, *Journal of Energy Resources and Technology*, **120**, 226-232 (1998).

Test, F., Laminar Flow Heat Transfer and Fluid Flow for Liquids With Temperature-Dependent Viscosity, *Journal of Heat Transfer*, 385-393 (1968).

Xie, C. and Hartnett, J., Influence of Variable Viscosity of Mineral Oil on Laminar Heat Transfer in a 2:1 Rectangular Duct, *International Journal of Heat and Mass Transfer*, **35**, 641-648 (1992).

Yang, K., Laminar Forced Convection of Liquids in Tubes with Variable Viscosity, *Journal of Heat Transfer*, 353 -362(1962).

Yuan, Z., Tao, W. and Wnag, Q., Numerical Prediction for Laminar Forced Convection Heat Transfer in Parallel Plate Channels with Streamwise-Periodic Rod Disturbances, *International Journal of Numerical Fluids*, **28**, 1371-1380(1998).

Zimparov, V., Extended Performance Evaluation Criteria for Enhanced Heat Transfer Surfaces: Heat Transfer through Ducts with Constant heat Flux, *International Journal of Heat and Mass Transfer*, **44**, 169-180 (2001).